THE BELL SYSTEM

TECHNICAL JOURNAL

DEVOTED TO THE SCIENTIFIC AND ENGINEERING

ASPECTS OF ELECTRICAL COMMUNICATION

Volume 49 April 1970 Number 4

Performance of Burst-Trapping Codes

By S. Y. TONG

(Manuscript received November 6, 1969)

The performance of several burst-trapping codes has been estimated through computer simulation on three sets of field trial data over the switched telephone network (Alexander-Gryb-Nast, Townsend-Watts, Vestigial-Sideband). The results indicate that the codes are capable of giving better performance than interleaved codes based on the same coding redundancy and approximately the same storage requirement.

I. INTRODUCTION

An adaptive error control scheme called burst-trapping has been proposed as a means to combat errors in a channel where both random and burst disturbances occur.[1] Such a channel is called a compound channel. Error statistics derived from field trial data over telephone channels indicate that the switched telephone network is a prime example of a compound channel.

It is of interest to see how the proposed technique performs on telephone channels and to compare its performance with other known techniques. In this report, a computer simulation is used to determine the performance of such codes. A program has been written which simulates any burst-trapping code of rate $(b-1)/b$, b an integer. The program was used on the three well-known sets of telephone error data: the

Alexander-Gryb-Nast (AGN) data,[2] the Townsend-Watts (TW) data[3] and the Vestigial-Sideband (VSB) data.[4]

The output of the simulation program gives both the bit and block error rate before and after the application of burst-trapping error control. The simulated block error rate with a large interleaving degree shows an excellent agreement with the result of an analytical approach presented in the companion paper.[5] Since two independent approaches are used, the agreement seems to indicate both techniques are accurate. The analytical technique gives the tail of distribution which cannot be produced by the simulation without a large amount of raw data. On the other hand, the simulation technique can show the effect of interleaving on performance. Thus it is a valuable design tool to determine the size of interleaving required which in turn determines the cost of the error control system. (Note that in Ref. 5, interleaving is assumed to be sufficiently large that each subcode essentially has statistically independent error blocks.) Thus these two techniques complement each other for the evaluation of performance of a burst-trapping code.

II. A REVIEW OF BURST-TRAPPING CODES

The reader is assumed to be familiar with Ref. 1 on burst-trapping techniques. We shall therefore confine ourselves to a brief review and will restrict our attention to codes with rate $R = \frac{2}{3}$, as this is the lowest rate that reveals the general operation. For a general description, see Ref. 1.

Let C be a linear systematic binary block code of length n with k information bits per block, such that $k/n = \frac{2}{3}$. Let I_i^1 be a $k/2$-tuple representing the first $k/2$ information bits in the ith transmitted block and let I_i^2 be similarly defined for the second $k/2$ information bits. Let P_i be the parity digits in the code word associated with I_i^1 and I_i^2. (Note that P_i is also a $k/2$-tuple.) Finally, define Q_i as

$$Q_i \triangleq P_i + I_{i-1}^1 + I_{i-2}^2$$

where addition is bit-by-bit, modulo-2. Then the transmitted message consists of the sequence of $k/2$-tuples, $I_0^1, I_0^2, Q_0, I_1^1, I_1^2, Q_1, \cdots, I_i^1, I_i^2, Q_i, \cdots$, and so on, as shown in Fig. 1.

At the decoder there are two modes of operation, the *random* mode and the *burst-trapping* mode. Let the minimum distance of C be d_m and assume that the decoder is designed to correct up to t errors per block where $t \leqq [(d_m - 1)/2]$. Now assume the decoder has just received

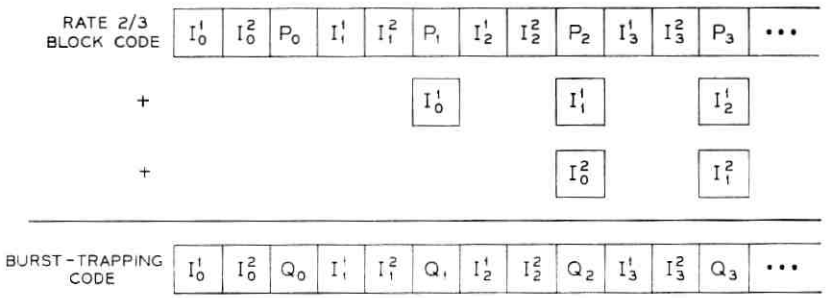

Fig. 1—Generation of $R = 2/3$ burst-trapping code.

the 0th block. If $I_i^j = 0, i < 0, j = 1, 2$, then $Q_0 = P_0$ and the sequence I_0^1, I_0^2, Q_0 forms a code word in C. If the decoder "thinks" that there are t or fewer errors in the received block, then it operates in the random mode and attempts to correct these errors. If the decoder is successful then I_0^1 can be subtracted from Q_1 and I_0^2 from Q_2 through feedback as shown in Fig. 2. As long as decoding proceeds correctly in this fashion, then, upon the arrival of each successive block, the effect of all past information bits will be removed and the decoder will be left with a code word in C plus any channel errors which may have occurred. Thus, in the random mode, the decoder acts like an ordinary block decoder. Let us now assume that at the first block the decoder detects an error pattern of weight greater than t. It then enters the burst-trapping mode, inhibits feedback of the information bits and delays the estimation of I_1^1 and I_1^2 until the second and third blocks have arrived. The course of action then taken by the decoder is shown graphically in Fig. 3. If the second block is correctly received, then P_2 can be calculated

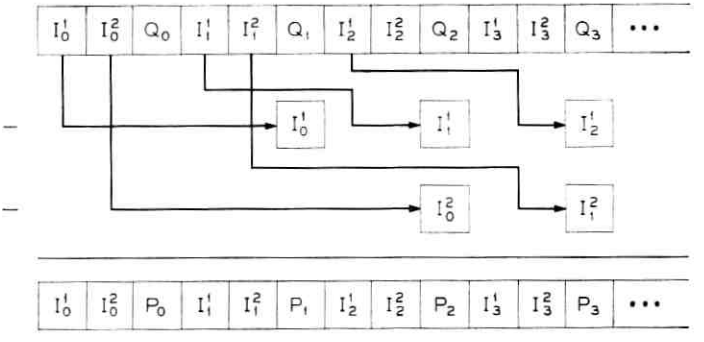

Fig. 2—Error correction in random code.

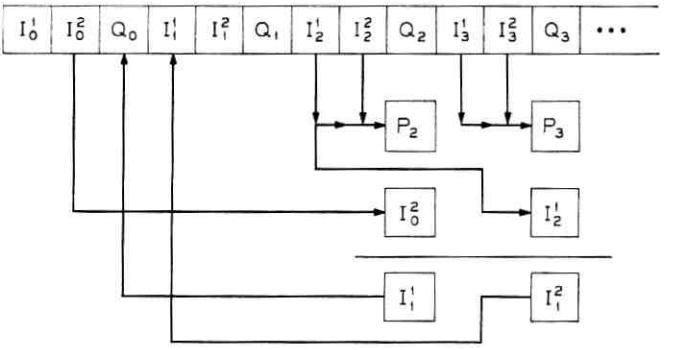

Fig. 3—Error correction in burst code.

from I_2^1 and I_2^2 and subtracted from Q_2. Assuming that the 0th block has been correctly decoded, I_0^2 may also be subtracted from Q_2, leaving I_1^1, which replaces the first $k/2$ discarded information bits in the first block. If the third block is also correctly received, then I_3^1 and I_3^2 may be used to calculate P_3 which, along with I_2^1, is subtracted from Q_3, leaving I_1^2 which, in turn, replaces the second $k/2$ discarded information bits in the first block. Thus I_1^1 and I_2^1 will be recovered error-free if and only if the second and third blocks are error-free. This is the guard space for correcting a burst in the first block. To summarize this discussion, a block error pattern which is detectable with C is correctable with the burst-trapping decoder if and only if the next two blocks are error-free. The probability of failing to detect an error can be made small by keeping t small. In such a case, most of the cosets of C are used for detection, with only a few being used for correction. Such a strategy is often successful on channels where the probability of error between bursts is quite low.

As with any feedback convolutional decoding algorithm, this discussion is valid only under the assumption that all previous blocks have been decoded correctly. In the event of a decoding error, it has been shown that error propagations are rare and are limited.[1] Now suppose Q_i is redefined as

$$Q_i \triangleq P_i + I_{i-\ell}^1 + I_{i-2\ell}^2 .$$

Then the code is said to be *block-interleaved to degree* ℓ. In the burst trapping mode, the decoder then recovers I_i^1 and I_i^2 from the $(i + \ell)$th and the $(i + 2\ell)$th blocks, respectively. Interleaving produces, in effect, ℓ distinct codes of the type described before and if a burst is limited to ℓ or fewer blocks, only one block in each code will be affected. It follows that a burst confined to ℓ successive blocks is correctable if

(*i*) no undetected errors occur in any of the ℓ blocks and (*ii*) the next 2ℓ blocks are error-free. The latter condition is not a necessary one since many burst patterns, particularly on telephone channels, will contain blocks with t or few errors. If this is true for, say, the kth block, then the $(k + \ell)$th and $(k + 2\ell)$th blocks need not be error free.

In the next section, the simulation results on bit error rates are given. It is shown that the burst-trapping codes, when used on telephone channels, seem to perform better than other known codes, with the same coding redundancy and same storage requirement.

III. SIMULATION RESULTS

AGN data was collected over the nation-wide switched network in 1959 with an FM data set operating at 600 b/s and 1200 b/s. Data from a total of about 1000 calls were recorded. The distribution of the average bit error per call is reproduced in Fig. 4. As will be shown later, the burst-trapping codes used in the test correct all the errors in at least 95 percent of the calls. Since the distribution of calls above 90 percent level is almost identical for both 600 and 1200 b/s calls, it was decided to combine the two types of calls together to simplify the discussion.

TW data was collected at 2000 b/s. A DATAPHONE 201A modem

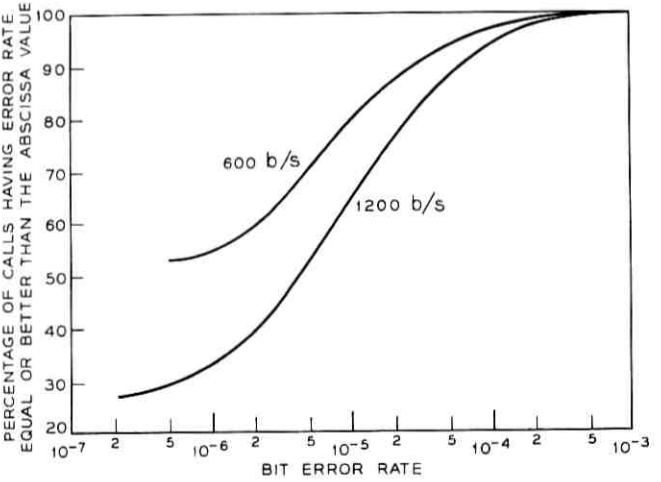

Fig. 4—Alexander-Gryb-Nast raw data statistics. Distribution of calls with respect to bit error rate and speed. Total number of calls—1000.

was used. A total of 502 usable calls* was recorded. The statistics of the calls are reproduced in Fig. 5.

VSB data used in this report consists of 85 selected calls. The statistics of the calls are shown in Fig. 6.

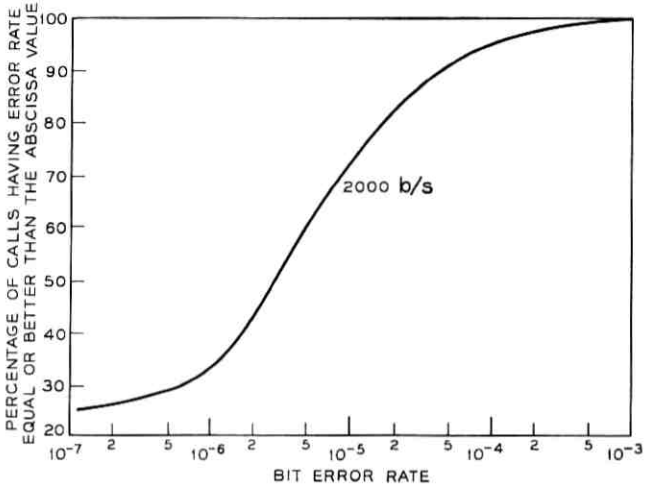

Fig. 5—Townsend-Watts (TW) raw data statistics. Distribution of calls with respect to bit error rate. Total number of calls = 502.

To simplify discussion, a quintuple (n, k, d_m, t, ℓ) is used to describe each burst-trapping code. Recall that a burst-trapping code is built on the basis of a (n, k, d_m) block code, where n is the block length, k is the number of information bits per block and d_m is the minimum distance of the block code. The parameter t denotes the number of random errors the burst-trapping decoder is designed to correct and ℓ is the interleaving degree. Roughly, with a (n, k, d_m, t, ℓ) burst-trapping code one may either correct t random errors in n bits or up to an $n\ell$-bit burst provided that a guard space of $n^2\ell/(n - k)$ bits exists. The storage requirement is $nk\ell/(n - k) + n + \ell$ bits. For more details, please refer to Ref. 1.

Figure 7 compares the performance of two rate $\frac{1}{2}$ codes on VSB data: a (24, 12) triple-error-correcting extended Golay code interleaved to

* Reference 3 indicates 548 completed calls. However, Ref. 6 indicates 503 completed calls of which 136 were error-free and 367 contained errors. The data available on magnetic tape and used in this study are consistent with the number of calls in Ref. 6 with the exception that one call was uninterpretable. Therefore, we shall use the calls from Ref. 6 with the exception of the aforementioned call leaving our sample to be of 502 calls of which 136 were error-free. (Courtesy of Messrs. F. X. Brophy and M. M. Buchner, Jr.)

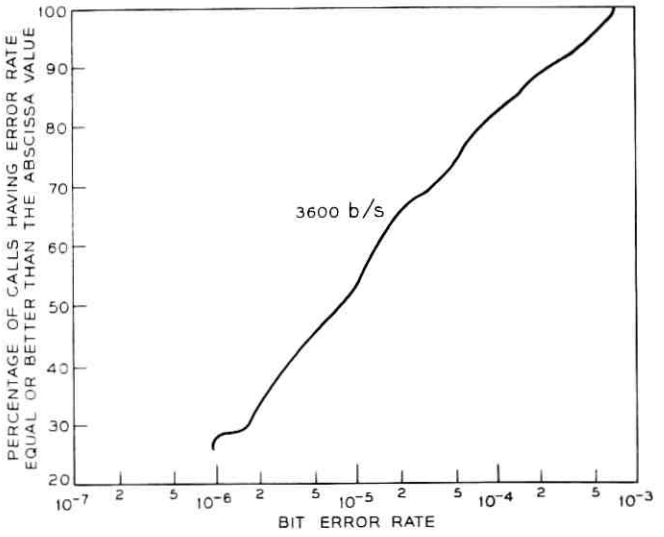

Fig. 6—Raw data statistics for multilevel Vestigial-Sideband (VSB) modem—with respect to bit error rate. Total number of calls = 85.

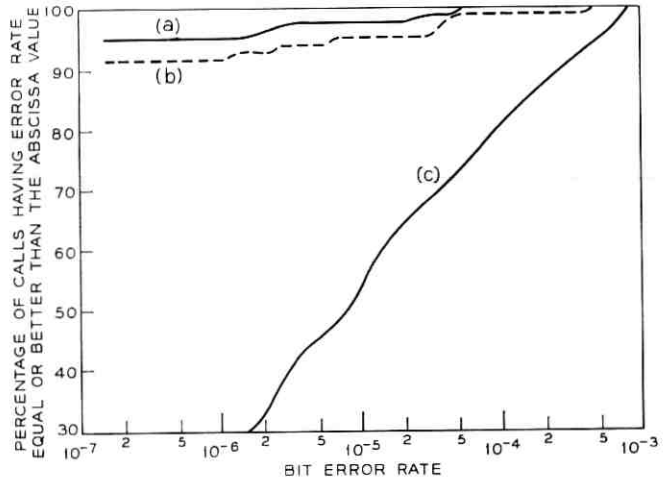

Fig. 7—Comparison of rate 1/2 codes. (a) (24, 12, 8, 1, 330) burst-trapping code. Using (24, 12) Golay code corrects single random error and burst up to 7920 bits. Storage = 4214 bits. (b) Interleaved (24, 12) extended Golay code corrects three errors. Interleaving degree = 175. Corrects bursts up to 525 bits. Storage = 4200. (c) VSB raw data.

degree 175 and a burst-trapping code based on the same Golay code but with single-error-correction only. As shown in the figure, their storage requirements are about the same; yet the (24, 12, 8, 1, 330) burst-trapping code out-performs the interleaved Golay code at a significantly lower cost (single-error correction vs. triple-error correction).

Figure 8 compares the performance of two rate $\frac{2}{3}$ codes: a (57, 38) triple-error-correcting shortened BCH code interleaved to degree 75

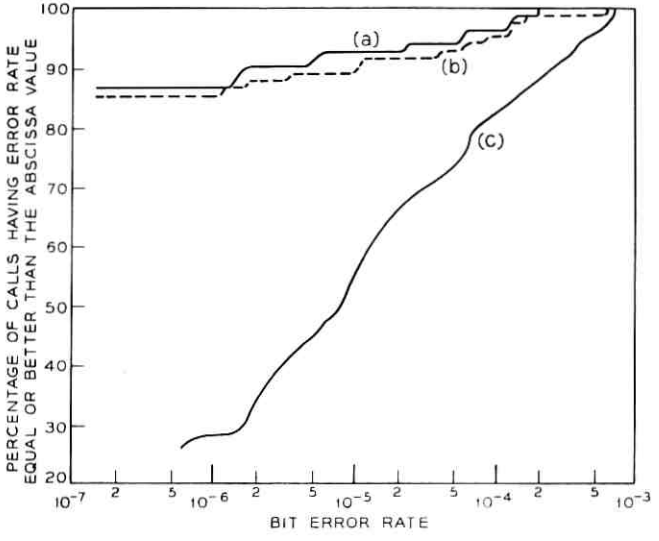

Fig. 8—Comparison of two rate 2/3 codes. (a) (57, 38, 8, 2, 50) burst-trapping code. Using (57, 38) BCH code corrects 2 random errors and bursts up to 2850 bits. Storage = 3957 bits. (b) Interleaved (57, 38) BCH code corrects three errors and bursts of 275 bits. Storage = 4275 bits. Interleaving degree = 75. (c) VSB raw data.

and a (57, 38, 8, 2, 50) burst-trapping code. Figure 9 also compares two rate-$\frac{2}{3}$codes: an interleaved (degree 25) (255,170) compound code* that corrects seven random errors and bursts of 1000 bits (after interleaving) and a (126, 84, 14, 6, 25) burst-trapping code. It is seen, that the burst-trapping code outperforms the compound code at smaller storage requirement and lower logic cost (six error vs. seven error correcting). A more striking result is shown in Fig. 10, where the performance of the (255, 170) compound code is compared with a (39, 26, 6, 1, 117) burst-trapping code, which performs better than the compound code; yet only single-error-correction is required (vs. seven error

* Taken from page 137 Table 1 of Ref. 7.

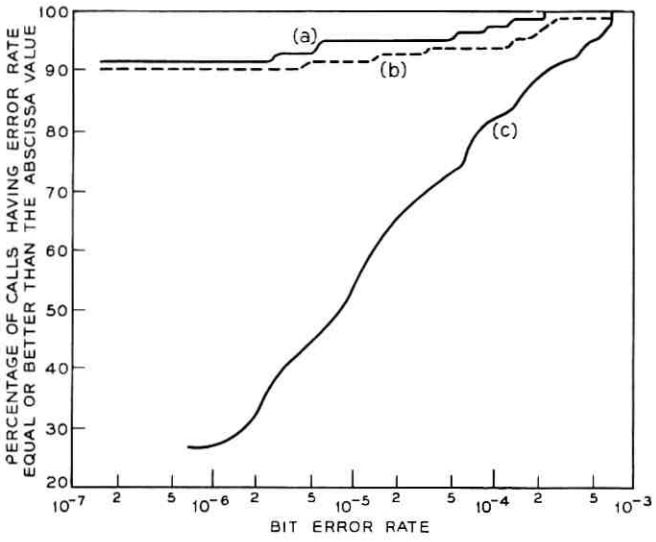

Fig. 9—(255, 170) compound code vs. (126, 84, 14, 6, 25) burst-trapping code. (a) (126, 84, 14, 6, 25) burst-trapping code using (126, 84) BCH code corrects 6 random errors and bursts up to 3150 bits. Storage required = 4376 bits. (b) Interleaved (255, 170) compound code that corrects 7 random errors and 1000-bit burst errors with interleaving degree 25. Storage required = 6375 bits. (c) VSB raw data.

correction required for the compound code). Note that the compound code chosen is a very powerful one. The comparison simply shows that this type of code might not be suitable for use on telephone channels.

Figure 11 shows the effect of the trade-off between random-error-correction and burst-error-correction for a typical burst-trapping code. In this case, a (57, 38) BCH code was used to correct 0, 1, 2 and 3 errors with correspondingly decreasing burst-error-detecting capability and consequently lower burst-correcting capability.

The (57, 38, 8, 0, 50) is simply a burst-error-correcting code. Its performance reflects the fact that telephone channels do not produce burst errors only. The (57, 38, 8, 3, 50) code is essentially a random-error-correcting code. Such a code, as expected, does not do well for telephone channels either. The (57, 38, 8, 1, 50) single-error-correcting and the (57, 38, 8, 2, 50) double-error-correcting burst-trapping codes perform better. This seems to confirm the assertion that telephone channels can be characterized as a type of compound channel.

Figures 12 through 16 show the performance of various burst-trapping codes on AGN and TW data. It is seen that more than 93 percent of

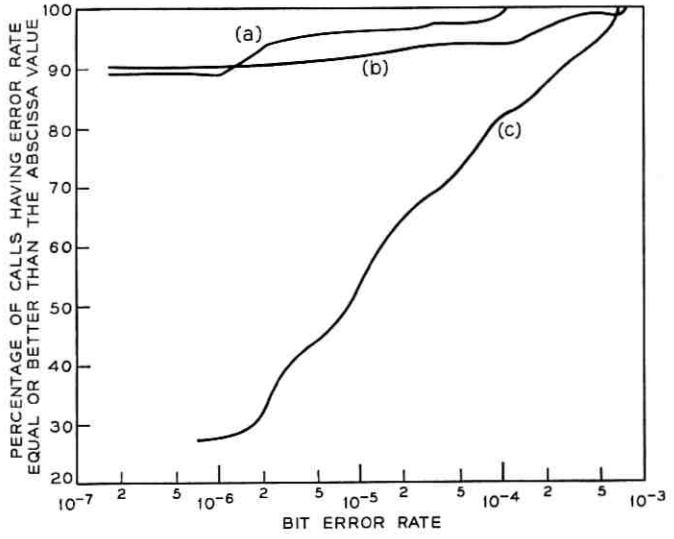

Fig. 10—(255, 170) compound code vs. (39, 26, 6, 1, 117) burst-trapping code. (a) (39, 26, 6, 1, 117) burst-trapping code which corrects single error and bursts up to 4563 bits. Storage required = 6357 bits. (b) Interleaved (255, 170) compound code which corrects 7 random errors and 1000-bit burst errors with interleaving degree 25. Storage required = 6375 bits. (c) VSB raw data.

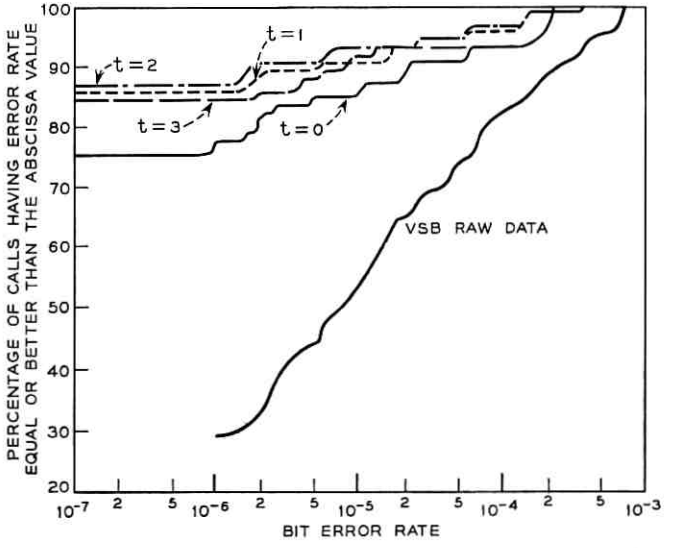

Fig. 11—Effect of trade off on VSB channels. Burst-trapping code using (57, 38) code with different mix of random and burst-error-correcting capability. Interleaving degree L = 50. Storage = 3957 bits.

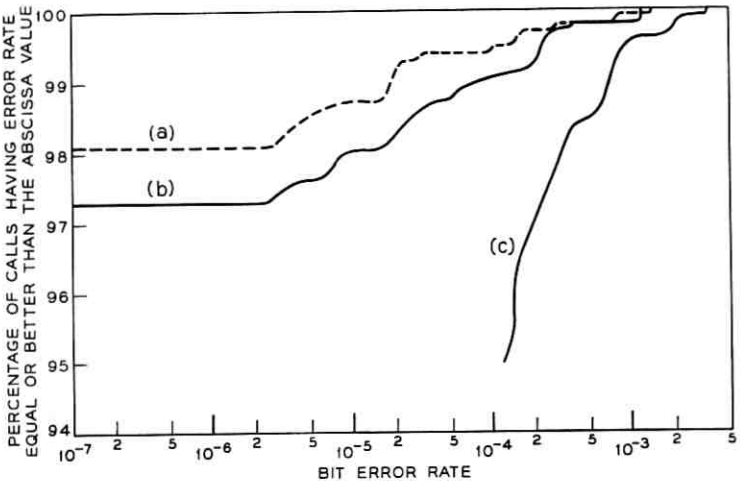

Fig. 12—Performance of two burst-trapping codes over AGN data. (a) (57, 38, 8, 2, 50) burst-trapping code corrects burst up to 2650 bits. Storage required = 3957 bits. (b) (57, 38, 8, 2, 26) burst-trapping code corrects bursts up to 1482 bits. Storage required = 2085 bits. (c) AGN raw data.

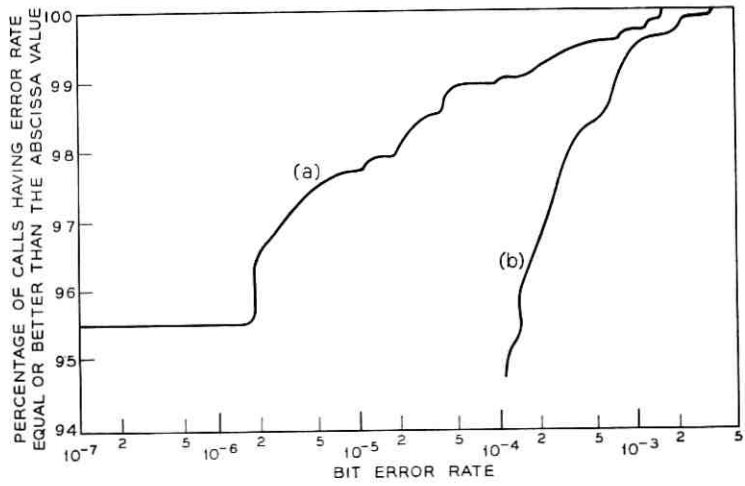

Fig. 13—Performance of (30, 20, 5, 1, 50) burst-trapping code. (a) (30, 20, 5, 1, 50) burst-trapping code corrects single error and bursts up to 1500 bits. Storage required = 2130 bits. (b) AGN raw data.

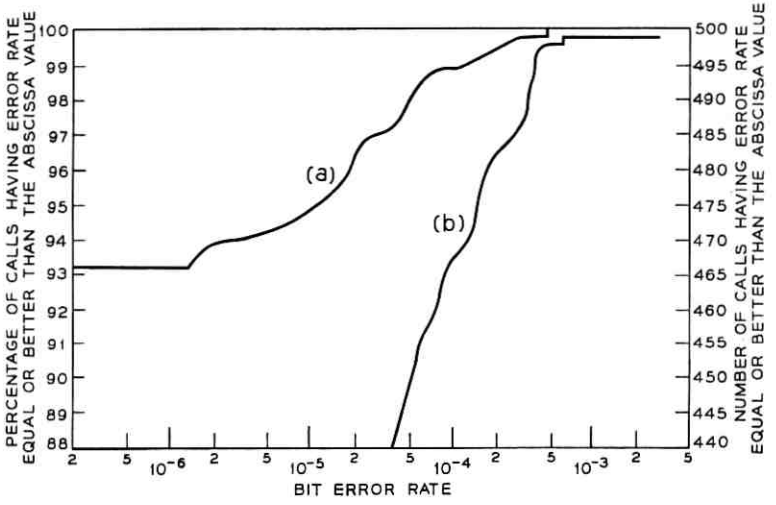

Fig. 14—Performance of (57, 38, 8, 2, 26) burst-trapping code over TW data. (a) (57, 38, 8, 2, 26) burst-trapping code corrects double errors and bursts up to 1482 bits. Storage required = 2085 bits. (b) TW raw data.

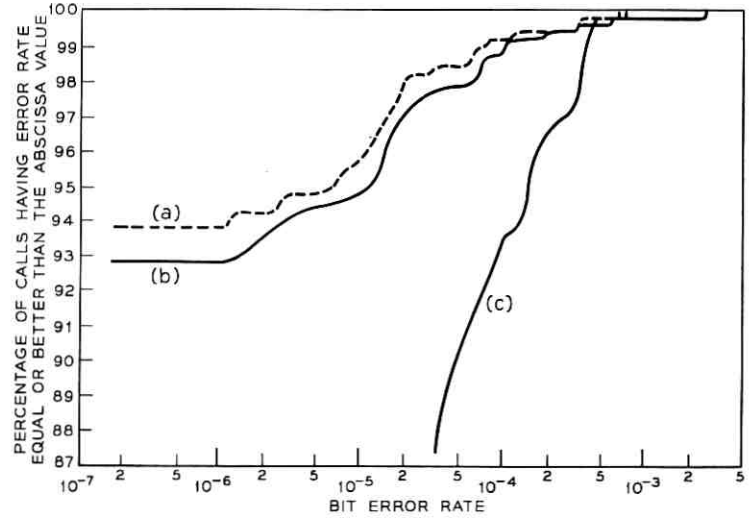

Fig. 15—Performance of two burst-trapping codes over TW data. (a) (39, 26, 6, 1, 80) burst-trapping code corrects burst up to 3120 bits. Storage required = 4379 bits. (b) (39, 26, 6, 1, 40) burst-trapping code corrects burst up to 1560 bits. Storage required = 2199 bits. (c) TW raw data.

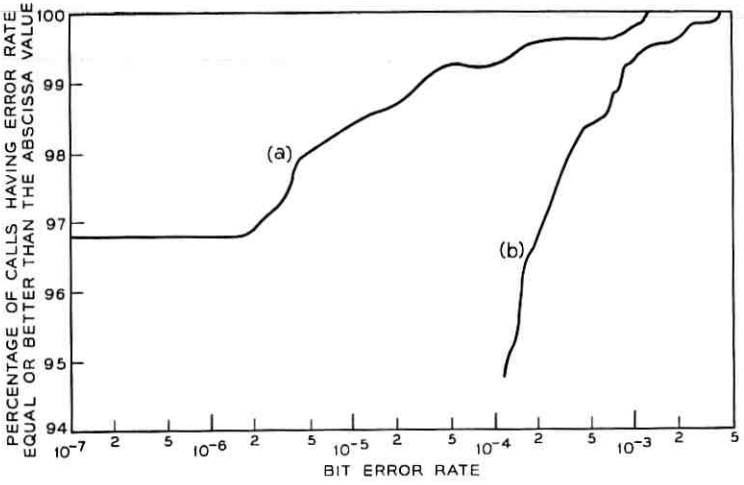

Fig. 16—Performance of (39, 26, 6, 1, 80) burst-trapping code. (a) (39, 26, 6, 1, 80) burst-trapping code corrects single error and bursts up to 3120 bits. Storage required = 4359 bits. (b) AGN raw data.

calls will be error-free if any of these codes is used for error control. All can be implemented at very modest cost.

Finally, we compare the performance of a (24, 20) convolutional single-error-correcting code interleaved to degree 127 with a burst-trapping code. The interleaved (24, 20) code is planned to be used in an optional error control unit for the 203 data set.[8,9] The performance of the (24, 20) code has been simulated by W. K. Pehlert with VSB data.[10]

Figure 17 curve (a) shows the performance of a (90, 75, 6, 1, 8) burst-trapping code with the same data; this code requires about the same storage* and has the same rate but performs better than (24, 20) code. Figure 17 curve (c) shows a more contrasting comparison. The (90, 75, 6, 1, 6) burst-trapping code requires only three-quarters as much storage yet still performs about the same as (24, 20) code. Before one attempts to draw any conclusion, however, it must be emphasized that the result is based on a relatively small sample size; hence wide variations are expected.

---

* We assume the (24, 20) code uses minimum storage, that is, 3048 bits although the actual implementation uses about 3600 bits of storage in order to simplify decoding logic.

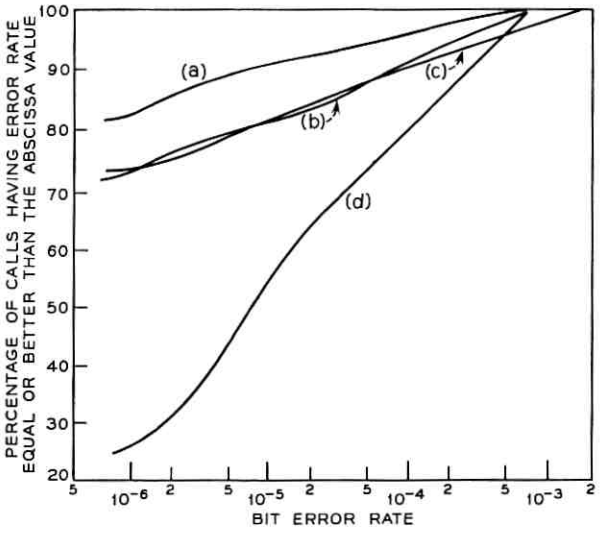

Fig. 17—Comparison of rate 5/6 error-correcting codes. (a) (90, 75, 6, 1, 8) burst-trapping code corrects burst up to 720 bits. Storage required = 3000 bits. (b) (24, 20) single error correcting code interleaved to degree 127. Corrects bursts up to 127 bits. Storage required = 3000 bits. (c) (90, 75, 6, 1, 6) burst-trapping code corrects bursts up to 540 bits. Storage required = 2250 bits. (d) VSB raw data.

IV. CONCLUSION

We have shown, through computer simulation, the performance of some burst-trapping codes, and have compared such codes with other known codes using telephone channel error statistics. It seems that several conclusions can be drawn, based on the available data.

(*i*) There are always a few percent of the calls that are so bad that it is difficult to improve them through forward error-control.

(*ii*) The performance of burst-trapping codes compares favorably with interleaved codes.

(*iii*) For a given level of performance, burst-trapping decoders are generally simpler to implement than decoders for other schemes that have been proposed for telephone channels.

V. ACKNOWLEDGMENTS

Thanks are due to H. O. Burton and E. R. Kretzmer for their valuable comments. W. K. Pehlert provided the simulated (24, 20) code performance data. The brief description of burst-trapping code is taken from a private memorandum co-authored by D. D. Sullivan and myself.

REFERENCES

1. Tong, S. Y., "Burst-Trapping Techniques for a Compound Channel," IEEE Trans. on Information Theory, *IT-15*, No. 6 (November 1969), pp. 710–715.
2. Alexander, A. A., Gryb, R. M., Nast, D. W., "Capabilities of the Telephone Network for Data Transmission," B.S.T.J., *39*, No. 3. (May 1960), pp. 431–476.
3. Townsend, R. E., and Watts, R. N., "Effectiveness of Error Control in Data Communication over the Switched Telephone Network," B.S.T.J., *43*, No. 6 (November 1964), pp. 2611–2638.
4. Farrow, C. W., and Holzman, L. N., "Nationwide Field Trial Performance of a Multilevel Vestigial-Sideband Data Terminal for Switched-Network Voice Channels," 1968 IEEE International Conference on Communications, Conference Record 68C20-COM (June 1968), pp. 782–787.
5. Pehlert, Jr., W. K. "Analysis of a Burst-Trapping Error Correction Procedure," B.S.T.J., this issue, pp. 493–519.
6. Townsend, R. L., unpublished work.
7. Hsu, H. T., Kasami, T., Chien, R. T., "Error-Correcting Codes for a Compound Channel," IEEE Trans. on Information Theory, *IT-14*, No. 1 (January 1968), pp. 135–139.
8. Mecklenburg, P., unpublished work.
9. Kretzmer, E. R., "Telephoning Data Faster," Bell Laboratories Record, *47*, No. 7 (August 1969), pp. 239–243.
10. Pehlert, Jr., W. K., unpublished work.

Analysis of a Burst-Trapping Error Correction Procedure

By W. K. PEHLERT, JR.

(Manuscript received November 6, 1969)

This paper presents an analysis technique for determining upper and lower bounds on the performance of a burst-trapping error control procedure. The analysis is valid for random, burst, or compound channels provided that a block interleaving degree $\ell \geqq 1$ can be found for the channel such that error patterns in blocks spaced ℓ blocks apart occur approximately independently. Good agreement is achieved between the theoretical performance of codes on telephone channels and the performance obtained by computer simulation.

I. INTRODUCTION

A burst-trapping error correction procedure for error control on compound channels such as the telephone channel has been described by S. Y. Tong.[1] An evaluation of the burst-trapping procedure by computer simulation of its performance on recorded telephone channel error data is presented in the companion paper.[2] An analysis technique for determining the performance of the burst-trapping procedure is presented here. The analysis technique permits determination of upper and lower bounds on the probability of block error. It is valid for random, burst, or compound channels provided that a block interleaving degree $\ell \geqq 1$ can be found for the channel such that error patterns in blocks spaced ℓ blocks apart occur (approximately) independently.

Expressions for upper and lower bounds on the probability of block error for codes of rate $\frac{1}{2}$ and $\frac{2}{3}$ are given in Table I. For higher rate codes, numerical determination of the stationary probabilities which yield the bounds seems preferable to determination of expressions for the bounds. The performance of a rate $\frac{2}{3}$ code, the (39, 26) shortened BCH code, has been computed using the expressions for probability of block error of Table I for two sets of recorded telephone channel error data. For both sets of data the computed performance agrees well with the performance obtained by computer simulation.

TABLE I—BOUNDS ON BLOCK ERROR PROBABILITY FOR RATE 1/2 AND RATE 2/3 CODES

RATE $\frac{1}{2}$ Codes

$$P_{eg} = \frac{\pi_1}{p_0 + p_c}\{p_d[1 - (p_0 + p_w)] + (K + p_u + p_w)\},$$

where $$\pi_1 = \frac{p_0 + p_c}{1 + p_d}.$$

$$P_{eu1} = \frac{\rho_1}{p_0 + p_c}\left\{p_d[1 - (p_0 + p_w)] + (K + p_u + p_w)\left(\frac{1 + p_0}{p_0^2}\right)\right\},$$

where $$\rho_1 = \frac{p_0 + p_c}{1 + p_d + \frac{1 + p_0}{p_0^2}(K + p_u + p_w)}.$$

$$P_{eu2} = P_{eu1}.$$

$$P_{eL} = \frac{\rho_1}{p_0 + p_c}\{p_d[1 - (p_0 + p_w)] + (K + p_u + p_w)\},$$

where $$K = p_d\{1 - [p_0 + \alpha(p_c + p_u + p_d)]\}.$$

RATE $\frac{2}{3}$ Codes, $t = 1$, $d_m \geqq 4$

$$P_{eg} = \frac{\pi_1}{p_0 + p_c}\{p_d[1 - (p_0 + p_w)^2] + (2K + p_u + p_w)\},$$

where $$\pi_1 = \frac{p_0 + p_c}{1 + 2p_d}.$$

$$P_{eu1} = \frac{\rho_1}{p_0 + p_c} \cdot \left\{p_d[1 - (p_0 + p_w)^2] + (2K + p_u + p_w) + \frac{D(1 - 2p_0^5 + p_0^6)}{p_0^5(1 - p_0)}\right\},$$

where $$\rho_1 = \frac{p_0 + p_c}{1 + 2p_d + \frac{D(1 - p_0^5)}{p_0^5(1 - p_0)}}.$$

$$P_{eu2} = \frac{\rho_1}{p_0 + \rho_c} \cdot \left\{p_d[1 - (p_0 + p_w)^2] + (2K + p_u + p_w) + \frac{D(1 - 4p_0^5 + 3p_0^6)}{p_0^5(1 - p_0)}\right\}$$

where $$s_1 = p_1.$$

$$P_{eL} = \frac{\rho_1}{p_0 + p_c}\{p_d[1 - (p_0 + p_w)^2] + (2K + p_u + p_w)\},$$

where $$D = p_u + p_w + p_d\{1 - [p_0 + \alpha(p_c + p_u + p_d)]^2\}.$$

II. ENCODING AND BURST-TRAPPING DECODING PROCEDURES

The encoding procedure and burst-trapping decoding technique have been described in detail elsewhere.[1] The code is a rate $(b-1)/b$ recurrent code[3] whose parity check matrix, A, is constructed from the parity check matrix, H, of an (n, k) linear systematic block code [where $k/n = (b-1)/b$] and the $(n-k) \times (n-k)$ identity matrix I. The truncated parity check matrix, A_N, for rate $\frac{2}{3}$ codes is given in Fig. 1. The constraint length of the code is $N = [(b-1)\ell + 1]n$ where $\ell \geqq 1$ is a block interleaving constant.

Although encoding is specified by the A matrix, it is useful to interpret encoding as the interleaved encoding of ℓ subcodes in the following way. Blocks $0, \ell, 2\ell, 3\ell, \cdots$ form the first subcode. The k-tuple of information bits, $I_{i\ell}$, of the $[i\ell]$th block $(i = 0, 1, 2, \cdots)$ is encoded into an n-tuple $M_{i\ell}$ which is the concatenation of $I_{i\ell}$ and a parity $(n-k)$-tuple $Q_{i\ell}$:

$$M_{i\ell} = I_{i\ell} \,||\, Q_{i\ell} . \tag{1}$$

$I_{i\ell}$ can be represented as the concatenation of $(b-1)$ equal length segments:

$$I_{i\ell} = I^1_{i\ell} \,||\, I^2_{i\ell} \,||\, \cdots \,||\, I^{b-1}_{i\ell}. \tag{2}$$

The parity $(n-k)$-tuple $Q_{i\ell}$ is

$$Q_{i\ell} = P_{i\ell} + I^1_{(i-1)\ell} + I^2_{(i-2)\ell} + \cdots + I^{b-1}_{(i-b+1)\ell} \tag{3}$$

where $P_{i\ell}$ is the parity $(n-k)$-tuple obtained by encoding $I_{i\ell}$ with the block code parity check matrix H. Thus each encoded subcode block is a block code word whose parity portion is modified by the addition of an information segment from each of the previous $(b-1)$ subcode blocks. Further the jth information segment of the $[i\ell]$th block is added to the information portion of the $[(i+j)\ell]$th block $(j = 1, 2, \cdots, b-1)$.

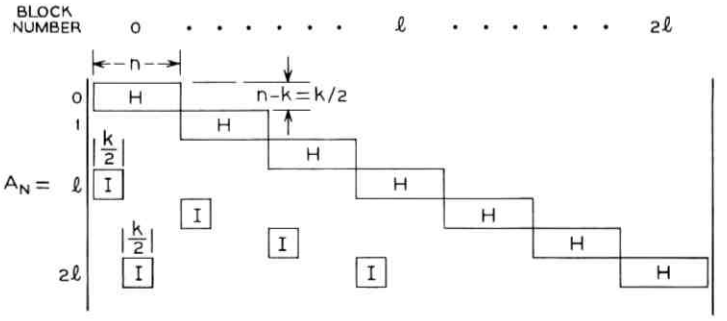

Fig. 1—A_N matrix of a rate 2/3 code.

A given block of a subcode is decoded by the burst-trapping procedure in one of three ways. Successive blocks of a subcode (blocks $0, \ell, 2\ell, \cdots$) are decoded by Random Error Decoding (RED) as long as the decoder decides that t or fewer errors occur in each block. When the decoder decides that more than t errors occur in a block, for example block $[i\ell]$, then that block is decoded by Burst-Trapping Decoding (BTD). The next $(b-1)$ subcode blocks {blocks $[(i+1)\ell]$, $[(i+2)\ell]$, $\cdots$, $[(i+b-1)\ell]$} are decoded by Blind Faith Decoding (BFD). Detailed descriptions of RED, BTD, and BFD are given below. Successive subcode blocks {blocks $[(i+b)\ell]$, $[(i+b+1)\ell]$, $\cdots$} are decoded by RED until the decoder again decides that a block has more than t errors.

Let $M_{i\ell}^*$, $I_{i\ell}^*$, $Q_{i\ell}^*$ be the received n-tuple at the $[i\ell]$th block, the received information k-tuple portion, and the received parity $(n-k)$-tuple portion respectively. Let $P_{i\ell}^*$ be the parity $(n-k)$-tuple obtained by encoding $I_{i\ell}^*$ with the block code parity check matrix H. Let $\bar{I}_{i\ell}$ be the decoded information k-tuple of the $[i\ell]$th block regardless of how the decoding is accomplished.

The primary method of decoding is RED. RED is attempted at the $[i\ell]$th block if none of blocks $[(i-b+1)\ell]$, $[(i-b+2)\ell]$, $\cdots$, $[(i-1)\ell]$ are decoded by BTD. RED is the removal of the effects of previous block information segments from the parity portion and the decoding of the block by bounded distance decoding of t or fewer errors. That is, to decode the $[i\ell]$th block the decoder computes

$$P'_{i\ell} = Q_{i\ell}^* + \bar{I}^1_{(i-1)\ell} + \bar{I}^2_{(i-2)\ell} + \cdots + \bar{I}^{b-1}_{(i-b+1)\ell} \tag{4}$$

and decodes $I_{i\ell}^* \,||\, P'_{i\ell}$ as a block code word. Following standard terminology for recurrent codes we will say that $\bar{I}^1_{(i-1)\ell}$, $\bar{I}^2_{(i-2)\ell}$, $\cdots$, $\bar{I}^{b-1}_{(i-b+1)\ell}$ are "fed back" to the $[i\ell]$th block.

The secondary method of decoding is BTD. BTD is effected when a RED attempt indicates that the block code word is detected in error but cannot be corrected by bounded distance decoding. If this occurs in block $[i\ell]$ then blocks $[(i+1)\ell]$, $[(i+2)\ell]$, $\cdots$, $[(i+b-1)\ell]$ are necessarily decoded by BFD (to be described subsequently) and decoding of block $[i\ell]$ is delayed until block $[(i+b-1)\ell]$ has been decoded. The information segments of block $[i\ell]$ are obtained from the corresponding parity portion of blocks $[(i+1)\ell]$, $[(i+2)\ell]$, $\cdots$, $[(i+b-1)\ell]$ as follows

$$\bar{I}^1_{i\ell} = Q^*_{(i+1)\ell} + P^*_{(i+1)\ell} + \bar{I}^2_{(i-1)\ell} + \bar{I}^3_{(i-2)\ell} + \cdots + \bar{I}^{b-1}_{(i-b+2)\ell}\,; \tag{5}$$

$$\bar{I}^2_{i\ell} = Q^*_{(i+2)\ell} + P^*_{(i+2)\ell} + \bar{I}^1_{(i+1)\ell} + \bar{I}^3_{(i-1)\ell} + \cdots + \bar{I}^{b-1}_{(i-b+3)\ell}\,; \tag{6}$$

$$\bar{I}^{3}_{i\ell} = Q^{*}_{(i+3)\ell} + P^{*}_{(i+3)\ell} + \bar{I}^{1}_{(i+2)\ell} + \bar{I}^{2}_{(i+1)\ell} + \bar{I}^{4}_{(i-1)\ell} + \cdots + \bar{I}^{b-1}_{(i-b+4)\ell} ; \tag{7}$$

$$\bar{I}^{b-1}_{i\ell} = Q^{*}_{(i+b-1)\ell} + P^{*}_{(i+b-1)\ell} + \bar{I}^{1}_{(i+b-2)\ell} + \bar{I}^{2}_{(i+b-3)\ell} + \cdots + \bar{I}^{b-2}_{(i+1)\ell} . \tag{8}$$

In equation (6), for example, we will say that $(Q^{*}_{(i+2)\ell} + P^{*}_{(i+2)\ell})$ and $\bar{I}^{1}_{(i+1)\ell}$ are "fed forward" and $\bar{I}^{3}_{(i-1)\ell}, \cdots, \bar{I}^{b-1}_{(i-b+3)\ell}$ are "fed back" to the $[i\ell]$th block.

The third method of decoding is BFD. BFD is effected at the $[i\ell]$th block if one of blocks $[(i-b+1)\ell], [(i-b+2)\ell], \cdots, [(i-1)\ell]$ has been decoded by BTD. BFD of $[i\ell]$th block is the use of the received information k-tuple as the decoded information k-tuple. That is

$$\bar{I}_{i\ell} \equiv I^{*}_{i\ell} . \tag{9}$$

III. COMMUNICATION CHANNEL

We consider channels where each block word (binary n-tuple) is subjected to the component-wise modulo-two addition of an error pattern (binary n-tuple) during transmission. We define a partition of the set of 2^n possible error patterns as follows.

C_0—is the set of one element—the pattern with no errors.
C_w—is the set of channel error patterns which are identical to nonzero code words.
C_c—is the set of nonzero channel error patterns which are correctable by RED (bounded distance decoding of t or fewer errors).
C_u—is the set of channel error patterns which are both uncorrectable by RED and undetectable (but are not nonzero code words).
C_d—is the set of channel error patterns which are detectable (but not correctable by RED).

We consider channels where error patterns separated by ℓ or more blocks occur independently. On burst or compound channels, proper design of the burst-trapping procedure requires sufficient block interleaving that the requirement of independent error patterns is approximately met. The nth power[4] of the binary symmetric channel with any $\ell \geq 1$ is included in the class of channels under consideration.

Let p_0, p_w, p_c, p_u, p_d be the probability that the channel error pattern for a particular block is in set C_0, C_w, C_c, C_u, C_d respectively. Let α be the probability that the information bits of a received word are unaffected by the channel error pattern given that the channel error pattern is either correctable, detectable, or undetectable. For the class

of communication channels under consideration the probability that the error patterns in successive blocks of a subcode are in sets C_i and C_j is $p_i p_j$, $i, j \epsilon \{0, w, c, u, d\}$.

IV. ANALYSIS OF PERFORMANCE

Since each subcode is independently and identically decoded it suffices to analyze the decoding of one subcode. The decoding of successive blocks of a subcode can be described by a set of states and a set of transition probabilities between states which form a Markov Chain. The set of states is partitioned into a set of "normal" states and a set of "anomalous" states. Given the block code parameters, the sequence of states is determined by the error pattern sequence. The block code parameters which are required are d_m , the minimum distance of the block code, and t, the amount of bounded distance random-error-correction done in RED.

Before enumerating the states we give a general description of the two sets of states. In all following discussion we assume the decoding of a single subcode. A block is decoded in a normal state *only* if all the blocks containing information segments fed back to that block are correctly decoded. Thus a block decoded in a normal state can only be in error due to its own error pattern or due to errors which are fed forward. A block is decoded in an anomalous state if one or more of the blocks containing information segments to be fed back to that block are incorrectly decoded. Once a block is decoded in an anomalous state the decoder is affected by fed back errors in addition to the channel error pattern sequence. Successive blocks are assumed to be decoded in anomalous states until a run of V blocks with no channel errors occurs. V is termed the recovery space for a subcode. V is determined in terms of d_m and t (independent of details of the specific code) so that if no channel errors occur in a period exceeding $(V - 1)$ blocks, then no errors are fed back to subsequent blocks regardless of the previous channel history. The first block after a run of V blocks free of channel errors is decoded in a normal state. A block decoded in an anomalous state can be in error due to its own error pattern, due to errors which are fed forward, and/or errors which are fed back. Error propagation which is due to fed back errors is bounded and can occur only in anomalous states.

Each normal state is numbered by means of the following notation:

The first digit represents the method of decoding

1—Random Error Decoding (RED),
2—Burst-Trapping Decoding (BTD),
3, 4, $\cdots$, $(b + 1)$—Blind Faith Decoding (BFD).

States whose first digit is 1 or 2 have a two digit number. States whose first digit is j, $3 \leqq j \leqq (b + 1)$, have a j digit number. The last digit is 0(1) to designate that the block is correctly (incorrectly) decoded. Interior digits for blocks with $3 \leqq j \leqq (b + 1)$ digit numbers designate the decoding history of the $(j - 2)$ previous blocks. An interior digit is 0(1) to designate that its corresponding block is correctly (incorrectly) decoded. For rate $(b - 1)/b$ codes there are 2^{b+1} normal states. Normal state diagrams illustrating this notation are given in Figs. 2 and 3 for rate $\frac{1}{2}$ and $\frac{2}{3}$ codes respectively. Throughout this paper a rate $\frac{2}{3}$ code will be used in a running example. The analysis technique is easily used for any rate $(b - 1)/b$ code.

Since the error pattern sequence determines the state sequence the transition probabilities between normal states can be expressed in terms of p_0, p_w, p_e, p_u, p_d and α. Transition probabilities between normal states are given in Figs. 2 and 3 and Appendix A for rate $\frac{1}{2}$ and $\frac{2}{3}$ codes. For simplicity of notation in writing the one step transition probabilities, $p_{i,j}$, from state i to state j the normal states are renumbered as in Figs. 2 and 3.

The normal state diagrams represent the possible state transitions until an undetected error occurs (state 11) or a BTD and its associated $(b - 1)$ BFD's occur [states $(b + 1)00 \cdots 0$ to $(b + 1)11 \cdots 1$]. Transitions from state $(b + 1)00 \cdots 0$ or state $(b + 1)10 \cdots 0$ (states marked with ϕ in Figs. 2 and 3) are the same as those from state 10 since the

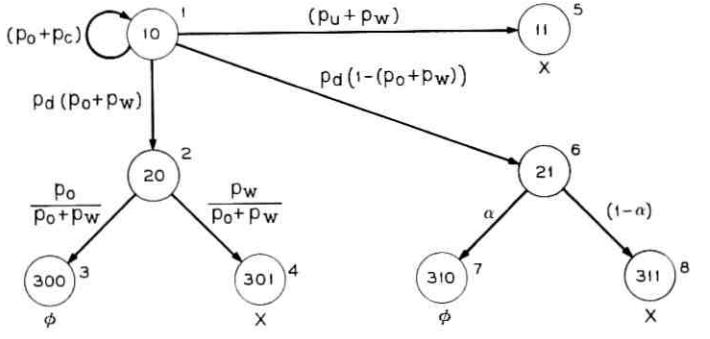

Fig. 2—Normal state diagram for rate 1/2 codes.

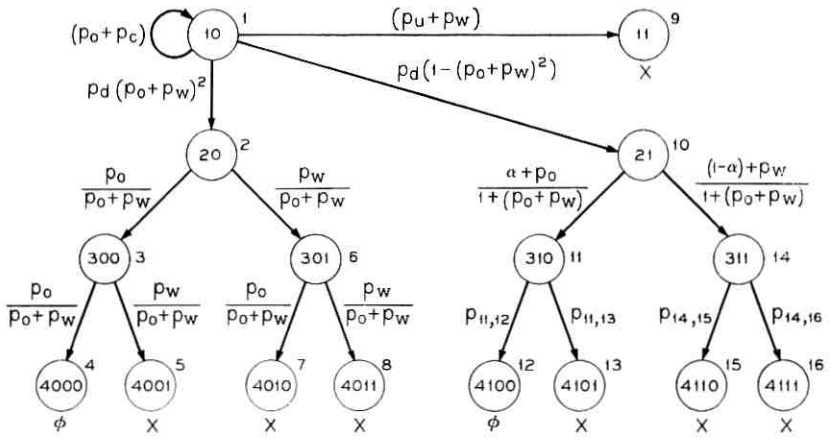

Fig. 3—Normal state diagram for rate 2/3 codes.

last $(b - 1)$ blocks containing information block segments to be fed back are correctly decoded. Transitions from other normal states (marked with X in Figs. 2 and 3) are to anomalous states since one or more of the last $(b - 1)$ blocks containing information block segments to be fed back are incorrectly decoded. The enumeration of the anomalous states is presented later.

V. AN OPTIMISTIC ESTIMATE OF THE PROBABILITY OF BLOCK ERROR

If we assume, for purposes of obtaining an optimistic estimate of performance, the presence of a Genie Decoder which corrects all fed back information, then transitions from normal states marked X (in Figs. 2 and 3) are the same as those from state 10 or the two states marked ϕ. Note that with the Genie Decoder blocks can still be incorrectly decoded and incorrect information can be fed forward but only correct information can be fed back. The assumption of a Genie Decoder in effect eliminates error propagation (which arises from erroneous feedback) and the only possible states are normal states. The entire transition probability matrix $[p_{i,j}]$ is then known from the normal state diagram (for example, Figs. 2 and 3) where $p_{i,j}$ is the one step transition probability from renumbered state i to renumbered state j. The Markov Chain is regular and therefore the stationary probabilities exist.[5] The stationary probability π_i of being in renumbered state i, $i = 1, 2, \cdots, 2^{b+1}$, can be obtained from

$$\pi_i = \sum_{j=1}^{2^{b+1}} \pi_j p_{j,i} \tag{10}$$

and

$$\sum_{i=1}^{2^{b+1}} \pi_i = 1. \tag{11}$$

The probability of block error with a Genie Decoder, P_{eg}, is the probability of being in a normal state whose identifying number has a last digit of 1. For rate $\frac{2}{3}$ codes,

$$P_{eg} = \pi_5 + \pi_6 + \pi_8 + \pi_9 + \pi_{10} + \pi_{13} + \pi_{14} + \pi_{16}. \tag{12}$$

Expressions for P_{eg} for rate $\frac{1}{2}$ and $\frac{2}{3}$ codes are given in Table I. For higher rate codes numerical determination of the stationary probabilities which yield P_{eg} seems preferable to determination of an expression for P_{eg}.

5.1 *Upper Bound on the Probability of Block Error*

An upper bound on the probability of block error can be obtained by considering worst case error propagation. The set of anomalous states is used to represent the decoder when error propagation can occur. Assume that one or more of blocks $[(i - b + 2)\ell]$ to $[i\ell]$ is incorrectly decoded and that block $[i\ell]$ has channel errors but all succeeding blocks $[(i + 1)\ell]$, $[(i + 2)\ell]$, $\cdots$ have no channel errors. Error propagation is the effect that, although no channel errors occur beyond block $[i\ell]$, decoding errors in block $[i\ell]$ and/or previous blocks may, through feedback, cause decoding errors to occur in some succeeding blocks $[(i + 1)\ell]$, $[(i + 2)\ell]$, $\cdots$.

The amount of error propagation, a, is the number of blocks after the last block with channel errors that have decoding errors. The length of error propagation, λ, is the number of blocks after the last block with channel errors up to and including the last block with decoding errors. Upper bounds A and Λ on a and λ respectively are derived in Appendix B and given in Table II for codes with $d_m \geqq 2t + 2$. In Table II the notation $\lfloor x \rfloor$ means the greatest integer less than or equal to x.

Another required quantity, the recovery space, is the minimum number of blocks after the last block with channel errors that must be free of channel errors to guarantee that error propagation ceases and to guarantee that the decoder has completed any BTD decoding and associated BFD decodings resulting from error propagation. Specifically, the recovery space, V, is defined as the minimum number of consecutive blocks free of channel errors (blocks $[(i + 1)\ell]$, $[(i + 2)\ell]$, $\cdots$, $[(i + V)\ell]$ required to guarantee that the decoder will return to one of normal states $\{10, 11, 20, 21\}$ at block $[(i + V + 1)l]$ regardless of the channel error sequence prior to block $[(i + 1)l]$. The

TABLE II—RECOVERY SPACE AND BOUNDS ON THE AMOUNT AND LENGTH OF ERROR PROPAGATION FOR CODES WITH $d_m \geq 2t + 2$

$b = 2$	$\Lambda = 1$ $A = 1$ $V = 2$		
$b = 3, t = 1$	$\Lambda = 2$ $A = 2$ $V = 5$		
	$d_m > b$	$d_m \leqq b$	
$b \geqq 4, t = 1$	$\Lambda = 3b - 8$ $A = b$ $V = 4b - 7$	$\Lambda = 3b - 8$ $A = (b - 1) + \left\lfloor \frac{b - 4}{d_m - 2} + 1 \right\rfloor$ $V = 4b - 7$	
	$d_m > bt$	$d_m \leqq bt$	
$b \geqq 3, t \geqq 2$	$\Lambda = 3b - 6$ $A = b$ $V = 4b - 7$	$d_m \leqq 3t$ $\Lambda = (2b - 3) + \left\lfloor \frac{(b - 2)t - 2}{d_m - 2t} \right\rfloor$ $A = (b - 1) + \left\lfloor \frac{(b - 2)t - 2}{d_m - 2t} + 1 \right\rfloor$ $V = (3b - 4) + \left\lfloor \frac{(b - 2)t - 2}{d_m - 2t} \right\rfloor$	$d_m > 3t$ $\Lambda = 3b - 6$ $A = (b - 1) + \left\lfloor \frac{(b - 2)t - 2}{d_m - 2t} + 1 \right\rfloor$ $V = 4b - 7$

recovery space for codes with $d_m \geqq 2t + 2$ is derived in Appendix B and is given in Table II. Values for A, Λ, and V are presented in Table III for typical values of b, t, and d_m.

The decoder can be represented by $(V + 1)$ anomalous states, as in Fig. 4, when it is not in a normal state. State A_0 exists whenever channel errors occur in a block. States $A_1, A_2, \cdots, A_V$ represent successive blocks free of channel errors. In Fig. 4 state X represents any normal state marked X in Figs. 2 and 3 from which the transition from normal state to anomalous state occurs. A complete state diagram includes both normal and anomalous states. The transition probability matrix is implicitly given in Figs. 2(3) and 4 for rate $\frac{1}{2}(\frac{2}{3})$ codes. The Markov

Chain is regular and therefore the stationary probabilities exist.[5] Let ρ_i, $i = 1, 2, \cdots, 2^{b+1}$, $A_0, A_1, \cdots, A_V$ be the stationary probabilities of being in the respective states.

An upper bound on the probability of block error, P_{eu1}, is obtained by summing the stationary probabilities that the decoder is in a normal state whose last digit is 1 or in an anomalous state A_0 through A_{V-1}. If the decoder reaches state A_V then correct decodings are assured in states $A_{\Lambda+1}$ to A_V, but if the decoder returns to state A_0 after state $A_{\Lambda+j}$, $j = 1, 2, \cdots, (V - \Lambda - 1)$ correct decodings are not assured in states $A_{\Lambda+1}$ to $A_{\Lambda+j}$. A tighter bound which accounts for this difference will be obtained next. For rate $\frac{2}{3}$ codes with $t = 1$ and $d_m \geqq 4$

$$P_{eu1} = \rho_5 + \rho_6 + \rho_8 + \rho_9 + \rho_{10} + \rho_{13} + \rho_{14} + \rho_{16} + \rho_{A_0} + \rho_{A_1} + \rho_{A_2} + \rho_{A_3} + \rho_{A_4}. \tag{13}$$

Expressions for P_{eu1} for rate $\frac{1}{2}$ and $\frac{2}{3}$ codes are given in Table I.

A tighter upper bound, P_{eu2}, is obtained by using $2V$ anomalous states as in Fig. 5. State B_0 exists whenever channel errors occur. States $B_1, B_2, \cdots, B_{V-1}$ represent successive blocks free of channel errors when the total number of consecutive blocks free of channel errors is less than V. States $C_1, C_2, \cdots, C_V$ represent successive blocks free of channel errors when the total number of consecutive blocks

TABLE III—A, Λ, V FOR TYPICAL VALUES OF CODE PARAMETERS

CODE PARAMETERS	A	Λ	V
$b = 2$, $d_m \geq 2t + 2$	1	1	2
$b = 3$, $t = 1$, $d_m \geq 4$	2	2	5
$t = 2$, $d_m \geq 6$	3	3	5
$t = 3$, $d_m \geq 8$	3	3	5
$t = 4$, $d_m = 10$	4	4	6
$d_m \geq 11$	3	3	5
$b = 4$, $t = 1$, $d_m \geq 4$	4	4	9
$t = 2$, $d_m = 6$	5	6	9
$d_m \geq 7$	4	6	9
$t = 3$, $d_m = 8$	6	7	10
$d_m = 9$	5	6	9
$d_m = 10$	5	6	9
$d_m \geq 11$	4	6	9
$t = 4$, $d_m = 10$	7	8	11
$d_m = 11$	6	7	10
$d_m = 12$	5	6	9
$d_m = 13$	5	6	9
$d_m = 14$	5	6	9
$d_m \geq 15$	4	6	9

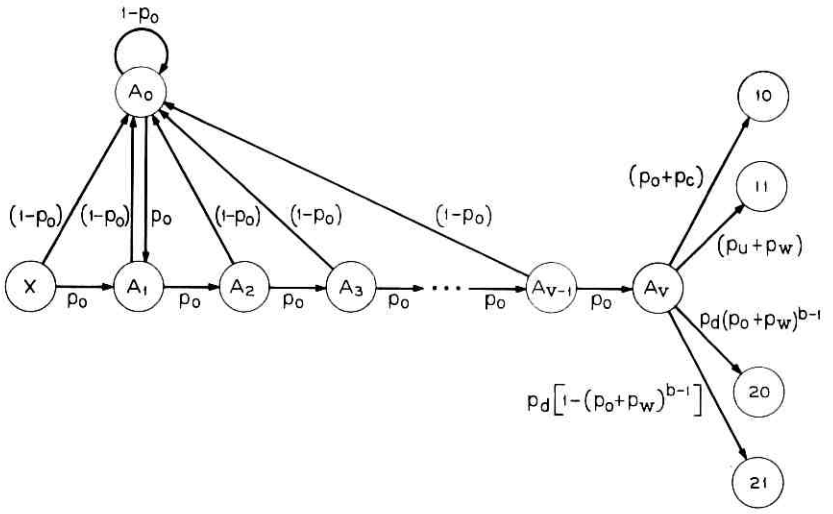

Fig. 4—$(V + 1)$ anomalous states for P_{eu1} bound on probability of block error.

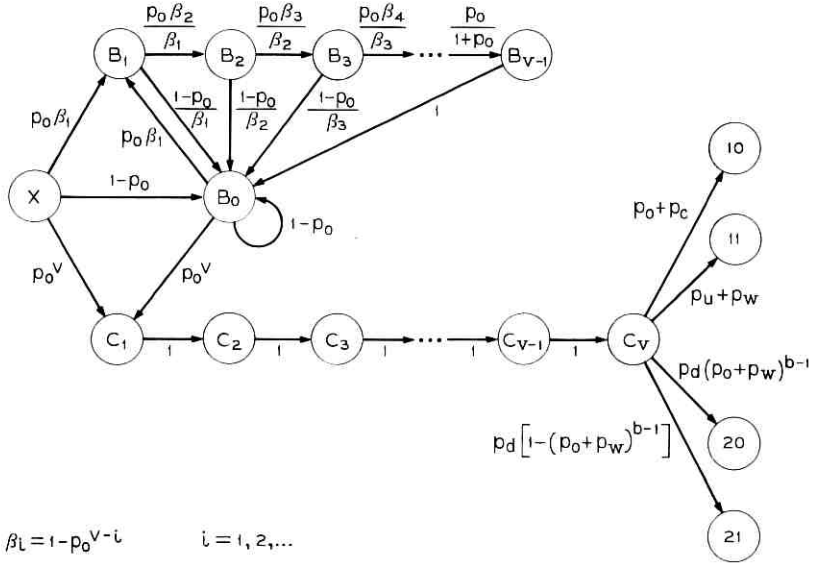

Fig. 5—$(2V)$ anomalous states for P_{eu2} bound on probability of block error.

free of channel errors is at least V. In Fig. 5 state X represents any normal state marked X in Figs. 2 and 3 from which the transition from normal state to anomalous state occurs. A complete state diagram includes both normal and anomalous states. The transition probability matrix is implicitly given in Figs. 2(3) and 5 for rate $\frac{1}{2}(\frac{2}{3})$ codes. The Markov Chain is regular and therefore the stationary probabilities exist.[5] Let s_i, $i = 1, 2, \cdots, 2^{b+1}, B_0, B_1, \cdots, B_{V-1}, C_1, C_2, \cdots, C_V$ be the stationary probabilities of being in the respective states.

P_{eu2} is obtained by summing the stationary probabilities that the decoder is in a normal state whose last digit is 1 or in an anomalous state B_0 through B_{V-1} or C_1 through C_A. For rate $\frac{2}{3}$ codes with $t = 1$ and $d_m \geqq 4$

$$P_{eu2} = s_5 + s_6 + s_8 + s_9 + s_{10} + s_{13} + s_{14} + s_{16} + s_{B_0} + s_{B_1} + s_{B_2} + s_{B_3} + s_{B_4} + s_{C_1} + s_{C_2} . \tag{14}$$

Expressions for P_{eu2} for rate $\frac{1}{2}$ and $\frac{2}{3}$ codes are given in Table I.

5.2 *Lower Bound on the Probability of Block Error*

A lower bound on the probability of block error, P_{eL}, is obtained by summing the stationary probabilities that the decoder is in a normal state whose last digit is 1. That is, it is assumed that no decoding errors are made when the decoder is in anomalous states. For rate $\frac{2}{3}$ codes with $t = 1$ and $d_m \geqq 4$

$$P_{eL} = \rho_5 + \rho_6 + \rho_8 + \rho_9 + \rho_{10} + \rho_{13} + \rho_{14} + \rho_{16} . \tag{15}$$

Expressions for P_{eL} are given in Table I.

VI. PERFORMANCE OF TWO CODES

The performance of a rate $\frac{1}{2}$ (18, 9) code of minimum distance $d_m = 6$ has been evaluated on the binary symmetric channel ($\ell = 1$). This code is obtained by extending the (17, 9) quadratic residue code of minimum distance $d_m = 5$ by one bit. Upper and lower bounds on the probability of block error for the (18, 9) code used in burst-trapping with $t = 1$ and $t = 2$ versus the binary symmetric channel transition probability, p, are given in Fig. 6. The probability of block error for maximum likelihood decoding of the (18, 9) code and the probability of block error for an uncoded 9 bit block are presented for comparison. It is interesting to note that the performance of the code is better with burst-trapping decoding ($t = 2$) than with maximum likelihood

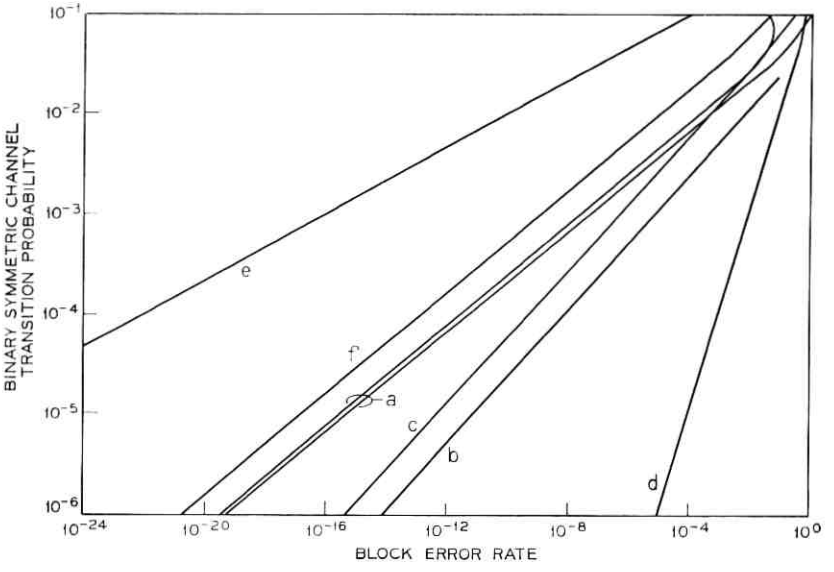

Fig. 6—Performance of (18, 9) code on binary symmetric channel. a. Upper and lower bounds for burst-trapping procedure, $t = 2$; b. Upper bound for burst-trapping procedure, $t = 1$; c. Maximum likelihood decoding; d. Uncoded 9-bit block; e. Decision feedback, $t = 0$; f. Decision feedback, $t = 2$.

decoding for values of p where the rate $\frac{1}{2}$ is much less than the channe capacity. Channel capacity is $\frac{1}{2}$ when $p = 0.11$. The probability of block error for two decision feedback systems using the (18, 9) code are also presented for comparison. In one system, ($t = 0$), repeat requests are made on all received n-tuples but code words. In the other system, ($t = 2$), single and double error corrections are made and repeat requests are made on all received n-tuples but code words or code words perturbed by one or two errors.

The performance of a rate $\frac{2}{3}$ (39, 26) shortened BCH code of minimum distance $d_m = 6$ with $t = 1$ has been computed on the basis of recorded telephone error data. One set of recorded telephone error data is the Vestigial-Sideband (VSB) data.[6,7] A selected set of 85 calls was used. Each call is an error sequence of about 3×10^6 bits recorded at 3600 b/s (4-level operation of the VSB modem). The 85 calls were divided into groups of calls of similar bit error rate as shown in Table IV and $P(m, 39)$ statistics[8] were determined for each group. $P(m, 39)$, $m = 1, 2, \cdots, 39$, is the probability that m errors occur in a block of 39 bits. Estimates of p_0, p_e, p_w, p_d, p_u, and α were obtained for each group by using

TABLE IV—GROUPING OF 85 VSB CALLS BY BIT ERROR RATE TO OBTAIN ESTIMATES OF p_0, p_e, p_w, p_d, p_u and α
[For (39, 26) Code with $d_m = 6$ and $t = 1$.]

Number of Calls in Group	Range of Bit Error Rate of Calls in Group	p_0	p_e	p_w	p_d	p_u	α
6	$4.30 \times 10^{-4} < p < 7.67 \times 10^{-4}$	0.982964	1.538×10^{-2}	5.407×10^{-8}	1.652×10^{-3}	2.173×10^{-6}	3.063×10^{-1}
6	$1.56 \times 10^{-4} < p < 3.83 \times 10^{-4}$	0.994869	4.418×10^{-3}	5.976×10^{-8}	7.106×10^{-4}	2.353×10^{-6}	2.899×10^{-1}
6	$7.01 \times 10^{-4} < p < 1.52 \times 10^{-4}$	0.996415	3.349×10^{-3}	7.652×10^{-9}	2.363×10^{-4}	3.103×10^{-7}	3.145×10^{-1}
6	$4.50 \times 10^{-5} < p < 6.81 \times 10^{-5}$	0.998643	1.078×10^{-3}	9.329×10^{-9}	2.785×10^{-4}	3.790×10^{-7}	2.757×10^{-1}
6	$2.20 \times 10^{-5} < p < 4.19 \times 10^{-5}$	0.999220	6.505×10^{-4}	4.221×10^{-9}	1.295×10^{-4}	1.646×10^{-7}	2.882×10^{-1}
6	$1.19 \times 10^{-5} < p < 1.79 \times 10^{-5}$	0.999604	3.170×10^{-4}	8.473×10^{-10}	7.863×10^{-5}	3.305×10^{-8}	2.844×10^{-1}
6	$7.86 \times 10^{-6} < p < 1.07 \times 10^{-5}$	0.999703	2.552×10^{-4}	5.065×10^{-10}	4.147×10^{-5}	1.975×10^{-8}	2.967×10^{-1}
6	$4.95 \times 10^{-6} < p < 7.85 \times 10^{-6}$	0.999842	1.138×10^{-4}	2.836×10^{-10}	4.413×10^{-5}	1.106×10^{-8}	2.623×10^{-1}
6	$1.91 \times 10^{-6} < p < 3.48 \times 10^{-6}$	0.999914	7.441×10^{-5}	0.0	1.191×10^{-5}	0.0	2.960×10^{-1}
7	$6.03 \times 10^{-7} < p < 1.87 \times 10^{-6}$	0.999957	2.990×10^{-5}	0.0	1.308×10^{-5}	0.0	2.607×10^{-1}
7	$p \sim 3.33 \times 10^{-7}$						
17	$p < 3.33 \times 10^{-7}$						

approximate code and coset weight spectra. A plot of the distribution of the percent of calls (quantized by the grouping of calls) with respect to raw (39 bit) block error rate and the upper and lower bounds on the distribution with respect to decoded block error rate is given in Fig. 7. The distribution of the percent of calls with respect to decoded block error rate as estimated by computer simulation[2] on the same 85 call sample is also given for comparison. For the comparison simulation a block interleaving degree $\ell = 117$ was used as this amount of interleaving attained approximate independence between successive blocks of the subcodes.

Another set of recorded telephone error data is the Alexander-Gryb-Nast (AGN) data.[9] AGN data consists of about 1000 calls recorded at data rates of 600 b/s and 1200 b/s on an FM data modem. These calls are from three classes of calls of approximately 3.6×10^5, 7.2×10^5, or 2.16×10^6 bits in length. The 294 calls with bit error rate greater than 10^{-5} were divided into groups as shown in Table V and estimates of p_0, p_c, p_w, p_d, p_u, and α were obtained as for the VSB data. A

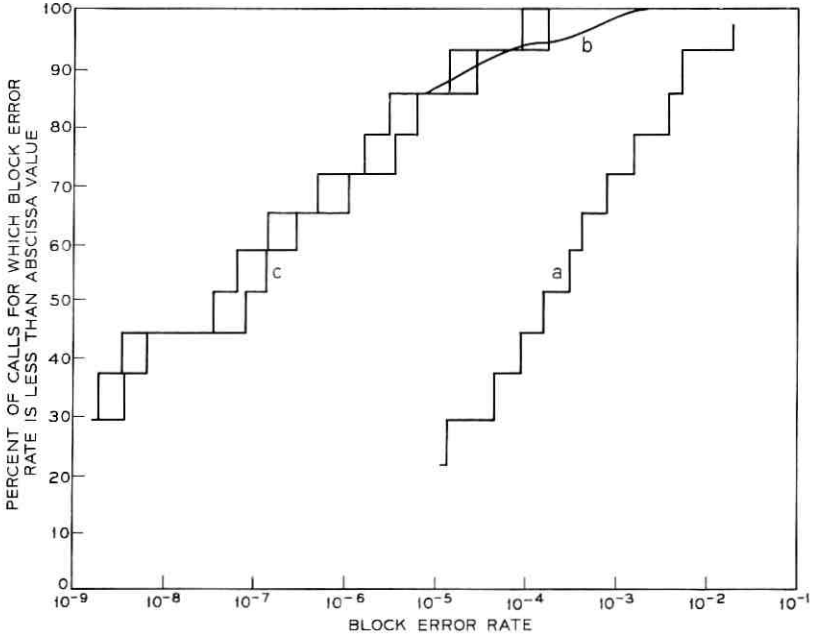

Fig. 7—Distribution of 85 call VSB sample with respect to block error rate. a. Uncoded 39 bit blocks; b. Simulation of (39, 26) code interleaved to degree 117; c. Upper and lower bounds for (39, 26) code.

plot of the distribution of the percent of calls (quantized by the grouping of calls) with respect to raw (39 bit) block error rate and the upper and lower bounds on the distribution with respect to decoded block error rate is given in Figs. 8 and 9. The performance as estimated by computer simulation[2] on the same call sample is also presented for comparison.

For both sets of data there is good agreement between the performance estimates obtained by the theory and simulation. Two advantages of the theoretical technique over the simulation technique are the ability to obtain the tail of the distribution and the ability to obtain the distribution from reduced data. This latter advantage is due to the fact that p_0 , p_c , p_w , p_d , p_u , and α can be approximately determined from reduced data such as $P(m, n)$ statistics.

VII. CONCLUSIONS

A technique for analyzing the performance of a burst-trapping error correction procedure has been described. The criterion of performance is the probability of block error. The analysis technique for burst-trapping procedures with block interleaving degree ℓ is valid on channels where error patterns in blocks separated by ℓ blocks are (approximately) independent. Thus the analysis technique is valid for random error channels or for properly designed burst-trapping procedures on burst or compound channels such as the telephone channel.

The performance of a rate $\frac{2}{3}$ code, the (39, 26) shortened BCH code, has been computed for two sets of recorded error data. For both sets of data the computed performance agrees with the performance obtained by computer simulation. An advantage of the theoretical technique over simulation is the ability to estimate performance on the basis of reduced data [$P(m, n)$ statistics] rather than on extensive error sequence data.

VIII. ACKNOWLEDGMENTS

The author acknowledges helpful discussions with H. O. Burton, D. D. Sullivan, and S. Y. Tong. E. J. Klieber wrote the computer programs required to obtain the performance estimates of the (39, 26) code.

APPENDIX A

Transition Probabilities for Normal State Diagrams

For simplicity the development of the one step transition probabilities $p_{i,j}$ from renumbered state i to renumbered state j is demonstrated for

TABLE V—GROUPING OF 294 AGN CALLS BY BIT ERROR RATE TO OBTAIN ESTIMATES OF p_0, p_c, p_w, p_d, p_u and α

[For (39, 26) Code with $d_m = 6$ and $t = 1$.]

Number of Calls in Group	Range of Bit Error Rate of Calls in Group	p_0	p_c	p_w	p_d	p_u	α
5	$1.306 \times 10^{-3} < p < 3.799 \times 10^{-3}$	0.959926	2.779×10^{-2}	3.328×10^{-7}	1.227×10^{-2}	1.318×10^{-5}	0.2512
10	$6.338 \times 10^{-4} < p < 9.444 \times 10^{-4}$	0.992275	3.186×10^{-3}	2.188×10^{-7}	4.530×10^{-3}	8.849×10^{-6}	0.1560
10	$2.667 \times 10^{-4} < p < 5.300 \times 10^{-4}$	0.990216	8.122×10^{-3}	1.851×10^{-8}	1.661×10^{-3}	7.356×10^{-7}	0.2901
10	$1.700 \times 10^{-4} < p < 2.662 \times 10^{-4}$	0.996270	2.725×10^{-3}	4.133×10^{-8}	1.003×10^{-3}	1.640×10^{-6}	0.2587
10	$1.335 \times 10^{-4} < p < 1.630 \times 10^{-4}$	0.997023	2.117×10^{-3}	1.720×10^{-8}	8.597×10^{-4}	7.081×10^{-7}	0.2528
10	$1.005 \times 10^{-4} < p < 1.278 \times 10^{-4}$	0.996567	2.855×10^{-3}	2.939×10^{-9}	5.777×10^{-4}	1.305×10^{-7}	0.2913
10	$7.964 \times 10^{-5} < p < 9.770 \times 10^{-5}$	0.997792	1.834×10^{-3}	9.263×10^{-9}	3.740×10^{-4}	3.816×10^{-7}	0.2859
10	$6.659 \times 10^{-5} < p < 7.691 \times 10^{-5}$	0.998481	1.251×10^{-3}	1.058×10^{-8}	2.677×10^{-4}	4.205×10^{-7}	0.2844
10	$6.111 \times 10^{-5} < p < 6.565 \times 10^{-5}$	0.998498	1.208×10^{-3}	6.632×10^{-9}	2.937×10^{-4}	2.727×10^{-7}	0.2789
10	$5.410 \times 10^{-5} < p < 6.110 \times 10^{-5}$	0.998618	1.028×10^{-3}	4.837×10^{-9}	3.537×10^{-4}	2.177×10^{-7}	0.2603
10	$4.447 \times 10^{-5} < p < 5.290 \times 10^{-5}$	0.998998	6.673×10^{-4}	5.683×10^{-9}	3.350×10^{-4}	2.376×10^{-7}	0.2415
10	$3.611 \times 10^{-5} < p < 4.446 \times 10^{-5}$	0.998900	8.475×10^{-4}	1.572×10^{-9}	2.524×10^{-4}	7.452×10^{-8}	0.2728
10	$3.240 \times 10^{-5} < p < 3.607 \times 10^{-5}$	0.999076	7.674×10^{-4}	2.129×10^{-9}	1.569×10^{-4}	9.580×10^{-8}	0.2860
10	$2.914 \times 10^{-5} < p < 3.117 \times 10^{-5}$	0.999087	7.702×10^{-4}	7.433×10^{-10}	1.431×10^{-4}	2.899×10^{-8}	0.2953
10	$2.779 \times 10^{-5} < p < 2.914 \times 10^{-5}$	0.999529	3.182×10^{-4}	4.958×10^{-9}	1.521×10^{-4}	2.033×10^{-7}	0.2408
10	$2.505 \times 10^{-5} < p < 2.778 \times 10^{-5}$	0.999377	4.590×10^{-4}	2.613×10^{-9}	1.640×10^{-4}	1.106×10^{-7}	0.2613
20	$2.223 \times 10^{-5} < p < 2.504 \times 10^{-5}$	0.999367	4.710×10^{-4}	1.319×10^{-9}	1.620×10^{-4}	5.776×10^{-8}	0.2657
20	$1.953 \times 10^{-5} < p < 2.223 \times 10^{-5}$	0.999462	4.277×10^{-4}	1.878×10^{-9}	1.107×10^{-4}	7.775×10^{-8}	0.2772
20	$1.714 \times 10^{-5} < p < 1.950 \times 10^{-5}$	0.999471	4.119×10^{-4}	3.444×10^{-10}	1.170×10^{-4}	1.756×10^{-8}	0.2768
20	$1.528 \times 10^{-5} < p < 1.671 \times 10^{-5}$	0.999706	1.628×10^{-4}	1.944×10^{-9}	1.309×10^{-4}	8.102×10^{-8}	0.2084
20	$1.340 \times 10^{-5} < p < 1.526 \times 10^{-5}$	0.999622	2.918×10^{-4}	6.556×10^{-10}	8.591×10^{-5}	2.819×10^{-8}	0.2722
20	$1.113 \times 10^{-5} < p < 1.340 \times 10^{-5}$	0.999660	2.571×10^{-4}	1.516×10^{-10}	8.320×10^{-5}	1.046×10^{-8}	0.2682
19	$1.017 \times 10^{-5} < p < 1.112 \times 10^{-5}$	0.999735	2.021×10^{-4}	1.175×10^{-9}	6.251×10^{-5}	4.758×10^{-8}	0.2687

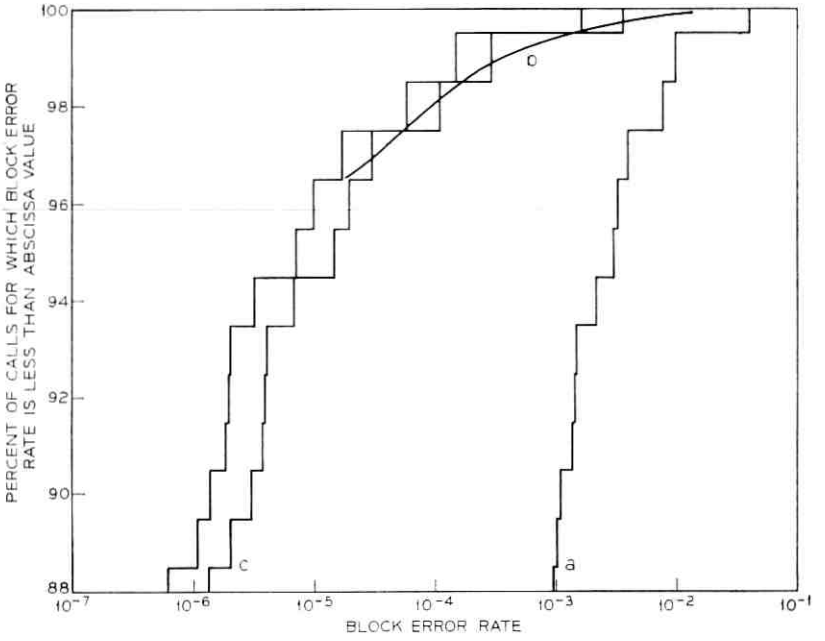

Fig. 8—Distribution of AGN call sample with respect to block error rate. a. Uncoded 39 bit blocks; 2. Simulation of (39, 26) code interleaved to degree 117; c. Upper and lower bounds for (39, 26) code.

rate $\frac{2}{3}$ codes (Fig. 3). The technique is easily generalized to rate $(b-1)/b$ codes, $b \geqq 2$. Obviously,

$$p_{1,1} = p_0 + p_e \ ; \tag{16}$$

$$p_{1,9} = p_u + p_w \ ; \tag{17}$$

$$p_{1,2} + p_{1,10} = p_d \ . \tag{18}$$

Let $p_{i,j}(b)$ be the b step transition probability from renumbered state i to renumbered state j. Due to the structure of the normal state diagram it is easily seen that,

$$p_{1,2} = p_{1,4}(3) + p_{1,5}(3) + p_{1,7}(3) + p_{1,8}(3); \tag{19}$$

$$p_{2,3} = (1 - p_{2,6}) = \frac{p_{1,4}(3) + p_{1,5}(3)}{p_{1,2}} \ ; \tag{20}$$

$$p_{3,4} = (1 - p_{3,5}) = \frac{p_{1,4}(3)}{p_{1,2}p_{2,3}} \ ; \tag{21}$$

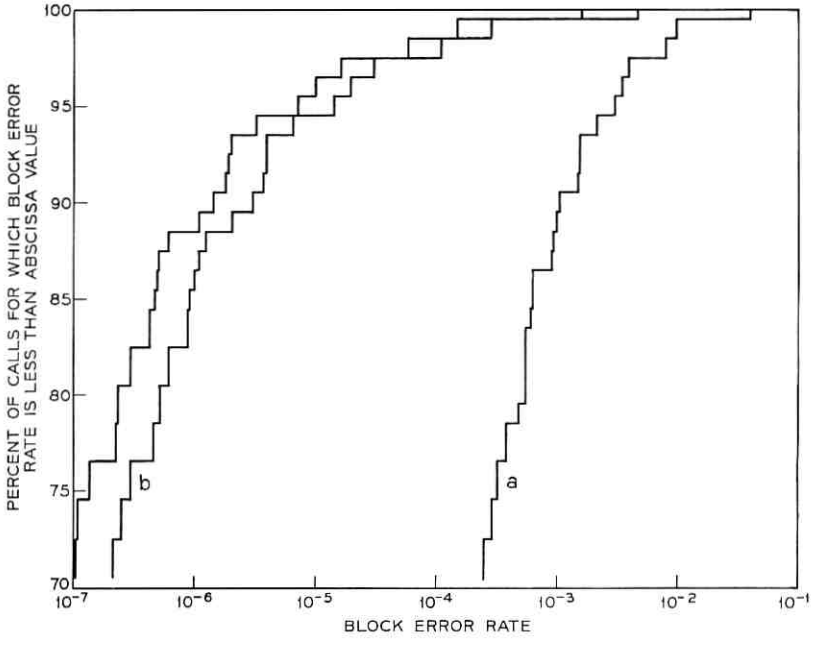

Fig. 9—Distribution of AGN call sample with respect to block error rate. a. Uncoded 39 bit block; b. Upper and lower bounds for (39, 26) code.

$$p_{6,7} = (1 - p_{6,8}) = \frac{p_{1,7}(3)}{p_{1,2}p_{2,6}}. \tag{22}$$

The three step transition probabilities $p_{1,4}(3)$, $p_{1,5}(3)$, $p_{1,7}(3)$, $p_{1,8}(3)$ can be computed by summing the probabilities of all combinations of three successive error patterns which cause transition from normal state 10 to normal states 4000, 4001, 4010, and 4011 respectively.

$$p_{1,4}(3) = p_d p_0^2 \ ; \tag{23}$$

$$p_{1,5}(3) = p_d p_0 p_w \ ; \tag{24}$$

$$p_{1,7}(3) = p_d p_w p_0 \ ; \tag{25}$$

$$p_{1,8}(3) = p_d p_w^2 \ . \tag{26}$$

Further,

$$p_{1,10} = p_{1,12}(3) + p_{1,13}(3) + p_{1,15}(3) + p_{1,16}(3); \tag{27}$$

$$p_{10,11} = (1 - p_{10,14}) = \frac{p_{1,12}(3) + p_{1,13}(3)}{p_{1,10}} ; \tag{28}$$

$$p_{11,12} = (1 - p_{11,13}) = \frac{p_{1,12}(3)}{p_{1,10}p_{10,11}} ; \tag{29}$$

$$p_{14,15} = (1 - p_{14,16}) = \frac{p_{1,15}(3)}{p_{1,10}p_{10,14}} . \tag{30}$$

The three step transition probabilities $p_{1,12}(3)$, $p_{1,13}(3)$, $p_{1,15}(3)$, $p_{1,16}(3)$ can be computed by summing the probabilities of all combinations of three successive error patterns which cause transition from normal state 10 to normal states 4100, 4101, 4110, 4111 respectively.

$$p_{1,12}(3) = p_d\{\alpha^2(p_e + p_u + p_d)^2 + 2p_0\alpha(p_e + p_u + p_d)\} ; \tag{31}$$

$$p_{1,13}(3) = p_d\{\alpha(1 - \alpha)(p_e + p_u + p_d)^2 + p_0(1 - \alpha)(p_e + p_u + p_d) + \alpha(p_e + p_u + p_d)p_w\} ; \tag{32}$$

$$p_{1,15}(3) = p_{1,13}(3) ; \tag{33}$$

$$p_{1,16}(3) = p_d\{(1 - \alpha)^2(p_e + p_u + p_d)^2 + 2p_w(1 - \alpha)(p_e + p_u + p_d)\} . \tag{34}$$

The transition probabilities for rate $\frac{1}{2}$ codes are given in Fig. 2. The transition probabilities for rate $\frac{2}{3}$ codes with the exception of

$$p_{11,12} = \frac{\alpha^2(p_e + p_u + p_d) + 2\alpha p_0}{\alpha + p_0} ; \tag{35}$$

$$p_{11,13} = \frac{(1 - \alpha)\alpha(p_e + p_u + p_d) + p_0(1 - \alpha) + \alpha p_w}{\alpha + p_0} ; \tag{36}$$

$$p_{14,15} = \frac{(1 - \alpha)\alpha(p_e + p_u + p_d) + p_0(1 - \alpha) + \alpha p_w}{(1 - \alpha) + p_w} ; \tag{37}$$

$$p_{14,16} = \frac{(1 - \alpha)^2(p_e + p_u + p_d) + 2(1 - \alpha)p_w}{(1 - \alpha) + p_w} ; \tag{38}$$

are given in Fig. 3.

APPENDIX B

Bounds on the Amount and Length of Error Propagation and Determination of the Recovery Space

We consider codes in which $d_m \geqq 2t + 2$. Let $0 \leqq e_i \leqq k$ be the maximum number of errors possible in the information part of the decoded word at block $[i\ell]$. The value of e_i depends on the method of decoding the block and the error pattern sequence. We will say that

$$f_i = \sum_{j=i-b+2}^{i} e_j \tag{39}$$

is the maximum number of errors "available" for feedback to blocks after block $[i\ell]$. As in the text, assume that one or more of blocks $[(i - b + 2)\ell]$ to $[i\ell]$ is incorrectly decoded and that block $[i\ell]$ has channel errors, but all succeeding blocks $[(i + 1)\ell]$, $[(i + 2)\ell]$, $\cdots$, have no channel errors. We consider three mutually exclusive and exhaustive cases. We use the fact that a block code of minimum distance d_m is simultaneously capable of correcting t errors and detecting $d \geqq t$ errors if $d_m = t + d + 1$.

B.1 *Case 1*

Assume that no error detections (BTD's) occur in blocks $[(i + 1)\ell]$, $[(i + 2)\ell]$, $\cdots$. Under this hypothesis error propagation cannot occur beyond block $[j\ell]$ if $f_j < d_m - t$. The maximum length of error propagation is then the smallest integer Λ_1 such that $f_{i+\Lambda_1} < d_m - t$. Since $f_i = (b - 1)k$, blocks $[(i + 1)\ell]$ to $[(i + b - 1)\ell]$ are subject to decoding error due to error propagation and therefore $f_{i+b-1} = (b - 1)t$. Each subsequent block, $[(i + b)\ell]$, $[(i + b + 1)\ell]$, $\cdots$, which is correctly (incorrectly) decoded removes t $(d_m - 2t)$ errors from the maximum number available for feedback. Therefore

$$\Lambda_1 = \begin{cases} (b - 1) + \left\lfloor \dfrac{(b - 2)t}{d_m - 2t} \right\rfloor, & \text{if } d_m - 2t \leqq t \\ (b - 1) + \left\lfloor \dfrac{bt - 2(d_m - 2t)}{t} \right\rfloor, & \text{if } d_m - 2t > t \end{cases} \tag{40}$$

where $\lfloor x \rfloor$ is the greatest integer less than or equal to x.

The maximum amount of error propagation is

$$A_1 = (b - 1) + \left\lfloor \frac{(b - 2)t}{d_m - 2t} \right\rfloor. \tag{41}$$

Blocks $[(i + \Lambda_1 + b)\ell]$, $[(i + \Lambda_1 + b + 1)\ell]$, $\cdots$ are correctly decoded by RED in normal state 10.

B.2 *Case 2*

Assume that an error detection (BTD) occurs in block $[(i + j)\ell]$, $1 \leqq j \leqq b - 1$. Under this hypothesis error propagation cannot occur

beyond block $[(i + j)\ell]$. The maximum length of error propagation is

$$\Lambda_2 = b - 1 \tag{42}$$

and the maximum amount of error propagation is

$$A_2 = b - 1. \tag{43}$$

Blocks $[(i + \Lambda_2 + b)\ell]$, $[(i + \Lambda_2 + b + 1)\ell]$, $\cdots$, are correctly decoded by RED in normal state 10.

B.3 *Case 3*

Assume that an error detection (BTD) occurs in block $[(i + j)\ell]$, $b \leqq j \leqq J$, where J is the maximum value of j such that block $[(i + j)\ell]$ can be detected in error when the last channel errors occur in block $[i\ell]$ and blocks $[(i + 1)\ell]$, $[(i + 2)\ell]$, $\cdots$ are free of channel errors. Under this hypothesis, error propagation cannot occur beyond block $[(i + j)\ell]$. For block $[(i + J)\ell]$ to be detected in error it must have $t_1 \geqq t + 1$ errors fed back to it. For $b = 2$ (rate $\frac{1}{2}$ codes) $J = b - 1$, and Case 3 cannot occur.

As in Case 1, $f_i = (b - 1)k$, and blocks $[(i + 1)\ell]$ to $[(i + b - 1)\ell]$ are subject to decoding error due to error propagation. Therefore, $f_{i+b-1} = (b - 1)t$. Each subsequent block, $[(i + b)\ell]$, $[(i + b + 1)\ell]$, $\cdots$, which is correctly (incorrectly) decoded removes $t(d_m - 2t)$ errors from the maximum number available for feedback. Let H_a be the largest integer such that $f_{i+H_a} \geqq t + 1$. Then when $b \geqq 3$

$$H_a = \begin{cases} (b - 1) + \left\lfloor \dfrac{(b - 2)t - 1}{d_m - 2t} \right\rfloor, & \text{if } d_m - 2t \leqq t; \\ 2b - 4 & \text{if } d_m - 2t > t. \end{cases} \tag{44}$$

Since errors must be fedback to block $[(i + J)\ell]$ from at least two blocks to get $t_1 > t$ feedback errors,

$$J = H_a + (b - 2). \tag{45}$$

B.3.1 *Case 3a*

Assume block $[(i + j)\ell]$ is correctly decoded by BTD. Then

$$\Lambda_3 = H_a ; \tag{46}$$

$$A_3 = (b - 1) + \left\lfloor \frac{(b - 2)t - 1}{d_m - 2t} \right\rfloor. \tag{47}$$

Blocks $[(i + J + b)\ell]$, $[(i + J + b + 1)\ell]$, $\cdots$ are correctly decoded in normal state 10.

B.3.2 *Case 3b*

Assume block $[(i + j)\ell]$ is incorrectly decoded by BTD. Now $b \leqq j \leqq G \leqq J$, where G is the maximum value of j such that block $[(i + j)\ell]$ can be detected in error and incorrectly decoded due to error propagation when the last channel errors occur at block $[i\ell]$ and blocks $[(i + 1)\ell]$, $[(i + 2)\ell]$, $\cdots$ are free of channel errors. For block $[(i + G)\ell]$ to be detected in error it must have $t_1 \geqq t + 1$ errors fed back to it to cause the detection and $t_2 \geqq 1$ errors fed back during the BTD to cause erroneous decoding.

If $f_{i+b-1} = (b - 1)t < t + 2$, $G = b - 1$ and Case 3b cannot occur. Let H_b be the largest integer such that $f_{i+H_b} > t + 1$. Then when $b \geqq 3$ and $(b - 2)t \geqq 2$

$$H_b = \begin{cases} (b - 1) + \left\lfloor \dfrac{(b - 2)t - 2}{d_m - 2t} \right\rfloor, & \text{if} \quad d_m - 2t \leqq t; \\ (b - 1) + \left\lfloor \dfrac{(b - 2)t - 2}{t} \right\rfloor, & \text{if} \quad d_m - 2t > t. \end{cases} \tag{48}$$

Since errors must be fed back to block $[(i + G)\ell]$ from at least two blocks (three blocks if $t = 1$) to get $t_1 + t_2 \geqq t + 2$ feedback errors

$$\Lambda_4 = G = \begin{cases} H_b + (b - 2), & \text{if} \quad t \geqq 2; \\ H_b + (b - 3), & \text{if} \quad t = 1. \end{cases} \tag{49}$$

$$A_4 = (b - 1) + \left\lfloor \frac{(b - 2)t - 2 + d_m - 2t}{d_m - 2t} \right\rfloor. \tag{50}$$

Blocks $[(i + \Lambda_4 + b)\ell]$, $[(i + \Lambda_4 + b + 1)\ell]$, $\cdots$ are correctly decoded in normal state 10.

Table I is constructed by taking

$$\Lambda = \max \{\Lambda_1, \Lambda_2, \Lambda_3, \Lambda_4\} \tag{51}$$

and

$$A = \max \{A_1, A_2, A_3, A_4\}.$$

By definition the recovery space is the minimum number of consecutive blocks free of channel errors required to guarantee the return of the decoder to one of normal states {10, 11, 20, 21} at block $[(i + V+1)\ell]$ regardless of the channel error sequence prior to block $[(i+1)\ell]$. We say that V is a necessary recovery space if fewer than V consecutive blocks free of channel errors do not guarantee transition to one of normal states {10, 11, 20, 21} at block $[(i + V + 1)\ell]$. We say that

V is a sufficient recovery space if V consecutive blocks free of channel errors guarantee transition to one of normal states {10, 11, 20, 21} at block $[(i + V + 1)\ell]$. For Cases 1, 2, and 4 $V_i = \Lambda_i + (b - 1)$, $i = 1, 2$, and 4, is a necessary and sufficient recovery space. For Case 3 $V_3 = \Lambda_3 + (2b - 3)$ is a necessary and sufficient recovery space. Since in all cases $V \geqq V_i$, $i = 1, 2, 3, 4$, is a sufficient recovery space $V = \max \{V_1, V_2, V_3, V_4\}$ is a necessary and sufficient recovery space.

APPENDIX C

List of Symbols

ℓ —block interleaving constant
b —parameter determining rate of recurrent code
A —recurrent code parity check matrix
H —component block code parity check matrix
N —constraint length of recurrent code
A_N —recurrent code truncated parity check matrix
n —block length of component block code
k —number of information bits per block of component block code
$I_{i\ell}$ —k-tuple of information bits of $[i\ell]$th block
$M_{i\ell}$ —n-tuple of transmitted bits of $[i\ell]$th block
$Q_{i\ell}$ —$(n - k)$-tuple of parity bits of $[i\ell]$th block
$I^j_{i\ell}$ —jth segment of $I_{i\ell}$
$M^*_{i\ell}$ —n-tuple of received bits of $[i\ell]$th block
$I^*_{i\ell}$ —k-tuple of received information bits of $[i\ell]$th block
$Q^*_{i\ell}$ —$(n - k)$-tuple of received parity bits of $[i\ell]$th block
$P^*_{i\ell}$ —parity $(n - k)$-tuple obtained by encoding $I^*_{i\ell}$ with H
$\bar{I}_{i\ell}$ —k-tuple of decoded information bits of $[i\ell]$th block
$P'_{i\ell}$ —$Q^*_{i\ell}$ as modified by fed back information segments
$\bar{I}^j_{i\ell}$ —jth segment of $\bar{I}_{i\ell}$
C_0 —the set of one element—the pattern with no errors
C_w —the set of channel error patterns which are identical to nonzero code words
C_c —the set of nonzero channel error patterns which are correctable by RED
C_u —the set of channel error patterns which are both uncorrectable by RED and undetectable
C_d —the set of channel error patterns which are detectable
α —the probability that the information bits of a received word are unaffected by the channel error pattern given that the channel error pattern is correctable, detectable, or undetectable

p_0 —the probability that the channel error pattern is in set C_0
p_w —the probability that the channel error pattern is in set C_w
p_e —the probability that the channel error pattern is in set C_e
p_u —the probability that the channel error pattern is in set C_u
p_d —the probability that the channel error pattern is in set C_d
d_m —minimum distance of the component block code
t —amount of error correction done in RED
V —recovery space
$p_{i,j}$ —single step transition probability from state i to state j
π_i —stationary probability of being in state i with Genie Decoder
P_{eg} —probability of block error with Genie Decoder
a —amount of error propagation
A —upper bound on a
λ —length of error propagation
Λ —upper bound on λ
A_i —designation of anomalous states for upper bound one on block error probability
ρ_i —stationary probability of being in state i for upper bound one
P_{eu1} —upper bound one on probability of block error
B_i, C_i —designation of anomalous states for upper bound two on block error probability
s_i —stationary probability of being in state i for upper bound two
P_{eu2} —upper bound two on probability of block error
P_{eL} —lower bound on probability of block error
$p_{i,j}(3)$—three step transition probability from state i to state j
e_i —maximum number of errors possible in decoded information k-tuple at block $[i\ell]$
f_i —maximum number of errors available for feedback to blocks after block $[i\ell]$
d —amount of error detection capability of component block code

REFERENCES

1. Tong, S. Y., "Burst-Trapping Techniques for a Compound Channel," IEEE Transactions on Information Theory, *IT-15*, No. 6 (November 1969), pp. 710–715.
2. Tong, S. Y., "Performance of Burst-Trapping Codes," B.S.T.J., this issue, pp. 477–491.
3. Wyner, A. D., and Ash, R. B., "Analysis of Recurrent Codes," IEEE Transactions on Information Theory, *IT-9*, No. 3 (July 1963) pp. 143–156.
4. Fano, R. M., *Transmission of Information*, New York: MIT Press and John Wiley and Sons, Inc., 1961, p. 183.
5. Kemeny, J. G., and Snell, J. L., *Finite Markov Chains*, Princeton, New Jersey: D. Van Nostrand Co., Inc., 1960, pp. 69–73.
6. Farrow, C. W., and Holzman, L. N., "Nationwide Field Trial Performance of a

Multilevel Vestigial-Sideband Data Terminal for Switched-Network Voice Channels," 1968 IEEE International Conference on Communication, Conference Record 68C20-COM, (June 1968), pp. 782–787.
7. Pehlert, Jr., W. K., "Performance of Error Control for High Speed Data Transmission on the Voice-Band Switched Telephone Network," 1969 IEEE International Conference on Communication, Conference Record 69C29-COM, (June 1969), pp. 39–19 to 39–25.
8. Elliott, E. O., "A Model of the Switched Telephone Network for Data Communications," B.S.T.J., *44*, No. 1 (January 1965), pp. 89–109.
9. Alexander, A. A., Gryb, R. M., and Nast, D. W., "Capabilities of the Telephone Network for Data Transmission," B.S.T.J., *39*, No. 3 (May 1960), pp. 431–476.

Synthesis of Stochastic Representations of Ground Motions

By S. C. LIU

(Manuscript received December 4, 1969)

In this paper, we study a number of stochastic models including stationary, nonstationary, and linear processes for the purpose of simulating earthquake- or explosion-induced ground motions. The important statistical characteristics of each model and their effects on structural systems are investigated in some detail. We obtain expressions for the mean-square response of simple linear mass-spring oscillators to each model. We discuss numerical procedures for time series simulations of these models. The objectives of this paper are (i) to examine and compare the statistical properties and effects on structures of all possible stochastic processes applicable to model ground motions and (ii) to offer engineers a basis for forming their own judgments.

I. INTRODUCTION

A primary concern in problems dealing with earthquake or blast response is the proper definition of random force environments. Typical problems include the design of earthquake-resistant frames for electronic or mechanical facilities in a building, and the estimation of structural damage resulting from nuclear detonation in a given area. Normally it is necessary to create ground-motion data artificially from information derived from limited recordings. Therefore, in ground-motion analysis, as in many other fields of engineering physics, time series modeling or simulation problems emerge. This paper carries forward the concern with such problems.

In a previous paper the statistical characteristics of a collection of earthquake ground-motion data were analyzed.[1] It was shown that a stationary random process of finite duration could be used to model the high-intensity phase of a ground-motion accelerogram. It was suggested that a narrowband stationary process be used. However, the narrowband process, like many other stationary models, fails to produce

the initial buildup and the decaying terminations which are apparent in many real ground-motion accelerograms. To simulate these portions, nonstationary models must be used. In this paper we investigate a number of physically realizable stationary, nonstationary, and linear stochastic models, when applicable to the simulation of ground motions. We derive the important statistics of these models and discuss numerical simulation procedures. The covariance, autocorrelation function, and power spectral density of the response process of a class of linear time-invariant systems excited by the input process represented by each model are examined. It is hoped that by comparing these models for basic definition, for simulation procedure, and for effects on induced structural responses, a practicing engineer will be able to select one that will be suitable for the analysis of his specific problem. It is the intent of this paper not only to sum up the current state of the art/science but also to give to researchers in the field of ground motion study such hints and directions for the development of advanced stochastic models as mathematical sophistication permits.

II. STOCHASTIC MODELS

2.1 *Stationary Models*

A typical ground-motion accelerogram from an earthquake or nuclear detonation consists of three phases: an initial rapid-buildup phase, a high-intensity primary phase, and a gradually decaying tail—all obviously nonstationary phenomena. However, many researchers still prefer to model earthquakes by stationary processes because the low-amplitude starting and ending portions of an accelerogram do not significantly affect the structural response as compared with the response induced by the primary phase. Therefore it appears legitimate to model the primary phase by a stationary process of finite duration. Furthermore, the stationariness assumption greatly simplifies the response evaluations and numerical simulation procedures. This feature is particularly important from the practical viewpoint. Three stationary models, designated as $x_1(t)$, $x_2(t)$, and $x_3(t)$, along with their autocorrelation function and power spectral density are defined in Table I.

The first model, white noise $x_1(t)$, defined as a stationary random signal having gaussian probability amplitude distribution and a constant spectral density for all frequencies, is the simplest one of all. Numerically, it can be simulated by generating a sequence of gaussian independent samples of gaussian random numbers g_n, spacing them at small time interval Δt, and assuming linear variation between amplitudes

TABLE I—STATIONARY MODELS AND CORRESPONDING AUTOCORRELATION AND SPECTRAL DENSITY FUNCTIONS

MODEL	I	II	III
NAME	White Noise	Filtered White Noise	Impulse Process
Definition, $x(t)$	$x_1(t)$	$x_2(t) = \int_{-\infty}^{\infty} h_0(t-\tau)x_1(\tau)d\tau$	$x_3(t) = \sum_{n=-\infty}^{\infty} a_n\delta(t-t_n)$
Autocorrelation Function, $R_x(\tau)$	$2\pi S_0\delta(\tau)$	$2\pi S_0 \int_0^{\infty} h_0(t)h_0(t+\tau)d\tau$	$\beta\left[\rho(0)\delta(\tau) + \sum_{n=1}^{\infty}\rho(n)p_n(\lvert\tau\rvert)\right]$
Spectral Density Function, $S_x(\omega)$	S_0	$\lvert H_0(i\omega)\rvert^2 S_0$	$\frac{\beta}{2\pi}\left[\rho(0) + 2Re\sum_{n=1}^{\infty}\rho(n)P_n(i\omega)\right]$

over each Δt. Bycroft[2] has studied this overly simplified model on an analog computer. This model fails to provide any frequency descriptions of the motions that are so important to the structural response analysis; its use results solely from its mathematical simplicity.

For model $x_2(t)$, the filtered white noise, symbols $h_0(t)$ and $H_0(\omega)$ in Table I represent the transfer function in the time and frequency domains, respectively. The process $x_2(t)$ is a gaussian, covariance stationary, narrowband process. The use of $x_2(t)$ in modeling earthquake ground motions is based upon the resemblance of the autocorrelation function, the power spectral density, and the response spectra of strong motion earthquakes to those of the narrowband process.[1,3,4] The numerical simulation of $x_2(t)$ based on prescribed power spectral density is a routine exercise using the basic relationship between the power spectral densities $S_{x1}(\omega)$ and $S_{x2}(\omega)$ of the input and output of the linear filter:

$$S_{x2}(\omega) = |H_0(\omega)|^2 S_{x1}(\omega). \tag{1}$$

This equation suggests that a signal $x_2(t)$ can be created from the random process $x_1(t)$ whose spectral density $S_{x1}(\omega) \equiv 1$ by passing $x_1(t)$ through a filter whose transfer function $H_0(\omega)$ satisfies $|H_0(\omega)|^2 = S_{x2}(\omega)$. A detailed approach to simulating stationary processes with a rational spectral density function, which is represented by a quotient of two polynomials in ω, has been described by Franklin.[5] Methods of estimating ground-motion spectral densities are given by Liu and Jhaveri.[1,4] A sample function of process $x_2(t)$, generated digitally by passing a white noise through a linear filter with a natural frequency of 10 rad/s and a damping ratio of 5 percent, is shown in Fig. 1 which demonstrates a typical appearance of a narrowband process. The justification for using this process to model ground motions is that both its power spectral density function and its response spectrum resemble and can be made to match those of real-world records. It reflects the predominant effects of the site on motion and, by using a modal analysis, $x_2(t)$ can model ground motions which exhibit multiple peaks in their frequency spectrograms.[4]

For $x_3(t)$ as defined in Table I the random impulses $\{a_n\}$ form a stationary discrete parameter process, and $\{t_n\}$ is a stationary point process independent of $\{a_n\}$.[6,7] As in the expressions for autocorrelation function and power spectral density, β is the average number of impulses per unit time interval and $p_n(t)$ represents the probability density function for n consecutive intervals of $\{t_n\}$ within a time duration t; $\rho(n)$ and $P_n(i\omega)$ are defined as

$$\rho(n) = E[a_m a_{m+n}] \qquad (\text{any } m) \tag{2}$$

$$P_n(i\omega) = \int_0^\infty p_n(t) \exp(-i\omega t)\, dt \tag{3}$$

in which $E[\ ]$ denotes ensemble averages.

Notice that the model $x_3(t)$ allows correlation $\rho(n)$ to exist among the random amplitudes a_n which are assumed to be independent for many other stochastic models. The simulation of $x_3(t)$ can be achieved by the spectral approach as described by Franklin or by the correlation approach based on the matrix factorization procedure as proposed by Moore and Anderson.[8] However, when $p_n(t)$ is poisson with mean arrival rate β and Markov correlation $\rho(n) = \rho^{|n|}$ and $|\rho| \leqq 1$, a sample function of $x_3(t)$ can be created by simultaneous simulations of independent samples of $\{a_n\}$ and $\{t_n\}$. In this case the probability density function of the waiting time $\tau_k = t_{k+1} - t_k$ is an exponential distribution, that is, $p(\tau_k) = \beta \exp(-\beta\tau_k)$ and therefore a sequence τ_k can be generated from a sequence of uniformly distributed random numbers w_k:

$$\tau_k = -\frac{1}{\beta} \ln(1 - w_k), \qquad 0 \leqq w_k < 1. \tag{4}$$

The correlation $\rho^{|n|}$ can be introduced into $\{a_n\}$ by using an autoregressive transformation of a sequence of gaussian random numbers g_n with zero mean and unit variance:

$$\begin{aligned} a_n &= (1 - \rho^2)^{\frac{1}{2}} a'_n \\ a'_n &= \rho a'_{n-1} + g_n \ . \end{aligned} \tag{5}$$

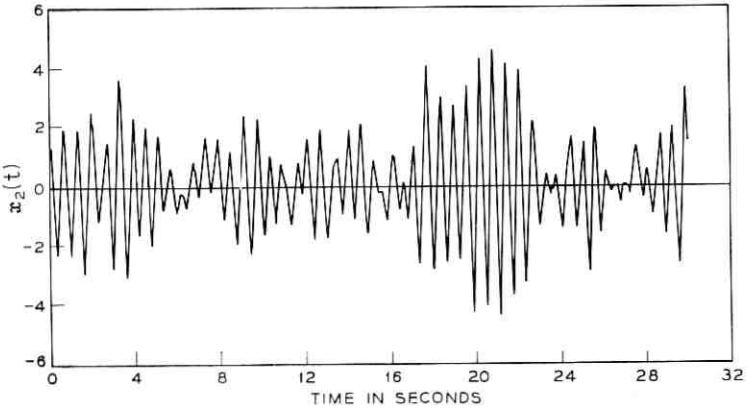

Fig. 1—Sample function of process $x_2(t)$.

A digitally simulated sample of $x_3(t)$ with $\rho = 0.5$, $\beta = 1.0$, and poisson distribution for $p_n(\tau)$ is shown in Fig. 2(a); its autocorrelation function and power spectral density are shown, respectively, in Figs. 2(b) and (c). The time response of a linear filter having a natural frequency $\omega = 10.0$ rad/s and a damping ratio $\zeta = 5$ percent to this input sample member of $x_3(t)$ is shown in Fig. 3(a). The corresponding autocorrelation function and power spectral density of the sample response are shown in Figs. 3(b) and (c), respectively. Notice that Fig. 3(b) exhibits a damped oscillatory motion with a frequency $\omega = 10.0$ rad/s which is the natural frequency of the filter. At this frequency there is a peak in the power spectral density as shown in Fig. 3(c) which is similar to that of strong-motion earthquakes. Notice also that in comparison with $x_3(t)$, which shows abrupt peaks and dips in the waveform, the filtered impulse process more closely resembles a ground-motion accelerogram. Based on these results, it appears that a filtered impulse process may be more appropriate than the impulse process $x_3(t)$ itself in modeling earthquake motions.

When ground motions are represented by stationary processes, it is extremely important to properly determine the duration and intensity of the processes because the induced response of structures depends heavily on these two parameters. To those who are reluctant to neglect the nonstationary effect resulting from the starting and tail portions of earthquake accelerograms, the stationary models I through III obviously are not satisfactory. One might therefore consider using the following nonstationary models.

2.2 *Nonstationary Models*

Five useful nonstationary models, $x_4(t)$ through $x_8(t)$, are defined in Table II.

The model $x_4(t)$ is a frequency-modulated nonstationary function. For its definition in Table II, b_i , α_i , and ω_i are given sets of real positive numbers, and w_i are independent random variables from uniform distribution over 0 and 2π. The use of $x_4(t)$ is based on the result that the skewed bell shape covariance function of $x_4(t)$ is similar to and can be made to match that of an earthquake. Numerical simulations of $x_4(t)$ present no special difficulty as its sample members can be created directly for given sets of b_i , α_i , and ω_i according to its definition. It may be expected that use of a large number of terms as given by $x_4(t)$ will produce member functions that look much more like real earthquake accelerograms.[9]

For the model $x_5(t)$, $\phi(t)$ is a deterministic or envelope function and

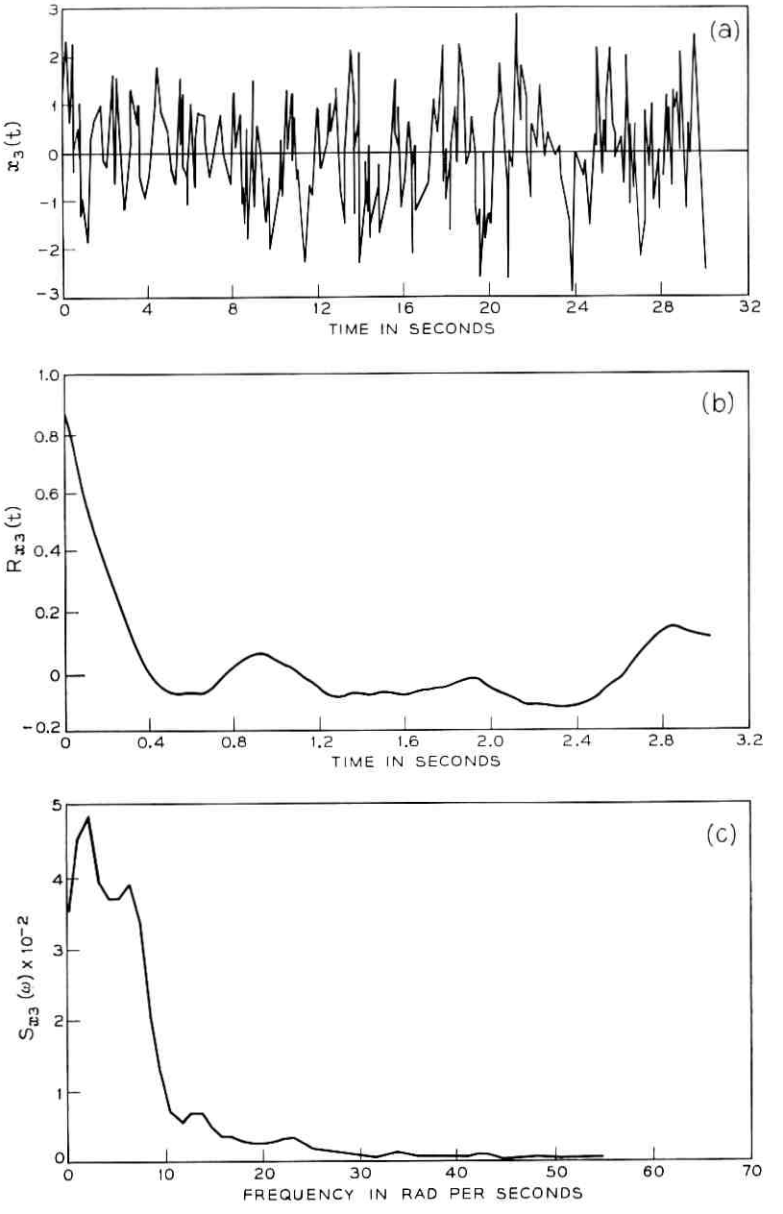

Fig. 2(a)—Digital realization of sample $x_3(t)$, the impulse process.
Fig. 2(b)—Autocorrelation function of sample $x_3(t)$.
Fig. 2(c)—Power spectral density function of sample $x_3(t)$.

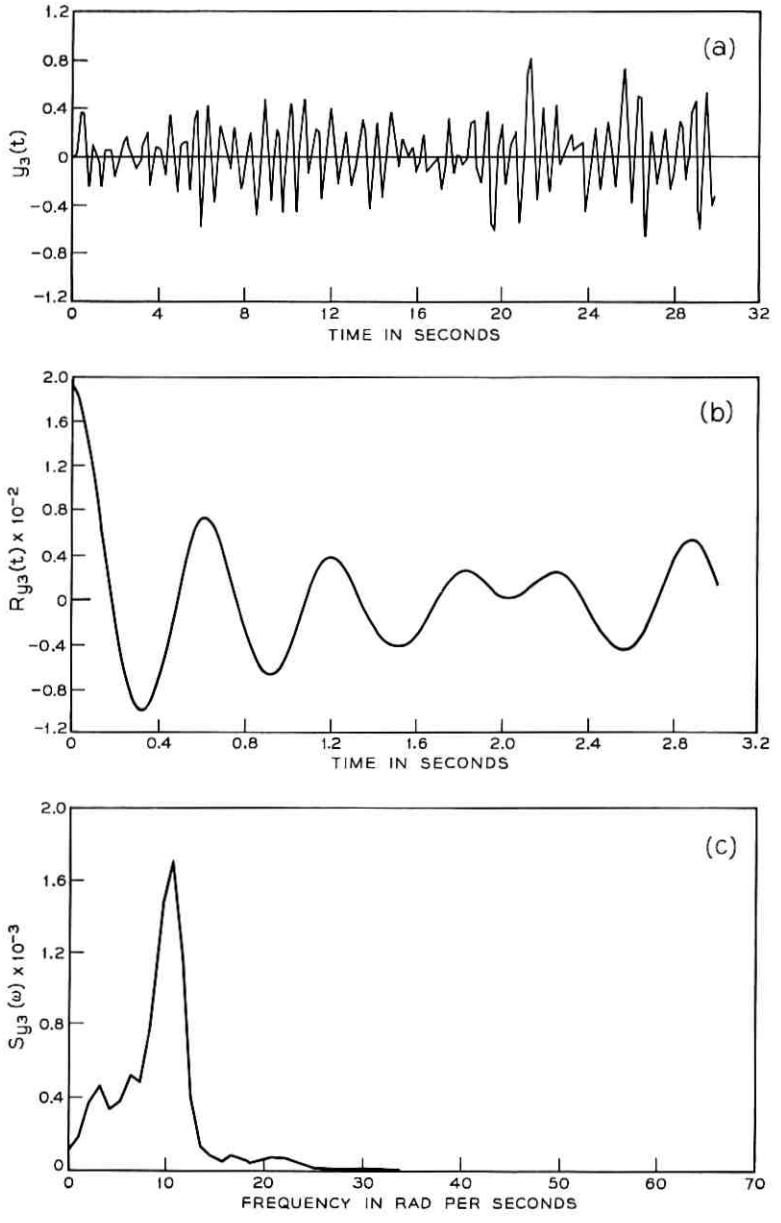

Fig. 3(a)—Digital realization of sample response of $x_3(t)$.
Fig. 3(b)—Autocorrelation function of sample response of $x_3(t)$.
Fig. 3(c)—Power spectral density function of sample response of $x_3(t)$.

TABLE II—DEFINITION OF NONSTATIONARY MODELS

MODEL	NAME	DEFINITION
IV	Frequency Modulated Random Function	$x_4(t) = \sum_{j=1}^{n} b_j \exp(-\alpha_j t) \cos(\omega_j t + w_j)$
V	Separable Nonstationary Process	$x_5(t) = \phi(t) f(t)$
VI	Filtered Separable Nonstationary Process	$x_6(t) = \int_{-\infty}^{\infty} h_0(t - \tau) x_5(\tau) d\tau$
VII	Shot Noise	$x_7(t) = \sum_{r} a(t_r) \delta(t - t_r)$
VIII	Filtered Shot Noise	$x_8(t) = \sum_{k} a_k h_0(t - t_k)$

$f(t)$ is a stationary random process with given autocorrelation function and power spectral density. The function $f(t)$ may be any one of processes $x_1(t)$, $x_2(t)$, and $x_3(t)$. This model in its various forms has been studied by Peterson and Pullen[10,11] and by MacNeal, and others.[12] The process $x_5(t)$ has been suggested for model earthquake motions by Shinozuka and Sato[13] and by Jennings, and others.[14] The process $x_6(t)$ is the response function of $x_5(t)$. In Fig. 4 is shown a sample member of $x_5(t)$ with $\phi(t) = \sin(\pi t/30)$ and $f(t)$ as the sample member of $x_2(t)$ in Fig. 1. Its response function to a linear filter with a natural frequency of 10 rad/s and a damping ratio of 5 percent is shown in Fig. 5 which represents a sample of the process $x_6(t)$. Figure 4 clearly illustrates that the waveform is enveloped by a half-sine wave which produces a strong phase between the times of 17 and 23 seconds. The high-amplitude tail observed in Fig. 5 is obviously undesirable in modeling ground motion. However, notice that this figure shows only the response history cutoff at the end of excitation. If free vibration is allowed after the termination of the input, the highly amplified portion will gradually decay, and the resulting waveform will then compare more favorably with real ground-motion records as shown.

A nice feature of process $x_5(t)$ is its separable property which greatly simplifies the mathematics required to evaluate the response statistics. Furthermore, the envelope function $\phi(t)$ can be chosen so that the pattern of the rise and fall of the simulated waveforms is similar to that of a real earthquake motion. However, because the choice of $\phi(t)$ is arbitrary, when using $x_5(t)$ the associated nonstationary effects resulting from the

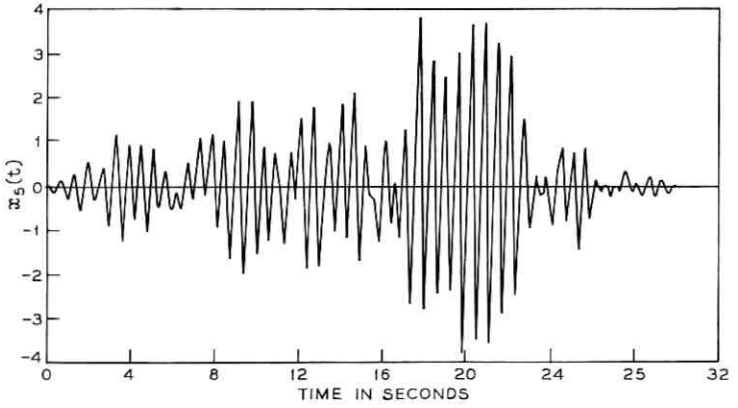

Fig. 4—Sample function of process $x_5(t)$.

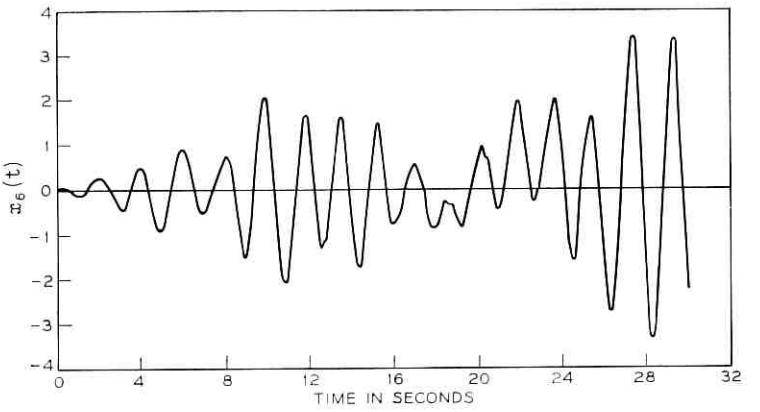

Fig. 5—Sample function of process $x_6(t)$.

total time duration, the time proportion of the three distinct phases of the ground motion, and the rate of buildup and decay must be carefully examined.

The shot noise $x_7(t)$ and the filtered shot noise $x_8(t)$ are the nonstationary counterparts of the stationary white noise $x_1(t)$ and filtered white noise $x_2(t)$, respectively. The nonstationariness is introduced into these models by two sources: the time-dependent mean arrival rate $\beta(t)$ and the time-dependent amplitude joint probability density function $p(a_i , t_i ; a_j , t_j)$. However, it is assumed that the impulse amplitudes are completely uncorrelated, that is, the joint probability density function is separable:

$$p(a_1 , t_1 ; a_2 , t_2) = p(a_1 , t_1)p(a_2 , t_2).$$

Further, the probability of n impulses in a small interval dt is negligible for $n \geqq 2$. Based upon these conditions, it can be shown that the covariance functions of $x_7(t)$ and $x_8(t)$ are also time-dependent:

$$\text{Cov}_{x8}(t_1 , t_2) = \int_\Gamma h_0(t_1 - \tau)h_0(t_2 - \tau)E[a^2(\tau)]\beta(\tau)\, d\tau; \tag{6}$$

$$\begin{aligned}\text{Cov}_{x7}(t_1 , t_2) &= \int_\Gamma \delta(t_1 - \tau)\ \delta(t_2 - \tau)E[a^2(\tau)]\beta(\tau)\, d\tau \\ &= E[a^2(t_1)]\beta(t_1)\ \delta(t_1 - t_2) \\ &= I(t_1)\ \delta(t_1 - t_2);\end{aligned} \tag{7}$$

where Γ denotes the appropriate time domain, and $I(t)$ is the strength

function of the shot noise defined as

$$E[x_7(t)x_7(t+\tau)] = I(t)\ \delta(\tau).$$

Notice that, when $I(t)$ is a constant, both $x_7(t)$ and $x_8(t)$ become stationary.

The process $x_7(t)$ can be constructed by generating independent gaussian random variables a_n with zero mean and variance equal to $I(t_n)\ \Delta t$, and by linearly connecting them over Δt along the time axis. The process $x_8(t)$ can be obtained in a similar way simply by shaping each impulse with the transfer function $h_0(t)$ according to its definition in Table II. Amin and Ang[15] have used process $x_8(t)$ with a second-order filter to model earthquakes. Both $x_7(t)$ and $x_8(t)$ are justified on the basis of the similarity between real and nonstationary waveforms and on the matching (*i*) of their time-varying covariance functions and (*ii*) of the induced response spectra with those of the real ground-motion data.

2.3 *Linear Models*

Special cases of the mixed autoregressive-moving average process x_t of order (m, n) as defined below also can be used to model ground motions:

$$x_t = \sum_{i=1}^{m} \phi_i x_{t-i} + g_t + \sum_{i=1}^{n} \theta_i g_{t-i}\ , \qquad t = 0, \pm 1, \pm 2, \cdots \tag{8}$$

where ϕ_i and θ_i are characterization parameters, and process $\{g_t\}$ is a white noise. An m-order autoregressive (ar) process is given by the first sum of equation (8), that is,

$$x_t = \sum_{i=1}^{m} \phi_i x_{t-i} + g_t \tag{9}$$

and an n-order moving average (ma) process by the second sum

$$x_t = g_t - \sum_{i=1}^{n} \theta_i g_{t-i}\ . \tag{10}$$

The ar processes given in equation (9) are particularly useful in time series simulations because they are very flexible and can be used to model a wide range of real-world random data. For example, the autocorrelation function of a second-order ar process, involving only two parameters, can produce a wide variety of autocorrelation functions. Therefore by matching the ground-motion autocorrelation function of the damped oscillatory type, one can estimate parameters ϕ_i and fit the observed motion to an appropriate linear stochastic model.

III. RESPONSE ANALYSIS

Because a ground-motion model when chosen will be used to specify vibration environments for structural testing and design, it is important to examine its effects on the time and frequency response of some representative systems. In what follows we shall compute and compare the mean-square response of a class of second-order linear systems to stochastic inputs represented by models as described in the previous section. The linear systems are characterized by two constant parameters, the damping coefficient ζ and a natural frequency ω_n, and have transfer functions

$$\begin{aligned} h(t) &= \frac{\exp(-\zeta\omega_n t)}{p}\sin pt, \qquad t \geqq 0; \\ &= 0 \qquad\qquad\qquad\qquad t < 0; \end{aligned} \tag{11}$$

where $p = \omega_n(1 - \zeta^2)^{\frac{1}{2}}$.

Let the response function to $x_i(t)$ be $y_i(t)$; $i = 1, 2, \cdots, 8$, for systems defined by equation (11). The mean-square response is given by

$$E[y_i(t)^2] = \int_\Gamma \int_\Gamma h(t - \tau)h(t - \tau')g_i(\tau, \tau')\, d\tau\, d\tau', \qquad i = 1, 2, \cdots, 8. \tag{12}$$

The function $g_i(\tau, \tau')$ for each model is

$$\begin{aligned} g_1 &= 2\pi S_0\, \delta(\tau - \tau'), \\ g_2 &= R_{x2}(\tau - \tau') = 2\pi \int_0^\infty h_0(t)h_0(t + \tau - \tau')\, dt, \\ g_3 &= R_{x3}(\tau - \tau') = \beta\left[\rho(0)\, \delta(\tau - \tau') + \sum_{n=1}^{\infty} \rho(n)p_n(|\, \tau - \tau'\, |)\right], \\ g_4 &= \tfrac{1}{2} \sum_1^n \tau\tau' a_i^2 \exp(-\alpha_i(\tau + \tau'))\cos\omega_i(\tau' - \tau), \\ g_5 &= \phi(\tau)\phi(\tau')R_f(\tau - \tau'), \\ g_6 &= \int_\Gamma \int_\Gamma h_0(\tau - \theta_1)h_0(\tau' - \theta_2)\phi(\theta_1)\phi(\theta_2)R_f(\theta_2 - \theta_1)\, d\theta_1\, d\theta_2, \\ g_7 &= E[a^2(\tau)]\beta(\tau)\, \delta(\tau - \tau') = I(\tau)\, \delta(\tau - \tau'), \\ g_8 &= \int_\Gamma h_0(\tau - \theta)E[a(\theta)]\beta(\theta)\, d\theta \int_\Gamma h_0(\tau' - \theta)E[a(\theta)]\beta(\theta)\, d\theta \\ &\quad + \int_\Gamma h_0(\tau - \theta)h_0(\tau' - \theta)E[a^2(\theta)]\beta(\theta)\, d\theta. \end{aligned} \tag{13}$$

The explicit expression for the mean-square response to stationary models can be obtained by integrations using equations (11) through (13):

$$E[y_1^2(t)] = \frac{\pi S_0}{2\zeta\omega_n^2} + \frac{\pi S_0}{2p^2\omega_n} \cdot(\zeta \cos 2pt - (1 - \zeta^2)^{\frac{1}{2}} \sin 2pt - 1/\zeta) \exp(-2\zeta\omega_n t), \quad (14)$$

$$E[y_2^2(t)] \simeq \frac{\pi S_{x2}(\omega_n)}{2\zeta\omega_n^3} \cdot\left[1 - \frac{\exp(-2\omega_n\zeta t)}{p^2}\{p^2 + 2(\omega_n\zeta)^2 \sin^2 pt + \omega_n p\zeta \sin 2pt\}\right]. \quad (15)$$

It is assumed in equation (15) that $S_{x2}(\omega)$, the power spectral density of $x_2(t)$, is given, and the main contribution of $x_2(t)$ to the response comes from the region around $\omega = \omega_n$.[16] And:

$$E[y_3^2(t)] = \beta c_1 + \beta \exp(-2\zeta\omega_n t)\left[c_2 \cos 2pt + c_3 \sin 2pt + \frac{\beta\rho}{p^2}(\zeta^2\omega_n^2 - a^2) \sin^2 pt + \frac{\beta\rho}{\gamma} \cos^2 pt - \frac{\beta\rho a\mu}{2p^2\zeta\omega_n}\right] - \frac{2\beta^2\rho}{p\gamma} \exp(-(\zeta\omega_n + a)t)[(a + \zeta\omega_n) \sin pt + p \cos pt] \quad (16)$$

in which $a = (1 - \rho)\beta$, $\mu = a^2 + (1 - 2\zeta^2)\omega_n^2$, $\gamma = (a^2 + \omega_n^2)^2 - 4a^2\zeta^2\omega_n^2$, and

$$c_1 = \frac{\beta\rho}{\gamma}\left(1 + \frac{a\mu}{2\zeta\omega_n^3} - \frac{a\zeta}{\omega_n}\right) + \frac{1}{4\zeta\omega_n^3}$$

$$c_2 = \frac{1}{\omega_n}\left[\frac{1}{2p^2}\left(\frac{a\beta\rho\zeta\mu}{\gamma} - \frac{1}{2\zeta}\right) + \frac{a\beta\rho\zeta}{\gamma}\right]$$

$$c_3 = \frac{1}{p}\left[\frac{\beta\rho\zeta}{\gamma}(\omega_n + a\zeta) - \frac{1}{2\omega_n^2}\left(\frac{1}{2} + \frac{a\beta\rho\mu}{\gamma}\right)\right].$$

Notice that, as time increases, mean-square response to each of three stationary models approaches its steady-state level, that is,

$$\lim_{t\to\infty} E[y_i^2(t)] = \begin{cases} \dfrac{\pi S_0}{2\zeta\omega_n^3}, & i = 1 \\ \dfrac{\pi S_{x2}(\omega_n)}{2\zeta\omega_n^3}, & i = 2 \\ \beta c_1, & i = 3. \end{cases} \quad (17)$$

Let the rate of convergence of the mean-square response be defined as

$$\epsilon_i = \frac{\lim_{t\to\infty} E[y_i^2(t)] - E[y_i^2(t)]}{\lim_{t\to\infty} E[y_i^2(t)]} \tag{18}$$

and $N = \omega_n t/2\pi$ be the number of cycles of the motion required to reach ϵ_i. A lower bound to the estimate of N can be easily established for processes $x_1(t)$ and $x_2(t)$ as the following:

$$N \geqq \frac{1}{4\pi\zeta} \ln \left[\frac{1 + \zeta^2 + \zeta(1 - \zeta^2)^{\frac{1}{2}}}{(1 - \zeta^2)\epsilon} \right], \qquad 0 < \zeta < 1. \tag{19}$$

From this it is noted that N is independent of the natural frequency ω_n of the system but is heavily dependent on the damping ratio ζ. Figure 6 shows that systems with high damping, when excited by $x_1(t)$ and $x_2(t)$, will approach steady-state level faster than those with low damping. A system with 10 percent damping will reach 90 percent of its steady-state response in two cycles of motion.

Because the mean-square response to $x_3(t)$ involves more parameters than that to $x_1(t)$ or $x_2(t)$, the response convergence rate for $x_3(t)$ is more difficult to evaluate. However, ζ remains as the dominant factor, not β or ρ. The mean-square response of $x_3(t)$, as of $x_1(t)$ and $x_2(t)$, approaches its steady-state value rapidly when ζ is high, slowly when ζ is low.

Explicit expression for the mean-square response to nonstationary models can also be obtained similarly from equation 13 although the integration involved in the time domain is quite cumbersome. Bogdan-

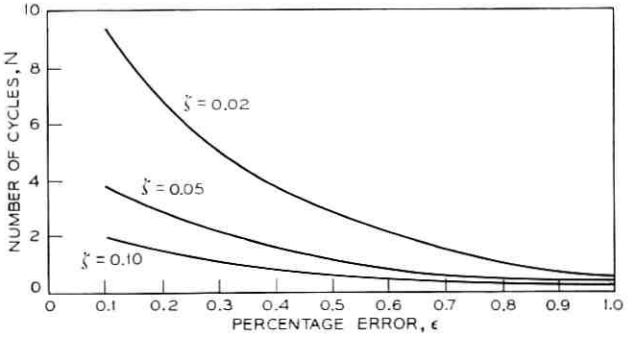

Fig. 6—Convergence of mean-square response of processes $x_1(t)$ and $x_2(t)$.

off, and others,[9] have shown that

$$E[y_4^2(t)] = \frac{1}{p^2} \exp(-2\zeta\omega_n t) \sum_1^n \frac{a_i^2 \gamma_i(t)}{\chi_i^2} \tag{20}$$

where $\gamma_i(t)$ and χ_i are both functions of α_i, ω_i, and p.

Sometimes it is more convenient to calculate the mean-square response by integration in the frequency domain than in the time domain. For example, Brown[17] has generalized Miller's[18] result for the process $x_5(t)$ to the case where $\phi(t)$ is bounded on $(-\infty, \infty)$ and integrable on every finite subinterval of $(-\infty, \infty)$. His frequency formulation is

$$\mathrm{Cov}_{y5}(t_1, t_2) = \frac{1}{2\pi} \int_{-\infty}^{\infty} B(\omega, t_1) B^*(\omega, t_2) S_f(\omega)\, d\omega \tag{21}$$

$$E[y_5^2(t)] = \frac{1}{8\pi^3} \int_{-\infty}^{\infty} \left| \int_{-\infty}^{\infty} H(\omega_1)\Phi(\omega_1 - \omega_2) \exp(i\omega_1 t)\, d\omega_1 \right|^2 S_f(\omega_2)\, d\omega_2 \tag{22}$$

where $H(\omega)$, $\Phi(\omega)$, and $B(\omega, t)$ are the Fourier transforms of $h(t)$, $\phi(t)$, and $h(t - \tau)\phi(\tau)$, respectively, and the star denotes the complex conjugate. Barnoski and Maurer,[19] using equation (21), evaluated $E[y_5^2(t)]$ numerically for cases where $\phi(t)$ is the unit step and rectangular functions and $f(t)$ is both white noise and noise with an exponentially decaying harmonic correlation function, that is, $R_f(\tau) = A \exp(-a \mid \tau \mid) \cos b\tau$. It was shown for white noise modulated by a unit step function that the system mean-square response will not exceed its stationary value for white noise. For correlated noise modulated in this same way, the system mean-square response may overshoot its stationary value. Note from equations (13) and (21) that

$$g_5(\tau, \tau') = \mathrm{Cov}_{y5}(\tau, \tau').$$

Substitution of this relation into equation (12) yields

$$\begin{aligned} E[y_5^2(t)] &= \int_\Gamma \int_\Gamma h(t - \tau)h(t - \tau') \mathrm{Cov}_{y5}(\tau, \tau')\, d\tau\, d\tau' \\ &= \frac{1}{p^2} \int_\Gamma \int_\Gamma \exp(\zeta\omega_n(\tau + \tau')) \sin p(t - \tau) \sin p(t - \tau') \\ &\quad \cdot \mathrm{Cov}_{y5}(\tau, \tau')\, d\tau\, d\tau'. \end{aligned} \tag{23}$$

Substitution of g_n in equation (13) into equation (12) yields

$$\begin{aligned} E[y_7^2(t)] = \frac{1}{2p^2} \exp(-2\zeta\omega_n t) &\int_\Gamma I(\tau) \exp(2\zeta\omega_n \tau)\, d\tau \\ &- \int_\Gamma I(\tau) \exp(2\zeta\omega_n \tau) \cos p(t - \tau)\, d\tau. \end{aligned} \tag{24}$$

Using the relation $g_s(\tau, \tau') = \mathrm{Cov}_{v\tau}(\tau, \tau')$ and letting $h_0(t)$ with parameters ω_0, ζ_0, and p_0 be of the same form as $h(t)$ in equation (11), it can be shown that

$$
\begin{aligned}
&E[y_s^2(t)] \\
&= \frac{1}{2p^2p_0^2} \exp(-2\zeta\omega_n t) \\
&\quad \cdot \int_\Gamma \int_\Gamma \Big\{ \exp[(\zeta\omega_n - \zeta_0\omega_0)(\tau + \tau')] \sin p(t - \tau) \sin p(t - \tau') \\
&\quad \cdot \Big[\cos p_0(\tau - \tau') \int_\Gamma I(\theta) \exp(2\zeta_0\omega_0\theta)\, d\theta \\
&\quad - \int_\Gamma I(\theta) \exp(2\zeta_0\omega_0\theta) \cos p_0(\tau + \tau' - 2\theta)\, d\theta \Big] \Big\} d\tau\, d\tau'. \qquad (25)
\end{aligned}
$$

It should be noted that, in equations (24) and (25), $I(\tau) = E[a^2(\tau)]\beta(\tau)$.

The mean-square response to linear first-order moving average and autoregressive processes (assuming a sampling interval Δt) for first-order and second-order filters are also found. Let the transfer function for the first-order filter be $h(t) = \exp(-a_0 t)$ (corresponding to a differential operator $p = d/dt + a_0$) and that for the second-order system be as given in equation (9), we obtain for the first-order ma process

$$
E[y^2(t)] = \frac{c}{2a_0}[(1 + \theta_1^2) - q\theta_1](1 - \exp(-2a_0 t)), \qquad (26)
$$

(first-order filter);

$$
\begin{aligned}
E[y^2(t)] &= \frac{c}{2p^2} \exp(-2\zeta\omega_n t) \\
&\quad \cdot \Big\{ (1 + \theta_1^2) \Big[\frac{1}{2\zeta} (\exp(2\zeta\omega_n t) - 1) - \frac{\zeta}{2} \exp(2\zeta\omega_n t) \\
&\quad + \zeta \cos 2pt - (1 - \zeta^2)^{\frac{1}{2}} \sin 2pt \Big] \\
&\quad + \theta_1 \Big[(1 - \zeta^2)^{\frac{1}{2}} \sin 2pt - \zeta \cos 2pt \\
&\quad + \zeta \exp(2\zeta\omega_n t) + \frac{1}{\zeta}(1 - \exp(2\zeta\omega_n t)) \Big] \Big\}, \qquad (27)
\end{aligned}
$$

(second-order filter);

and for first-order ar process

$$E[y^2(t)] = \frac{1}{1 - \theta_1^2} \frac{[1 - (\phi_1 \exp(a_0))^{-t}][(\exp(-a_0)\phi_1)^t - 1]}{(\ln \phi_1)^2 - a_0^2}, \quad (28)$$

(first-order filter);

$$E[y^2(t)] = \frac{[\exp(-a_1 t)(-a_1 \sin pt - p \cos a_1 t) + p]}{(1 - \phi_1^2)p^2(a_1^2 + p^2)(a_2^2 + p^2)} \cdot \frac{[\exp(-a_2 t)(-a_2 \sin pt - p \cos a_2 t) + p]}{(1 - \phi_1^2)p^2(a_1^2 + p^2)(a_2^2 + p^2)}, \quad (29)$$

(second-order filter).

In the above

$$c = \Delta t E[g_t^2],$$
$$q = 2 \exp(a_0 \Delta t),$$
$$a_1 = \zeta\omega_n + \ln \phi_1,$$
$$a_2 = \zeta\omega_n - \ln \phi_1.$$

It follows from equations (26) and (27) that the mean-square response to the first-order ma process approaches a steady-state value

$$\lim_{\substack{\Delta t \to 0 \\ t \to \infty}} E[y^2(t)] = \frac{c}{2a_0}(1 - \theta_1)^2, \quad \text{(first-order filter)}; \quad (30)$$

$$= \frac{c(1 + \theta_1^2)}{4\omega_n^3 \zeta}, \quad \text{(second-order filter)}. \quad (31)$$

Similarly from equations (28) and (29)

$$\lim_{\substack{\Delta t \to 0 \\ t \to \infty}} E[y^2(t)] = \frac{1}{(1 - \phi_1^2)[a_0^2 - (\ln \phi_1)^2]}, \quad \text{if} \quad 0 < \phi_1 \leqq 1, \quad (32)$$

(first-order filter);

$$= \frac{1}{(1 - \phi_1^2)\{[(\ln \phi_1)^2 + \omega_n^2]^2 - 4\zeta^2\omega_n^2(ln\ \phi_1)^2\}}, \quad (33)$$

(second-order filter).

The above results indicate that the mean-square response of linear systems to either of the ar and ma processes approaches a certain stationary value when the time of passage is sufficiently long.

IV. CONCLUSIONS

When selecting a stochastic model it is important to consider not only the matching of statistical characterizations of real-world random data to those of the model, but also the effects of the model on vulnerable structural systems. The statistical characterizations are provided by joint probability distribution functions of the process conditioned on its duration and intensity. Ordinary power spectra and time-variable spectra such as the running spectrum

$$S(i\omega, t) = \int_0^t x(\tau) \exp(-i\omega\tau)\, d\tau$$

or the instantaneous spectrum

$$\rho(\omega, t) = \frac{\partial}{\partial t} \mid S(i\omega, t) \mid^2$$

can be used to characterize and form the simulation basis for the stationary and nonstationary processes, respectively. For the latter case, a second variable enters into the spectrum formulations and therefore complicates the analysis considerably. One alternative for analyzing nonstationary processes is to follow Priestley's theory of evolutionary processes and spectra.[20-22] Its applicablility to ground motion and earthquakes will be investigated in a separate report. In general one must exercise engineering judgment upon consideration of the specific problem he studies in making an intelligent choice among all possible models. At the present time it appears that an earthquake ground-motion accelerogram can reasonably be treated as sectionally stationary when broken into three distinct phases. Each phase of the motion can be regarded as a short process and the corresponding power spectral density estimated by standard approaches to form the simulation bases for the $x_2(t)$ model. The applicability of this procedure is illustrated in Fig. 7 which shows the power spectrum densities associated with three distinct phases of recorded S21W ground motion during the Taft, California, 1952 earthquake. It is apparent from this earthquake that most of the input power to structures is provided by the midsection (from 3.3 to 13.6 seconds) of the motion. The power contained in low-intensity fluctuations preceding and following this stationary portion is relatively small.

Finally it should be pointed out that the stochastic models investigated in this paper can be easily realized by using a computer. The response statistics of these models are also reasonably easy to find. Although the

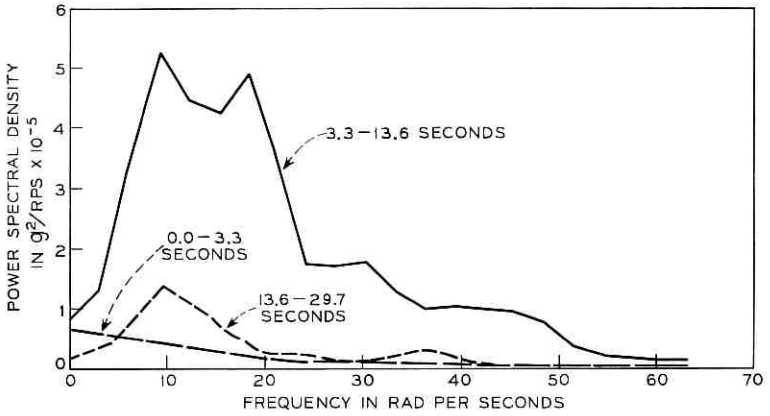

Fig. 7—Power spectral densities of Taft, California, S21W, July 21, 1952 earthquake.

current study is concerned primarily with ground-motion simulation, the results obtained can be applied also to many other engineering problems when time series modeling is required.

REFERENCES

1. Liu, S. C., "Statistical Analysis and Stochastic Simulation of Ground Motion Data," B.S.T.J., *47*, No. 10 (December 1968), pp. 2273–2298.
2. Bycroft, G. N., "White Noise Representation of Earthquakes," Proc. Amer. Soc. Civil Engineers, *86*, No. EM2 (April 1960), pp. 1–16.
3. Housner, G. W., and Jennings, P. C., Jr., "Generation of Artificial Earthquakes," Proc. Amer. Soc. Civil Engineers, *90*, No. EM1 (February 1964), pp. 113–150.
4. Liu, S. C., and Jhaveri, D. P., "Spectral Simulation and Earthquake Site Properties," J. of Eng. Mech. Div., Proc. Amer. Soc. Civil Engineers, *95*, No. EM-5 (October 1969), pp. 1145–1168.
5. Franklin, J. N., "Numerical Simulation of Stationary and Nonstationary Gaussian Random Processes," SIAM Review, *7*, No. 1 (January 1965), pp. 68–80.
6. Leneman, O. A. Z., "Random Sampling of Random Processes: Impulse Processes," Inf. and Contr., *9*, No. 6 (August 1966), pp. 347–363.
7. Beutler, F. J., and Leneman, O. A. Z., "The Spectral Analysis of Impulse Processes," Inf. and Contr., *12*, No. 3 (March 1968), pp. 236–258.
8. Moore, J. B., and Anderson, B. D. O., "Simulation of Stationary Stochastic Processes," Proc. IEEE, *115*, No. 2 (February 1968), pp. 337–339.
9. Bogdanoff, J. L., Goldberg, J. E., and Bernard, M. C., "Response of a Simple Structure to a Random Earthquake Type Disturbance," Bull. Seismological Soc. Amer., *54*, No. 1 (February 1964), pp. 263–276.
10. Peterson, H. C., and Pullen, C. L., "Response of a Dynamic System to a Separable Nonstationary Random Excitation," J. Spacecraft Rockets, *3*, No. 8 (August 1966), pp. 1299–1300.
11. Pullen, C. L., and Peterson, H. C., "Spectral Analysis of the Transient Response of a System to Random Excitation," Trans. Amer. Soc. Mech. Engineers, J. Appl. Mech., *33*, Series E, No. 3 (September 1966), pp. 700–702.
12. MacNeal, R., Barnoski, R. L., and Bailie, J. A., "Response of a Simple Oscillator to Nonstationary Random Noise," J. Spacecraft Rockets, *3*, No. 3 (March 1966), pp. 441–443.

13. Shinozuka, M., and Sato, Y., "Simulation of Nonstationary Random Process," Proc. Amer. Soc. Civil Engineers, *93*, No. EM1 (February 1967), pp. 11–40.
14. Jennings, P. C., Housner, G. W., and Tsai, N. C., "Simulated Earthquake Motions," Tech. Rept., Earthquake Engineering Research Lab., Calif. Inst. Tech., Pasadena, California, April 1968.
15. Amin, M., and Ang, A. H. S., "A Nonstationary Model for Strong Motion Earthquakes," Proc. Amer. Soc. Civil Engineers, *94*, No. EM2 (April 1968), pp. 559–583.
16. Caughey, T. K., and Stumpf, H. J., "Transient Response of a Dynamic System Under Random Excitation," J. Appl. Mech., Trans. Amer. Soc. Mechanical Eng., *28*, No. E-4 (December 1961), pp. 563–566.
17. Brown, J. L., "A Correlation Result for Nonstationary Inputs," Quart. Appl. Math., *24*, No. 1 (April 1966), pp. 93–95.
18. Miller, K. S., "A Note on Input-Output Spectral Densities," Quart. Appl. Math., *21*, No. 1 (October 1963), pp. 249–252.
19. Barnoski, R. L., and Maurer, J. R., "Mean-Square Response of Simple Mechanical System to Nonstationary Excitation," J. Appl. Mech., Trans. Amer. Soc. Mechanical Eng., *36*, Series E, No. 2 (June 1969), pp. 221–228.
20. Priestley, M. B., "Evolutionary Spectra and Nonstationary Processes," J. R. Statist. Soc. B., *27*, No. 2 (1965), pp. 204–237.
21. Priestley, M. B., "Power Spectral Analysis of Non-stationary Random Processes," J. Sound Vib., *6*, No. 1 (July 1967), pp. 86–97.
22. Priestley, M. B., and Rao, T. S., "A Test for Non-stationarity of Time-series," J. R. Statist. Soc. B, No. 1 (1969), pp. 140–149.

Limiting Behaviors of Randomly Excited Hyperbolic Tangent Systems

By S. C. LIU and D. K. COHOON

(Manuscript received October 22, 1969)

We investigate the steady-state probability density distribution of a large class of random processes by solving the governing Fokker–Planck equation. The random response statistics of a nonlinear single-degree-of-freedom mechanical model with hyperbolic tangent stiffness are discussed in some detail. The probability density of such systems is of the sech-power type which belongs to a class of distributions whose behaviors are carefully examined at the limits where the system parameter b approaches zero and infinity. Other important response statistics such as the mean square response, zero crossings, and peak distributions are also studied.

I. INTRODUCTION

In recent years, random vibrations of nonlinear systems have attracted considerable attention among engineers.[1] In this paper we investigate the Fokker–Planck equations[2,3] associated with a class of random processes whose steady-state probability density distributions, of the Liapunov potential function type.

The random response statistics of a nonlinear single-degree-of-freedom model having a hyperbolic tangent stiffness function can be described as a softening spring whose force-deflection relationship is asymptotic to some maximum force level. Such a model can be used to represent an elastic-perfect-plastic system, material often encountered in classical mechanics. Limiting situations for a class of probability density functions such as those obtained in this study are examined. We show that the limiting behavior of the steady-state output probability density function of a system having a generalized hyperbolic tangent stiffness function, $F(u) = (k_0/b^{\alpha-1}) \tanh bu$, is closely related to the range of the parameter α. At the limit $b \to \infty$, the probability density function becomes a Dirac delta (impulse) function or an exponential distribution, or identically approaches zero for all u, depending upon whether α

is less than, equal to, or greater than 1. At the limit $b \to 0$, it vanishes identically for all u and becomes a normal distribution or a Dirac delta function, depending upon whether α is less than, equal to, or greater than 2. In addition, we study statistics of other response parameters such as the mean square output, zero crossings and peak output distribution, which are relevant to the control of the failure modes of the system.

The motion of a dynamic system under purely random disturbance is described by a Markoff process $\mathbf{y}(t) = [y_1(t), y_2(t), \cdots, y_n(t)]$ in the n-dimensional phase space. It can be shown[3,4] that for the initial condition

$$p(\mathbf{y}_o) = \prod_{i=1}^{n} \delta(y_i - y_{io})$$

where $\mathbf{y}_o$ is the initial state of $\mathbf{y}(t)$ and δ is the Dirac delta function, the conditional probability density function $p(\mathbf{y} \mid \mathbf{y}_o, t)$ of the process $\mathbf{y}(t)$ satisfies the forward Fokker–Planck equation,

$$\frac{\partial p}{\partial t} = -\sum_{i=1}^{n} \frac{\partial G_i(\mathbf{y})}{\partial y_i}, \qquad t \geqq 0 \tag{1}$$

where

$$G_i(\mathbf{y}) = A_i(\mathbf{y})p - \tfrac{1}{2} \sum_{j=1}^{n} \frac{\partial}{\partial y_j} [B_{ij}(\mathbf{y})p] \tag{2}$$

is the component of the probability current vector $p(\mathbf{y} \mid \mathbf{y}_o, t)$ in which

$$A_i(\mathbf{y}) = \lim_{\Delta t \to 0} \langle y_{i,\Delta t} - y_i \rangle \tag{3}$$

and

$$B_{ij}(\mathbf{y}) = \lim_{\Delta t \to 0} \langle (y_{i,\Delta t} - y_i)(y_{j,\Delta t} - y_j) \rangle \tag{4}$$

are intensity coefficients depending on the input and the properties of the system (the bracket indicating ensemble averaging).

We are interested in the solution of the steady-state equation (1), that is when $\partial p/\partial t = 0$, for cases where all generalized response variables of a system in the $2n$ phase-space coordinates are independent of one another. For this type of motion it is sometimes possible to find appropriate partial operators which, when linearly operated on functions of the type $g_i(y_i)p + h_i(y_i)(\partial p/\partial y_i)$, generate an equation equivalent to (1). More specifically, the steady-state equation (1) can be put in the form

$$\sum_{i=1}^{2n} L_i \left[g_i(y_i)p + h_i(y_i) \frac{\partial p}{\partial y_i} \right] = 0 \tag{5}$$

where the coefficients L_i are arbitrary first-order partial-differential operators. If there exists a $p(y)$ independent of initial conditions and satisfying each

$$g_i(y_i)p + h_i(y_i)\frac{\partial p}{\partial y_i} = 0, \qquad (i = 1, 2, \cdots, 2n),$$

then by Gray's uniqueness theorem such $p(y)$ is the unique solution of equation (5).[5] Such a solution is

$$p_{st}(\mathbf{y}) = C \prod_{i=1}^{2n} \exp\left[-\int_0^{y_i} \frac{g_i(\lambda_i)}{h_i(\lambda_i)}\, d\lambda_i\right] \tag{6}$$

and C is the normalization factor.

Equations (5) and (6) will be used in the following sections to analyze a class of nonlinear systems.

II. HYPERBOLIC TANGENT STIFFNESS MODEL

The mechanical system considered in this investigation is a single-degree-of-freedom oscillator with a mass m, a linear viscous damping c, and a nonlinear spring function $F(u)$. When the system is subjected to a base acceleration excitation $\ddot{x}_b(t)$, its response is characterized by the displacement $u(t)$ relative to the base. The equation of motion of the system is

$$\ddot{u} + 2\beta\dot{u} + \mathfrak{F}(u) = a(t) \tag{7}$$

where

$$\beta = \frac{c}{2m}, \qquad \mathfrak{F}(u) = \frac{F(u)}{m},$$

and

$$a(t) = -\ddot{x}_b(t).$$

Let $a(t)$ be a gaussian, stationary white noise with zero mean; that is, with the properties

$$\langle a(t)\rangle = 0$$

$$\langle a(t_1)a(t_2)\rangle = 2S_o\,\delta(t_1 - t_2)$$

where S_o is the constant power spectral density of $a(t)$. Then the associated steady-state Fokker–Planck equation for $\mathbf{u}(t) = [u(t), \dot{u}(t)]$ is

$$S_o\frac{\partial^2}{\partial \dot{u}^2}p(u, \dot{u}) - \frac{\partial}{\partial u}[\dot{u}p(u, \dot{u})] + \frac{\partial}{\partial \dot{u}}\{[2\beta\dot{u} + \mathfrak{F}(u)]\}p(u, \dot{u}) = 0. \tag{8}$$

For this two-dimensional case ($n = 2$), according to equations (5) and (6), the solution can be written down readily,

$$p(u, \dot{u}) = C \exp\left\{-\frac{2\beta}{\pi S_o}\left[\frac{\dot{u}^2}{2} + \int_0^u \mathfrak{F}(\xi)\, d\xi\right]\right\} \tag{9}$$

where C is the normalization factor determined by

$$\iint p(u, \dot{u})\, du\, d\dot{u} = 1.$$

A special kind of softening spring described by a hyperbolic tangent function will now be considered. The force-deflection characteristic is shown in Fig. 1 and given as follows:

$$F(u) = \frac{k_o}{b} \tanh bu, \qquad k_o, b > 0, \tag{10}$$

where k_o is the initial stiffness, and b is the rate of convergence of the force-deflection curve.

It should be noted that the spring force $F(u)$ developed during the motion is bounded between k_o/b and $-k_o/b$. Therefore k_o/b may be regarded as yielding force and $1/b$ the corresponding yielding displacement. The stiffness function $F(u)$ described in equation (10) then provides a good representation of the elastic-perfect-plastic behavior often encountered in the fields of classical mechanics and structural engineering.

Let $\omega_o^2 = k_o/m$ where ω_o represents the natural frequency of the linear

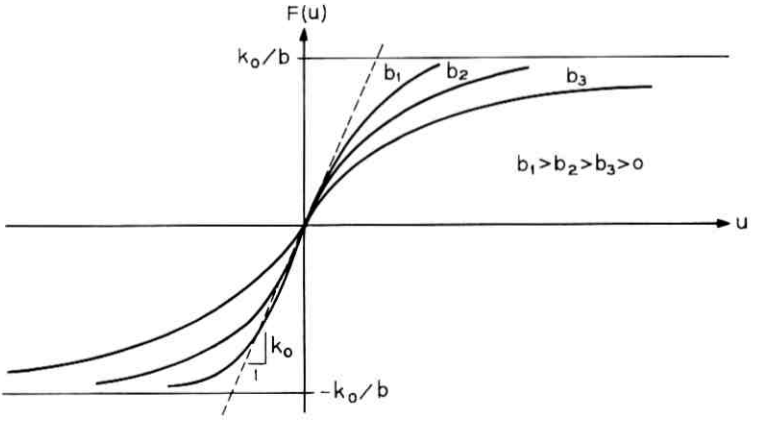

Fig. 1—Force-deflection relationship of hyperbolic tangent stiffness model.

oscillator with stiffness k_o ; then substitution of equation (10) into (9) yields

$$p(u, \dot{u}) = C \exp\left\{-\frac{\dot{u}^2}{2\omega_o^2\sigma_o^2} - \frac{1}{b^2\sigma_o^2} \ln \cosh bu\right\} \tag{11}$$

where $\sigma_o^2 = (\pi S_o/2\beta\omega_o^2)$ is the variance of the linear response [that is, if $F(u) = k_o u$].

Equation (11) shows that u and $\dot{u}$ are statistically independent. The probability density function for velocity $\dot{u}$ is normal with zero mean and variance $\sigma_o^2\omega_o^2$, that is,

$$p(\dot{u}) = \frac{1}{(2\pi)^{\frac{1}{2}}\sigma_o\omega_o} \exp\left(-\frac{\dot{u}^2}{2\sigma_o^2\omega_o^2}\right), \qquad -\infty < u < \infty. \tag{12}$$

The probability density function for the displacement u is

$$p(u) = C_1(b)[\operatorname{sech} bu]^{1/\sigma_o^2 b^2} \tag{13}$$

where

$$C_1(b) = \left(\int_{-\infty}^{\infty} \operatorname{sech}^{1/\sigma_o^2 b^2} b\xi \, d\xi\right)^{-1}. \tag{14}$$

Because $(\operatorname{sech} b\xi)^{1/b^2\sigma_o^2}$ converges to zero very rapidly as $\xi \to \infty$, $C_1(b)$ in equation (14) can be evaluated numerically for any positive b. If $1/b^2\sigma_o^2$ is an integer, equation (14) then becomes

$$C_1(b) = \frac{b}{2^D(D-1)!} \prod_{k=0}^{D-1} (2D - 2k - 1) \tag{15}$$

where $2D = 1/b^2\sigma_o^2$ are integers.[6] It is interesting to see that, if $\tanh bu$ is expanded into a power series, equation (13) then becomes

$$p(u) = C_1(b) \exp\left[-\frac{1}{2\sigma_o^2}\left(u^2 - \frac{b^2}{6}u^4 + \cdots\right)\right], \qquad |u| \leqq \frac{\pi}{2b},$$

which indicates that a cubic softening spring with nonlinear coefficient $k_o b^2/3$ is the first approximation of the hyperbolic tangent spring.

Values of $p(u)$ given by equation (13) for various $1/b^2\sigma_o^2$ are shown in Figs. 2 and 3.

III. LIMITING SITUATIONS OF $p(u)$

In connection with the examination of the limiting behaviors of $p(u)$ in equation (13), where the parameter b approaches zero and infinity alternately, three useful theorems are presented.

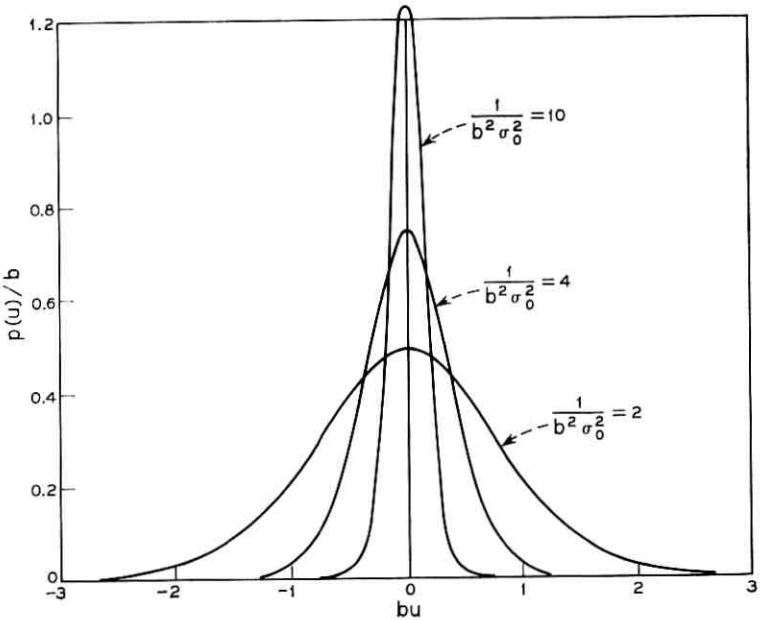

Fig. 2—Sech-power probability density distributions.

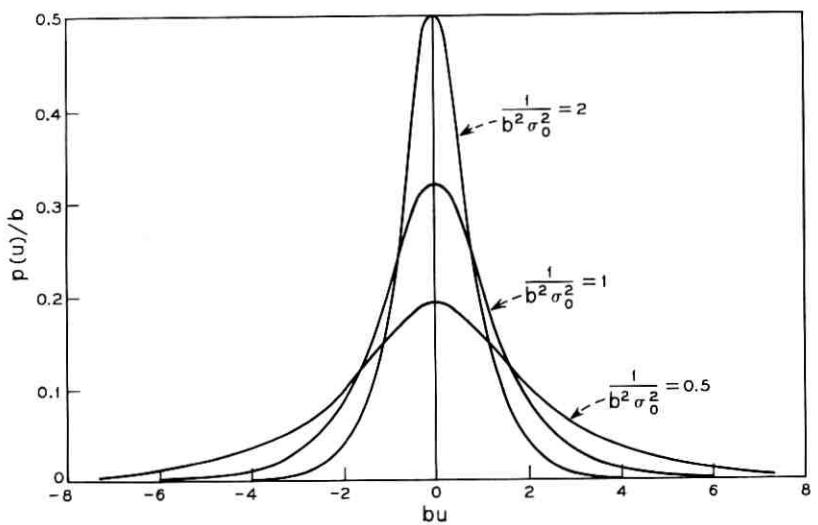

Fig. 3—Sech-power probability density distributions.

Theorem 1: *Let $f_n(x)$ be a sequence of nonnegative density functions integrable on $[-\infty, \infty]$. Suppose there exists a sequence of positive integrable $g_n(x)$ such that*

$$g_n(x) \geqq F_n(x) = f_n(x) \Big/ \int_{-\infty}^{\infty} f_n(s)\, ds$$

and

$$\lim_{n\to\infty} \left[\int_{\epsilon}^{\infty} g_n(x)\, dx + \int_{-\infty}^{-\epsilon} g_n(x)\, dx \right] = 0 \quad \text{for every} \quad \epsilon > 0.$$

Then

$$\lim_{n\to\infty} F_n(x) = \delta(x), \tag{16}$$

the Dirac delta function.

Proof: We must show that, for every h in $C_0^{\infty}(R)$, the space of test functions

$$\lim_{n\to\infty} \int_{-\infty}^{\infty} F_n(x)h(x)\, dx = h(0).$$

By the mean value theorem the following relationship holds:

$$\lim_{n\to\infty} \int_{-\infty}^{\infty} F_n(x)h(x)\, dx$$

$$= \lim_{n\to\infty} \int_{\epsilon}^{\infty} F_n(x)h(x)\, dx + \lim_{n\to\infty} \int_{-\infty}^{-\epsilon} F_n(x)h(x)\, dx + \lim_{n\to\infty} h(\xi) \cdot \int_{-\epsilon}^{\epsilon} F_n(x)\, dx$$

where ξ is some member of $[-\epsilon, \epsilon]$, depending on ϵ and n. The first two limits on the right side of the previous equation are zero by a comparison test; therefore, one can show that

$$\lim_{n\to\infty} \int_{-\epsilon}^{\epsilon} F_n(x)\, dx = 1.$$

Then

$$\lim_{n\to\infty} h(\xi) = \lim_{n\to\infty} \int_{-\infty}^{\infty} F_n(x)h(x)\, dx.$$

But the right side is independent of ϵ. Thus, letting ϵ approach zero,

we deduce that

$$h(0) = \lim_{n\to\infty} \int_{-\infty}^{\infty} F_n(x)h(x)\,dx,$$

which completes the proof.

Instead of considering $p(u)$ of equation (13), we shall investigate its more general form as

$$p_{(b,\alpha)}(u) = \frac{[\text{sech } (bu)]^{1/b^\alpha A}}{\int_{-\infty}^{\infty} [\text{sech } (by)]^{1/b^\alpha A}\,dy},$$

which is the steady-state displacement density function corresponding to a generalized hyperbolic tangent stiffness function

$$F(u) = \frac{k_o}{b^{\alpha-1}} \tanh bu \tag{17}$$

if $A = \sigma_o^2$.

Theorem 2: *Let* $p_\alpha(u) = \lim_{b\to\infty} p_{(b,\alpha)}(u)$, *then*

(*i*) $\alpha > 1$ *implies* $p_\alpha(u) = 0$,

(*ii*) $\alpha = 1$ *implies* $p_\alpha(u) = \left(\frac{1}{2A}\right)e^{-|u|/A}$,

and

(*iii*) $\alpha < 1$ *implies* $p_\alpha(u) = \delta(u)$.

Proof: First suppose $\alpha > 1$. We observe that

$$|\, p_{(b,\alpha)}(u)\,| \leqq \frac{1}{\int_{-\infty}^{\infty} [\text{sech } (by)]^{1/b^\alpha A}\,dy} \quad \text{for all} \quad u,$$

but

$$[\text{sech } (by)]^{1/b^\alpha A} \geqq \exp\,(-|\, y\,|/b^{\alpha-1}A),$$

thus

$$\int_{-\infty}^{\infty} [\text{sech } (by)]^{1/b^\alpha A}\,dy \geqq \int_{-\infty}^{\infty} \exp\,(-|\, y\,|/b^{\alpha-1}A)\,dy = 2b^{\alpha-1}A.$$

Thus, since

$$|\, p_{(b,\alpha)}(u)\,| \leqq 1/(2b^{\alpha-1}A) \tag{18}$$

for all u, we conclude that $\lim_{b\to\infty} p_{(b,\alpha)}(u) = 0$.

Now suppose that $\alpha = 1$. Then

$$\lim_{b\to\infty} \ln [\operatorname{sech}(bu)]^{1/bA} = \lim_{b\to\infty} (1/bA) \ln (\operatorname{sech} bu)$$
$$= \lim_{b\to\infty} (-1/bA) \ln (\cosh bu)$$
$$= \lim_{b\to\infty} [-\tanh (bu)/A] = -|u|/A.$$

Thus,

$$\lim_{b\to\infty} [\operatorname{sech}(bu)]^{1/bA} = \exp(-|u|/A).$$

By the Lebesgue dominated-convergence theorem

$$\lim_{b\to\infty} \int_{-\infty}^{\infty} [\operatorname{sech}(by)]^{1/bA}\, dy = \int_{-\infty}^{\infty} \exp(-|y|/A)\, dy = 2A.$$

Thus,

$$\lim_{b\to\infty} p_{(b,1)}(u) = (2A)^{-1} \exp(-|u|/A).$$

Finally, we suppose that $\alpha < 1$. Let

$$g_{(b,\alpha)}(u) = \frac{2^{1/b^{\alpha}A} \exp(-|u|\, b^{(1-\alpha)}/A)}{\int_{-\infty}^{\infty} \exp[-(b^{(1-\alpha)}\,|y|)/A]\, dy}$$

or, equivalently,

$$g_{(b,\alpha)}(u) = \left(\frac{2^{1/b^{\alpha}A} b^{(1-\alpha)}}{2A}\right) \exp(-|u|\, b^{(1-\alpha)}/A).$$

Then, since

$$\lim_{b\to\infty} \int_{\epsilon}^{\infty} g_{(b,\alpha)}(y)\, dy = \lim_{b\to\infty} \int_{-\infty}^{-\epsilon} g_{(b,\alpha)}(y)\, dy = 0$$

for every $\epsilon > 0$ and

$$g_{(b,\alpha)}(u) \geqq p_{(b,\alpha)}(u) \quad \text{for every} \quad u,$$

we conclude from Theorem 1 that

$$\lim_{b\to\infty} p_{(b,\alpha)}(u) = \delta(u),$$

and the proof is completed.

Theorem 3: *Let* $p_{\alpha}'(u) = \lim_{b\to 0} p_{(b,\alpha)}(u)$, *then*

(*i*) $\alpha > 2$ *implies* $p'_\alpha(u) = \delta(u)$,

(*ii*) $\alpha = 2$ *implies* $p'_\alpha(u) =$ *normal distribution with variance* σ_o^2, and

(*iii*) $\alpha < 2$ *implies* $p'_\alpha(u) = 0$ for all u.

Proof: The case $\alpha > 2$ implies $p'_\alpha(u) = \delta(u)$ is proved in Appendix A in which we also show that there exists for every $\gamma \in (0, 1)$ a $C_\gamma > 0$ such that

$$g_b(u) = C_\gamma \exp\left(-\frac{u^2}{b^{\alpha-2}A}\right)(2b^{\alpha-1}A)$$

$$\geqq \frac{[\operatorname{sech}(bu)]^{1/b^\alpha A}}{\int_{-\infty}^{\infty} [\operatorname{sech}(by)]^{1/b^\alpha A}\, dy} \quad \text{for} \quad |u| \leqq \frac{\gamma\pi}{2b}.$$

It follows from the above that

$$p'_\alpha(u) = 0 \quad \text{for} \quad 1 < \alpha < 2.$$

From equation (18) we immediately have $p'(u) = 0$ for $\alpha < 1$. Now we have only to consider the cases when $\alpha = 2$ and $\alpha = 1$. In Appendix B we show that when $\alpha = 2$, $p'_\alpha(u)$ is a normal distribution with variance σ_o^2. In Appendix C we show that when $\alpha = 1$, $p'_\alpha(u) = 0$ for all u. Therefore the proof is completed.

According to Theorem 3, for $p(u)$ given by equations (13) and (14), it follows that

$$\lim_{b\to 0} p(u) = \frac{1}{(2\pi)^{\frac{1}{2}}\sigma_o} \exp\left[-\frac{u^2}{2\sigma_o^2}\right], \qquad \text{a normal distribution,}$$

and according to Theorem 2

$$\lim_{b\to\infty} p(u) = 0. \tag{20}$$

At the limit $b \to \infty$, the yielding force $k_o/b \to 0$, that is, the system becomes perfect plastic. Thus one may expect an equal probability for all u on $[-\infty, \infty]$, as equation (20) indicated. As $b \to 0$, then $k_o/b \to \infty$, the system remains elastic on $[-\infty, \infty]$ with the initial stiffness k_o. It is well known that for linear systems the response probability distribution is gaussian, which agrees with the result of equation (19).

It is of interest to note that a similar force-deflection relationship as shown in Fig. 1 and as described by the hyperbolic tangent stiffness function given in equation (10) can be described by a full-wave smooth

limiter which is

$$G(u) = k_0 \int_0^u \exp\left(-\frac{\eta^2}{2d^2}\right) d\eta$$

in which $d^2 = 2/\pi b^2$.

It will be noted that in the above equation, $G(u)$ is proportional to the integral of a gaussian probability curve. Function $G(u)$ can also be used to evaluate the probability density function if made equivalent to $F(u)$ as given by equation (10) when both $G(u)$ and $F(u)$ have the same initial slope and spring resistance limits.

IV. OTHER IMPORTANT RESPONSE STATISTICS

The failure modes of a mechanical system are generally controlled by response parameters such as the mean square displacement, zero crossings, or the peak displacement distributions. These response statistics are closely related to $p(u)$ and will be briefly discussed.

The mean value of displacement response u vanishes because $p(u)$ in equation (13) is an even function. The mean square or the variance of the displacement is given by

$$\sigma_u^2(b) = \langle u^2 \rangle = \int_{-\infty}^{\infty} u^2 p(u)\, du$$

$$= 2C_1(b) \int_0^{\infty} u^2 \operatorname{sech}^{1/b^2\sigma_0^2} bu\, du, \tag{21}$$

which can be evaluated in the following manner*: Let

$$J(a) = \int_{-\infty}^{\infty} \frac{e^{2ax}\, dx}{(\cosh x)^{2\nu}},$$

then it can be shown[6] that

$$J(0) = \frac{(\pi)^{\frac{1}{2}}\Gamma(\nu)}{\Gamma(\nu + \frac{1}{2})},$$

and

$$\int_{-\infty}^{\infty} \frac{x^2\, dx}{(\cosh x)^{2\nu}} = \left[\frac{1}{4}\frac{\partial^2}{\partial a^2} J(a)\right]_{a=0} = \tfrac{1}{2} J(0)\psi'(\nu),$$

where $\psi'(\nu) = (d/d\nu)[\Gamma'(\nu)/\Gamma(\nu)]$ is the "trigamma" function and has been numerically tabulated.[7]

* This is pointed out by S. O. Rice.

From the above results and setting $x = bu$ and $\nu = b\sigma_o$ in equation (21) we finally obtain

$$\sigma_u^2(b) = \frac{1}{2b^3} C_1(b) J(0) \psi'(b\sigma_o). \tag{22}$$

Again according to Theorem 3, it is noted that

$$\lim_{b \to 0} \sigma_u^2(b) = \sigma_o^2 ,$$

and from Theorem 2 that

$$\lim_{b \to \infty} \sigma_u^2(b) = \infty .$$

Thus the mean square response $\sigma_u^2(b)$ with such limiting behavior can be illustrated as in Fig. 4.

The expected number of zero crossings ν_o^+ with positive slope per unit time (that is, the expected frequency) can be evaluated according to Rice,[8]

$$\nu_o^+(b) = \int_0^\infty \dot{u} p(0, \dot{u})\, d\dot{u} = \frac{C_1(b)}{2} \left(\frac{\pi}{\beta}\right)^{\frac{1}{2}} \tag{23}$$

where $C_1(b)$ is given by equation (14).

Also according to Theorem 3, it can be shown that

$$\lim_{b \to 0} \nu_o^+(b) = \frac{\omega_o}{2\pi} , \tag{24}$$

which is the frequency of the linear system.

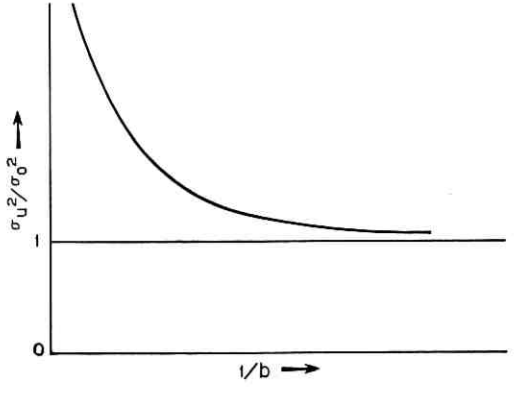

Fig. 4—Variation of mean-square displacement response.

The probability density of the peak amplitude of $u(t)$, from equation (13), is given by

$$p(a) = -\frac{\left|\frac{dp(u)}{du}\right|_{u=a}}{[p(u)]_{u=0}}$$

$$= \frac{1}{\sigma_o^2 b}(\operatorname{sech} ba)^{1/\sigma_o^2 b^2} \tanh ba. \tag{25}$$

By the same argument used in the proof of Theorem 2 it can be shown that

$$\lim_{b\to\infty} p(a) = \delta(a), \tag{26}$$

and it follows from Theorem 3 that

$$\lim_{b\to 0} p(a) = \lim_{b\to 0}\left(\frac{\tanh ba}{\sigma_o^2 b}\right) \lim_{b\to 0} \operatorname{sech}^{1/\sigma_o^2 b^2} ba$$

$$= \frac{a}{\sigma_o^2} \exp\left(\frac{-a^2}{2\sigma_o^2}\right), \tag{27}$$

which is the Rayleigh distribution as expected because at this limit ($b \to 0$) the system becomes linear. The peak probability density distribution $p(a)$ for various b in equation (25) is illustrated in Fig. 5. Notice that for all cases $p(a)$ approaches zero at large a; however, the rate of fall of $p(a)$ is reduced as b is increased.

It should be noted that when $\alpha = 1$, the forcing function described by equation (17) approaches a sgn function as $b \to \infty$, that is

$$\lim_{b\to\infty} (k_o \tanh bu) = k_o \operatorname{sgn} u.$$

Therefore, by taking appropriate limits to the density function previously obtained for second-order systems with a general hyperbolic tangent forcing function, we obtain the steady-state solution for the response density of systems governed by the following equation

$$\ddot{u} + 2\beta\dot{u} + k_o \operatorname{sgn} u = a(t).$$

The response density for the above equation is given precisely in statement (*ii*) of Theorem 2, which can also be verified by using equation (9).

V. ACKNOWLEDGMENTS

The authors wish to thank S. O. Rice and M. Lax for their interest in this work and their many valuable comments and suggestions.

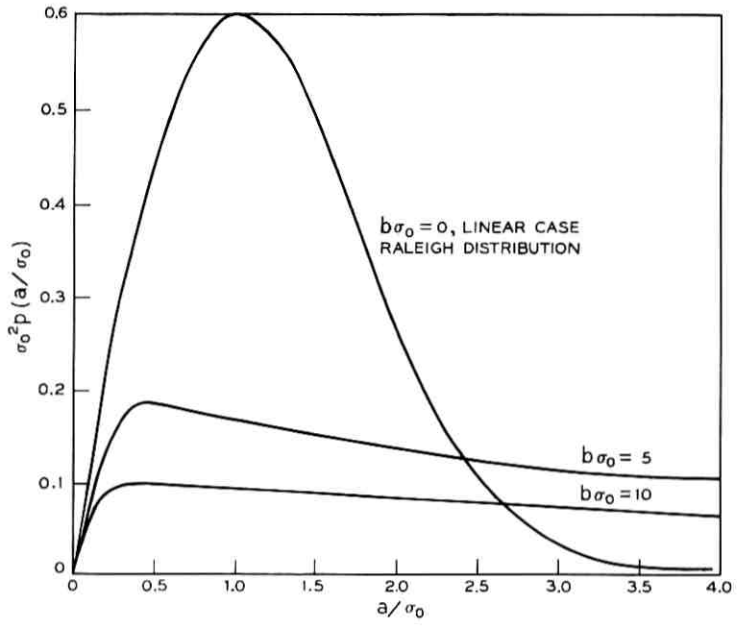

Fig. 5—Peak probability density distributions.

APPENDIX A

Partial Proof of Theorem 3 for Case $\alpha > 2$

We claim that if $\alpha > 2$, then

$$\lim_{b\to 0} \frac{\operatorname{sech}(bu)^{1/b^\alpha A}}{\int_{-\infty}^{\infty} \operatorname{sech}(by)^{1/b^\alpha A}\, dy} = \delta(u).$$

Proof: In view of Theorem 2 we have only to find functions

$$g_b(u) \geqq \frac{\operatorname{sech}(bu)^{1/b^\alpha A}}{\int_{-\infty}^{\infty} \operatorname{sech}(by)^{1/b^\alpha A}\, dy}$$

such that for every $\epsilon > 0$

$$\lim_{b\to 0} \int_{\epsilon}^{\infty} g_b(u)\, du = \lim_{b\to 0} \int_{-\infty}^{-\epsilon} g_b(u)\, du = 0$$

and such that $\sup \int_{-\infty}^{\infty} g_b(u)\, du < \infty$. We write

$$\operatorname{sech}(by)^{1/b^{\alpha}A} = \exp\{-\ln[\cosh(by)]/b^{\alpha}A\}.$$

We observe that if $|by| < \pi/2$, then

$$\ln[\cosh(by)]/b^{\alpha}A = \sum_{k=0}^{\infty}(1/b^{\alpha}A)(1/k!)\left[\lim_{\beta\to 0}\left(\frac{d}{d\beta}\right)^{k}\ln\cosh(\beta y)\right]b^{k}$$

$$= \sum_{k=2}^{\infty}(y/b^{\alpha}Ak!)\left[\lim_{\beta\to 0}\left(\frac{d}{d\beta}\right)^{k-1}\tanh(\beta y)\right]b^{k}.$$

We now make use of the fact that $|by| < 1$ implies

$$\tanh(by) = \sum_{n=1}^{\infty}\beta_n(-1)^{n+1}2^{2n}(2^{2n}-1)\frac{(by)^{2n-1}}{(2n)!}.$$

Thus, there is for every $\gamma \in (0, 1]$ a $C_\gamma > 0$ such that $|bu| < \gamma\pi/2$ implies

$$\operatorname{sech}(bu)^{1/b^{\alpha}A} \leqq C_\gamma \exp(-u^2/b^{\alpha-2}A).$$

Thus, since

$$\int_{-\infty}^{\infty}\left(\frac{2}{\exp(by)+\exp(-by)}\right)^{1/b^{\alpha}A}dy \geqq 2\int_{0}^{\infty}\left(\frac{2}{2\exp(by)}\right)^{1/b^{\alpha}A}dy$$

$$= 2b^{\alpha-1}A,$$

we therefore take

$$g_b(u) = C_\gamma \exp(-u^2/b^{\alpha-2}A)2b^{\alpha-1}A \quad \text{for} \quad |u| < \gamma\pi/2b$$

and

$$g_b(u) = 2b^{\alpha-1}A\operatorname{sech}(bu)^{1/b^{\alpha}A} \quad \text{for} \quad |u| > \gamma\pi/2b.$$

Note that

$$\int_{\gamma\pi/2b}^{\infty} g_b(u)\,du \leqq 2b^{\alpha-1}A\sum_{k=1}^{\infty}\left(\frac{k\gamma\pi}{2b}\right)\operatorname{sech}\left(\frac{bk\gamma\pi}{2b}\right)^{1/b^{\alpha}A}$$

$$= b^{\alpha-2}A\sum_{k=1}^{\infty}(k\gamma\pi)\operatorname{sech}\left(\frac{k\gamma\pi}{2}\right)^{1/b^{\alpha}A}$$

$$< C_2 2b^{\alpha-2}A.$$

Thus, for $\alpha > 2$

$$\lim_{b\to 0}\int_{\epsilon}^{\infty} g_b(u)\,du = \lim_{b\to 0}\int_{\epsilon}^{\gamma\pi/2b} C_\gamma \exp(-u^2/b^{\alpha-2}A)2b^{\alpha-1}A\,du$$

$$+ \lim_{b\to 0} 2b^{\alpha-2}A\sum_{k=1}^{\infty}(k\gamma\pi)\operatorname{sech}\left(\frac{k\gamma\pi}{2}\right)^{1/b^{\alpha}A}$$

$$= \lim_{b\to 0} \frac{\gamma\pi}{2b} C_\gamma \exp(-\epsilon^2/b^{\alpha-2}A)2b^{\alpha-1}A + 0$$

$$= 0.$$

Also, we observe that

$$\lim_{b\to 0} \int_{-\infty}^{-\epsilon} g_b(u)\, du = \lim_{b\to 0} \int_{\epsilon}^{\infty} g_b(u)\, du = 0.$$

APPENDIX B

Partial Proof of Theorem 3 for Case $\alpha = 2$

Let $p_b(x) = \theta(b)(\text{sech } bx)^{1/b^2\sigma_o^2}$, $b \geqq 0$ for all x on $[-\infty, \infty]$. We will first show $\lim_{b\to 0} \theta(b) = 0$, then $\lim_{b\to 0} p_b(x)$ converges pointwisely to a normal distribution with zero mean and variance σ_o^2.

Proof: From the definition of $p_b(x)$, it follows that

$$p_b(x) = \{\exp[\ln \theta(b) b^2\sigma_o^2](\text{sech } bx)\}^{1/b^2\sigma_o^2}$$

$$\ln p_b(x) = \ln \theta(b) + \frac{\ln \text{sech } bx}{b^2\sigma_o^2}.$$

Then

$$\lim_{b\to 0} \frac{1}{b^2\sigma_o^2} \ln \text{sech } bx = \lim_{b\to 0} \frac{-x \tanh bx}{2b\sigma_o^2}$$

by L'Hopital's rule. Thus, since

$$\lim_{b\to 0} \frac{\tanh bx}{b} = x,$$

we conclude that

$$\lim_{b\to 0} \ln p_b(x) = -\frac{x^2}{2\sigma_o^2},$$

or that

$$\lim_{b\to 0} p_b(x) = \exp\left(-\frac{x^2}{2\sigma_o^2}\right), \qquad \text{the normal distribution.}$$

By using these expressions and equation (17) we can conclude that $p_\alpha'(u)$ is a normal distribution with variance σ_o^2 when $\alpha = 2$.

APPENDIX C

Partial Proof of Theorem 3 for Case $\alpha = 1$

We claim that, when

$$p_{(b,1)}(u) = \frac{\operatorname{sech}(bu)^{1/bA}}{\int_{-\infty}^{\infty} \operatorname{sech}(by)^{1/bA}\, dy},$$

then

$$\lim_{b \to 0} p_{(b,1)}(u) = 0 \quad \text{for all} \quad u.$$

Proof: We observe that

$$p_{(b,1)}(u) \leqq \frac{\operatorname{sech}(bu)^{1/bA}}{\int_{-N}^{N} \operatorname{sech}(by)^{1/bA}\, dy}$$

for all positive integers N.

We show that for every $N > 0$ there is a $\mu > 0$ such that $b < \mu$ implies

$$p_{(b,1)}(u) \leqq 1/2N.$$

We can show, using L'Hopital's rule, that

$$\lim_{b \to 0} \operatorname{sech}(bu)^{1/bA} = 1$$

for all u and A. Thus, for every $\eta > 0$ no matter how small and every $N' \geqq N(1 + \eta)/(1 - \eta)$ we can show that there is a $\mu > 0$ such that by taking $b < \mu$, we have

$$p_{(b,1)}(u) \leqq \frac{1 + \eta}{\int_{-N'}^{N'} (1 - \eta)\, d\eta}.$$

Thus, $b < \mu$ implies

$$p_{(b,1)}(u) \leqq \left(\frac{1 + \eta}{1 - \eta}\right)\left(\frac{1}{2N'}\right) \leqq \frac{1}{2N}.$$

Thus, for every $N > 0$ there is a $\mu > 0$ such that $0 < b < \mu$ implies

$$p_{(b,1)}(u) \leqq \frac{1}{2N}.$$

Hence

$$\lim_{b \to 0} p_{(b,1)}(u) = 0.$$

The proof is completed.

REFERENCES

1. Crandall, S. H., and Mark, W. D., *Random Vibration in Mechanical Systems*, New York: Academic Press, 1963. p. 38.
2. Lax, M., *Brandeis Summer Institute in Theoretical Physical Lectures Notes*, New York: Gordon and Breach Science Publishers, Inc., 1968.
3. Wang, M. C., and Uhlenbeck, G. E., "On the Theory of Brownian Motion II," Rev. Mod. Phys., *17*, Nos. 2 and 3 (April–July 1945), pp. 323–342. Reprinted in *Selected Papers on Noise and Stochastic Processes*, N. Wax, ed., New York: Dover Publications, Inc., 1954.
4. Stratonovich, R. L., *Topics in the Theory of Random Noise*, New York: Gordon and Breach Science Publishers, Inc., 1963, Chapter 4, pp. 62–129.
5. Gray, A. H., "Uniqueness of Steady-State Solutions to the Fokker-Planck Equation," J. Math. Phys., *6*, No. 4 (April 1965), pp. 644–647.
6. Gradshteyn, I. S., and Ryzhik, I. M., *Table of Integrals Series and Products*, New York: Academic Press, 1965.
7. National Bureau of Standards, *Handbook of Mathematical Functions*, Appl. Math. Series 55, M. Abramowitz and I. A. Stegun, editors, 1964, pp. 267–270.
8. Rice, S. O., "Mathematical Analysis of Random Noise," B.S.T.J., *23*, No. 3 (July 1944), pp. 282–332, and *24*, No. 1 (January 1945), pp. 46–156. Reprinted in *Selected Papers on Noise and Stochastic Processes*, N. Wax, ed. New York: Dover Publications, Inc., 1954.

Masking of Crosstalk by Speech and Noise*

By TAPAS K. SEN

(Manuscript received September 24, 1969)

We performed three laboratory experiments of crosstalk thresholds using simulated telephone conversations. Two of these experiments involved masking of crosstalk by noise; the third involved masking of crosstalk by both noise and primary speech. In this paper, we present intelligibility and detectability threshold data from these experiments and discuss the usefulness of the intelligibility threshold data for determining telephone crosstalk objectives.

In general, the crosstalk threshold versus masking noise functions obtained from these experiments agreed fairly well with similar functions published earlier. These functions were found to be linear for high values of noise (about 20 dBrnC and higher) and markedly nonlinear for lower values of noise. For very low noise conditions (about 5-6 dBrnC or lower), crosstalk thresholds were almost independent of noise. Intelligibility thresholds were found to be 8-10 dB higher than the corresponding detectability thresholds and a difference of the same size was found between threshold values obtained (i) with background noise and (ii) with both background noise and background speech.

I. INTRODUCTION

1.1 *General Background*

In the process of transmitting speech over telephone channels, a portion of the speech energy occasionally gets transferred from one channel to another. This transferred energy is technically referred to as crosstalk. The presence of crosstalk in telephone circuits is objectionable for two main reasons. (*i*) Its presence may indicate to customers that they are receiving a telephone service which does not protect their

* The material of this paper was presented before the 74th Meeting of the Acoustical Society of America, 16 November 1967; "Masking of Crosstalk by Speech and Noise," J. Acoust. Soc. Am,. *42*, 1198(A)-1967.

own privacy. (*ii*) It may interfere with speech transmission and thus degrade the circuit quality.

Since the Bell System strives to maintain a certain standard of transmission quality and provide privacy to the customers, it is concerned with controlling all sources of circuit degradation, including crosstalk interference. Designing the telephone plant to guarantee complete absence of energy transfer between channels is not economically feasible. Therefore, to guarantee privacy and to maintain a certain standard of transmission quality, the usual engineering strategy (which is maintained with a high degree of probability) is to limit the crosstalk energy below a threshold such that (*i*) it is not intelligible and (*ii*) it does not subjectively degrade the circuit quality. This threshold is experimentally determined by subjective testing, using simulated telephone connections. It is then translated into engineering terms in the form of a transmission objective.

Prior to the completion of the tests reported here, crosstalk objectives for the telephone plant were based on the results of subjective tests conducted at Bell Telephone Laboratories about 30 years ago.[1] In the intervening period, however, there have been changes in the telephone plant, including the introduction of 500-type new telephone set and the 3A noise measuring set. Although it would have been possible to continue to use the previous data with appropriate conversion factors, a new series of tests was undertaken. This was done even though the difference between the near and earlier results was expected to be small, because small differences in objectives, even in the order of 1 dB, can indeed have important economic consequences in new designs.

One of the important areas of application for the present crosstalk data will be design requirements for new telephone sets. Here, the state-of-the-art now promises the possibility of increased telephone set gain at low cost. However, it also appears that loop crosstalk considerations will probably limit the extent to which this gain can be used to achieve economics in other parts of the plant. In order to facilitate studies of this type, it was considered important to have accurate and up-to-date subjective test results.

In addition to providing for the revision of the earlier crosstalk test results for the intelligibility threshold, the new test series afforded the opportunity to obtain data on the threshold of detectability and on the masking effects of speech as well as noise. Other factors which were considered worthy of study were differences between one-word and several-word intelligibility and the effect of letting the subject control the crosstalk level.

The primary results of the study are in terms of crosstalk coupling

loss which is flat with frequency in the band from approximately 300 to 3300 kHz. In order to apply the results to systems where capacitive rather than flat coupling exists, correction factors must be applied. Appropriate correction factors, based on the results of a comparison study, have been included in Section III of this paper.

1.2 *Purpose of the Experiments*

In order to check the adequacy of the existing crosstalk objectives, transmission engineers need, among other things, psychophysical data on speech intelligibility thresholds for various background noise conditions. Experiment I was designed to collect psychophysical data of this kind; that is, data which could be used by transmission engineers to set transmission objectives for crosstalk.

Experiment II was designed to obtain data on crosstalk thresholds with both noise and primary speech on the circuit. The primary purpose here was to determine the difference between crosstalk threshold values obtained with both background speech and noise, and those obtained with background noise only. Such information is useful in evaluating certain crosstalk phenomenon. However, it should be recognized that in most applications, speech may not always be present to provide additional masking, and objectives must normally be based on the masking effects of noise only. A second purpose of this experiment was to obtain, for each experimental condition, a rating by the subjects of the overall transmission quality. Data on transmission quality ratings serve as important guidelines for establishing Bell System transmission objectives. This paper, however, presents only the threshold data.

Experiment III had essentially the same purpose as Experiment I, but two changes were made in the procedure. First, instead of hearing short sentences for crosstalk as in Experiment I, the subjects heard a recorded 2-way simulated telephone conversation. Second, instead of simply reproducing the crosstalk words heard as was done in Experiment I, each subject used his own criterion for determining intelligibility thresholds. The purpose here was to find if the threshold values and the intersubject variability as obtained in Experiment I could be significantly affected by introducing a somewhat less stringent criterion, namely, the subjects' own judgment about the intelligibility threshold.

II. METHOD

2.1 *Definitions of Thresholds*

Two kinds of speech (or crosstalk) thresholds were measured in these experiments: (*i*) The threshold of detectability, defined as the speech

(or crosstalk) level at which the subject is just able to detect the presence of speech sounds with 50 percent probability. (*ii*) The threshold of intelligibility, defined as the speech (or crosstalk) level at which the subject is just able to understand the meaning of the speech content with 50 percent probability.

2.2 *Psychophysical Methods*

Of the various psychophysical methods which can be used for determining thresholds, we used two in the present experiments. In Experiments I and II, we used the *Method of Limit.* In this, the experimenter controlled the level of the stimulus (crosstalk material) presented to the subjects. The experiment started with the stimulus at a level well below the threshold. The level was increased by small but equal steps in subsequent presentations (a 3 dB step was used in this case). The series was stopped when the level was well above the intelligibility threshold. The next series started with the stimulus at some level above the intelligibility threshold and the level was decreased by the same step of 3 dB. The series was terminated when the level was well below the detectability threshold. At each presentation of the test condition, the subjects gave the desired response. For each subject, the midpoint of the transition between response and no response determined his threshold.

In Experiment III, we used a different psychophysical method, namely the *Method of Adjustment,* to determine the thresholds. This method required the subjects to adjust the stimulus level. For each experimental condition, the subject was first presented with a speech level well below the detectability threshold. He was asked to increase the level until speech was first detectable and then intelligible. Next, he started with a speech level well above the intelligibility threshold and decreased the level until it was no longer detectable.

2.3 *Experimental Conditions*

In Experiment I, five levels of white noise were presented to the subjects. These noise levels, as measured at the line terminals of the telephone set, were 18, 33.5, 38.5, 43.5 and 48.5 dBrnC respectively. (For explanation of dBrnC, see Aikens and Lewinski[2].) Short sentences taken from a list provided by Beranek served as crosstalk material.[3] For each noise level, two different sentences were used, one spoken by a male talker and the other by a female talker. There were thus a total of ten experimental conditions presented to the subjects.

In Experiment II, the same five noise levels used in Experiment I were each combined with five levels of primary speech, thus making a

total of 25 experimental conditions. These 5 speech levels as measured at the line terminals of the telephone set used were −30, −35, −40, −45, and −50 VU respectively.

For each experimental condition in Experiment II, the subjects heard a 30-second simulated telephone conversation between male or female talkers which served as the primary speech in the circuit. Short sentences like those used in Experiment I served as crosstalk materials. For each of the 25 experimental conditions, a different primary speech segment and a different crosstalk sentence were used. Both male and female talkers were used in both. Thus, a test condition could have only male, only female, or a combination of male and female talkers.

In Experiment III the five noise levels of Experiments I and II were retained. However, instead of short Beranek sentences, simulated conversation segments between talkers were used as crosstalk material.

A Northern Electric VU Meter was used for all speech level measurements. One experienced meter reader made all the measurements following recommendations made by Carter and Emling, and as quoted by Brady.[4]

Equivalent Peak Level (epl)[5] measurements were also made on about 25 percent of the speech samples in these experiments. On the average, epl was found to be 10 dB higher than the corresponding VU measure. The standard deviation of the difference (epl-VU) was 0.9 dB.

2.4 *Anchor Conditions*

It was mentioned earlier that the subjects were asked to rate the transmission quality of each experimental condition during Experiment II. In order to give them a general idea of the range of transmission quality usually encountered in the telephone plant, selected speech samples were presented prior to each test session. This was done to anchor their judgment at the extremes of the rating scale. A set of six test conditions was thus presented to the subjects at the beginning of each test session in Experiment II. These consisted of simulated telephone conversations between pairs of talkers which were heard by the subjects through some very poor and some very good simulated telephone connections.

2.5 *Room Noise*

The room noise for Experiments I and II as measured by a sound level meter was 37 dBt,* A-weighting. The similar value for Experiment III was 41 dBt. (Experiment III was performed in a different test room.)

* dBt = dB relative to 0.0002 dynes/cm². This measure was referred to as dBRAP in earlier crosstalk tests by Edson.[1]

2.6 *Experimental Apparatus*

Block diagrams of the laboratory system used in the present experiments are shown and discussed in Appendix A.

2.7 *Procedure*

Two rooms were used in Experiments I and II. The control room contained the equipment required for manipulation during the experiments; the experimental room contained part of the apparatus and the subjects' booths. A test administrator monitored the test conditions using one of 12 parallel receivers in the experimental room.

Normally, eight to ten subjects took part in each experimental session. Before each experiment began, the test administrator reviewed the instructions with the subjects. Each subject was provided with an instruction sheet before the administrator reviewed the instruction.

At the beginning of each session, the subjects listened to the six anchor conditions. They were not required to make any response to these conditions. The actual experimental conditions followed these anchor conditions with a short announcement. To each stimulus condition, the subjects were required to take these steps: (*i*) Indicate whether or not they detected any background speech (that is, crosstalk). (*ii*) Write down all the interfering words that were intelligible. (*iii*) For Experiment II only, rate the transmission quality of the circuit on a 5-point scale.

The 25 test conditions in Experiment II were divided into five groups, each group being presented in one test session. For each subject, five test sessions were required for Experiment II and one session for Experiment I. Each test session in Experiments I and II took from 90 to 100 minutes, and was divided into 2 halves by a short break. No subject took part in more than one session per day. A total of 24 test sessions was required to run all the subjects through Experiments I and II. This was spread over a period of 7 weeks. As indicated earlier, the *Method of Limit* was used in Experiments I and II.

In Experiment III the *Method of Adjustment* was used with one subject at a time taking part in the experiment. Here, the subject was required to adjust a variable attenuator for his threshold settings. Each subject made two settings each for both detectability and intelligibility threshold—one for the crosstalk level going up from low volume to high volume, and the other for the crosstalk level going down from high volume to low volume.

The crosstalk materials used in Experiment III were two 30-second simulated conversations, one between a pair of male talkers and the

other between a pair of female talkers. The same five circuit noise levels were used as in Experiments I and II. The subjects were given the following guidelines for their threshold criteria: (*i*) For the detectability threshold, the level should permit them to detect the presence of speech sounds without understanding them. (*ii*) For the intelligibility threshold, the level should permit them to understand about one complete sentence without appreciable effort. For each subject, one experimental session took approximately one hour.

For all experiments, the test conditions within a session were presented according to some predetermined random order which varied for different sessions. Also, the speech materials for crosstalk and primary conversation were recorded in such a way that the volume (in VU) was maintained at a fairly constant level across conversation segments.

2.8 *Subjects*

Thirty-one subjects, male and female, took part in Experiments I and II. Their ages ranged from 20 to 64. They were selected at random from employees at the Murray Hill location of Bell Telephone Laboratories. Six of these subjects had previous experience with psychoacoustic experiments; the rest had no such previous exposure.

In Experiment III, 39 subjects took part. Fifteen of them were subjects also in Experiments I and II including the six experienced subjects mentioned above.

The subjects were tested for hearing acuity before the experiments. All the subjects had about normal hearing in the range of 500–2000 Hz, considered important for speech intelligibility.

In general, it may be said that in terms of their age, sex, professional background and hearing level, the subjects represent a reasonably good cross section of Bell System customers.

III. RESULTS AND DISCUSSION

3.1 *Thresholds Data—Experiments I and II*

Figure 1 presents the group psychometric functions for detectability thresholds obtained from two experimental conditions providing the same amount of circuit noise. Curve a was obtained with a background noise of 18 dBrnC. Curve b was obtained with a background noise of 18 dBrnC and also a primary speech level of −30 VU. Both noise and VU measurements were made at the line terminals of the subjects' telephone set. The ordinate gives the percentage of the subjects detecting the crosstalk; the crosstalk volumes are plotted on the abscissa.

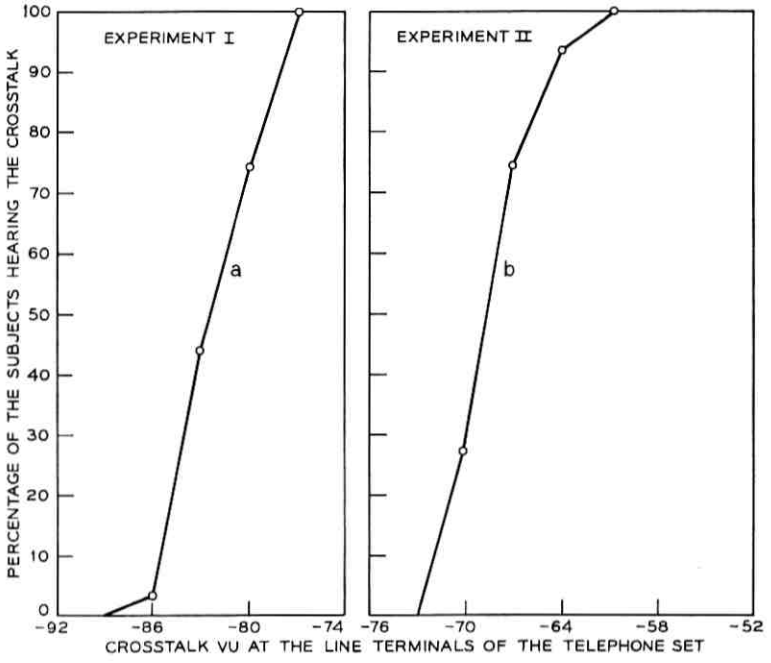

Fig. 1—Cumulative distributions of crosstalk detection, curves a and b refer to two experimental conditions: curve a, circuit noise 18 dBrnC; curve b, circuit noise 18 dBrnC, primary speech −30 VU. All measurements were made at the terminals of the telephone set.

The curves in Fig. 1 were drawn from the raw data. Similar detectability and intelligibility threshold (of one word or more) functions were drawn for all the experimental conditions in Experiments I and II. Since these functions appeared similar to cumulative normal curves, the raw data for each experimental condition were subjected to an unweighted-normal least-squares fit. The Kolmogorov–Smirnov[6] test was applied to determine any significant difference between the actual and the fitted cumulative normal curves. No difference was observed at the 5 percent level of significance. Group detectability and intelligibility thresholds were then obtained by finding the speech (or crosstalk) level corresponding to the 50 percent point on the fitted cumulative threshold function for each experimental condition.

Group threshold for each experimental condition was also calculated from the raw data by simply taking the average of all the subjects' individual thresholds for that condition as obtained from the *Method of Limit*.

A comparison between the threshold values of actual and fitted data for Experiments I and II is presented in Table I. Notice that the threshold values for corresponding experimental conditions are about the same. In Experiment I, two crosstalk sentences were used for each noise condition, one spoken by a male talker and the other by a female talker. In this table, they have been indicated by M and F respectively. The threshold values for these two sentences have been averaged for each noise condition since they were not significantly different. (In general, no significant difference in the threshold data was found between male and female talkers in any of the three experiments.) For Experiment II, the table presents the threshold values for each of the 25 experimental conditions. For each noise condition, the threshold values for the five primary speech levels were also averaged. All intelligibility threshold values in Table I are for intelligibility of *one word or more.*

Table II presents the standard deviation values corresponding to the mean thresholds of Table I as used for the least-squares normal fit. The data are presented for Experiment II only. On the average, variability in intelligibility threshold was found to be much larger than in detectability threshold.

For Experiment I, however, where there was no background speech as in Experiment II, variability in the threshold data was much lower and consistent over the range of noise levels used. For intelligibility threshold, standard deviation was of the order of 2.5 dB, and for detectability threshold, it was of the order of 2.0 dB. These values were used for the normal least-squares fit.

For any noise level in Experiment II, notice the change in threshold as a function of primary speech level as shown in Fig. 2. For detectability, no significant change in threshold values was observed over a 20 dB range of primary speech level (from -30 VU to -50 VU) for the four high noise levels between 33.5 and 48.5 dBrnC. However, with the low noise level (that is, 18 dBrnC), a threshold difference of 8.5 dB was found between the lowest and the highest speech level. In the case of intelligibility, the corresponding threshold shifts were found to be much larger. But here again, as in the case of detectability threshold, the ranges of the threshold shifts were relatively smaller for higher noise levels, as compared to the one obtained for 18 dBrnC.

Figure 3 presents the summary of the test results of Experiments I and II in terms of threshold as a function of circuit noise level. For Experiment II, each data point represents the average of the five threshold values (corresponding to five primary speech levels) for each circuit noise condition. For Experiment I, each data point represents the average of the two threshold values (male and female talkers) for each

TABLE I—GROUP CROSSTALK THRESHOLD FOR DIFFERENT EXPERIMENTAL CONDITIONS IN EXPERIMENTS I AND II

		Intelligibility Threshold Noise Level* (dBrnC)					Detectibility Threshold Noise Level (dBrnC)					
		18	33.5	38.5	43.5	48.5	18	33.5	38.5	43.5	48.5	
Fitted Data Primary Speech Level (VU)*	†M	−74.0	−62.9	−58.0	−50.9	−47.4	−82.0	−71.9	−67.6	−60.9	−55.2	Experiment I
	F	−76.0	−60.0	−55.0	−52.0	−45.3	−85.0	−73.1	−66.1	−61.8	−55.4	
	Avg.	−75.0	−61.4	−56.5	−51.4	−46.4	−83.5	−72.5	−66.8	−61.3	−55.3	
	−30	−50.4	−43.1	−40.5	−38.2	−31.9	−68.3	−60.9	−56.9	−52.0	−47.9	
	−35	−61.8	−44.1	−40.1	−43.0	−36.2	−72.4	−61.4	−57.2	−52.3	−47.8	
	−40	−54.6	−51.9	−47.4	−42.7	−40.9	−68.6	−63.6	−56.6	−54.3	−47.4	Experiment II
	−45	−53.0	−52.0	−47.3	−45.5	−39.1	−72.5	−65.4	−58.1	−57.0	−50.2	
	−50	−64.6	−54.4	−52.0	−46.3	−42.4	−78.5	−62.6	−62.7	−53.7	−46.7	
	Avg.	−56.9	−49.1	−45.5	−43.1	−38.1	−72.1	−62.8	−58.3	−53.9	−48.0	
Raw Data Primary Speech Level (VU)	M	−75.8	−62.8	−59.5	−50.2	−48.2	−82.2	−72.3	−67.7	−61.3	−55.0	Experiment I
	F	−77.2	−60.2	−54.1	−52.7	−44.2	−85.0	−72.8	−66.4	−62.0	−55.2	
	Avg.	−76.5	−61.5	−56.8	−51.4	−46.1	−83.6	−72.5	−67.0	−61.6	−55.1	
	−30	−51.0	−44.8	−40.3	−37.2	−33.5	−68.5	−61.3	−56.9	−52.2	−48.4	
	−35	−61.0	−45.0	−40.6	−41.3	−37.8	−73.8	−61.9	−57.0	−52.3	−48.8	Experiment II
	−40	−52.7	−50.8	−45.4	−41.9	−38.7	−68.0	−63.1	−57.9	−54.9	−48.1	
	−45	−54.3	−50.0	−45.8	−45.6	−39.4	−72.9	−65.5	−57.9	−56.5	−50.8	
	−50	−64.3	−54.0	−50.4	−47.2	−42.4	−77.7	−63.1	−62.8	−55.3	−48.7	
	Avg.	−56.7	−48.9	−44.5	−42.6	−38.4	−72.2	−63.0	−58.5	−54.2	−49.0	

* All noise and speech levels were measured at the line terminals of the subject's telephone set.
† M and F refer to male and female crosstalk sources respectively.

TABLE II—STANDARD DEVIATIONS ASSOCIATED WITH CORRESPONDING MEAN VALUES OF EXPERIMENT II PRESENTED IN TABLE I

	Intelligibility Threshold Noise Level (dBrnC)					Detectibility Threshold Noise Level (dBrnC)				
	18	33.5	38.5	43.5	48.5	18	33.5	38.5	43.5	48.5
−30	2.1	2.9	8.4	8.8	5.0	3.0	4.4	2.8	2.6	3.5
−35	6.3	7.0	8.1	5.5	5.2	4.7	2.0	2.1	3.0	3.6
−40	6.2	5.5	5.0	4.2	5.5	5.0	3.4	2.3	2.3	2.0
−45	8.9	8.0	5.3	2.9	1.7	3.4	2.6	3.1	1.9	3.5
−50	6.3	3.0	6.4	2.5	8.0	6.4	3.2	1.2	3.3	6.3

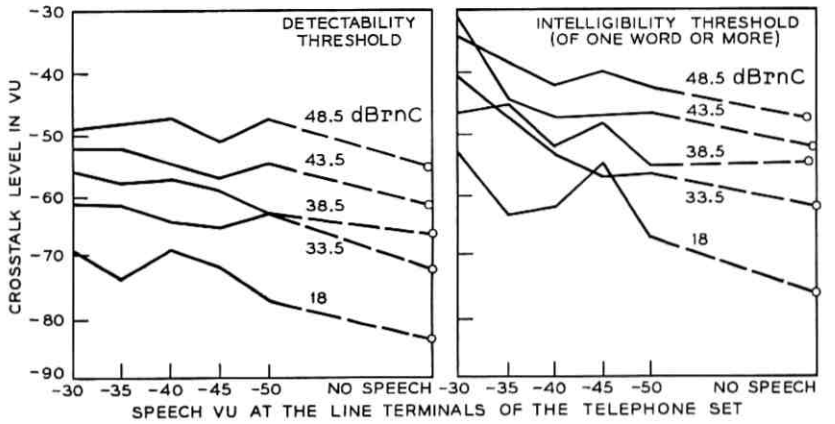

Fig. 2—Crosstalk threshold as a function of primary speech in the circuit. The different curves are for different values of circuit noise in dBrnC.

circuit noise condition. Two curves have been drawn for each experiment, one for the detectability threshold and one for the intelligibility threshold. These threshold functions show two important characteristics: (*i*) they are linear for the high noise levels and show a tendency to bend at the lower noise levels, and (*ii*) on the average, there is about a 10 dB shift between detectability threshold and intelligibility threshold.

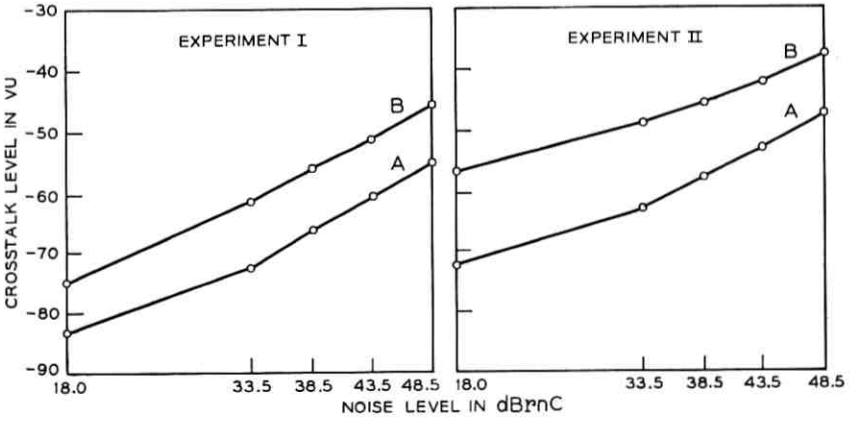

Fig. 3—Crosstalk threshold as a function of circuit noise. A represents detectability threshold; B, intelligibility threshold.

How do the threshold functions of Experiment I (with noise as background) compare with those of Experiment II (with both noise and primary speech as background)? Figure 4 presents this comparison. Two functions from each experiment have been presented, one for the detectability thresholds and one for the intelligibility thresholds. A very interesting finding comes out of this comparison: the detectability threshold function of Experiment II is about the same as the intelligibility threshold function of Experiment I. This suggests that crosstalk which is barely detectable in a circuit when people are talking becomes just intelligible when people pause or stop talking. Crosstalk objectives for the telephone plant are, however, based on threshold data obtained in the absence of any primary speech, that is, the kind of data obtained from Experiment I here.

3.2 *Comparison with Earlier Data*

Several other studies also have investigated the problem of masking of speech by noise. Unfortunately, due to lack of complete information, most of the previous data cannot be properly converted for precise comparison with the present data. However, there are two sets of data (Hawkins and Stevens[7] and Edson[8]) which could be compared with the present data (Experiment I) with proper conversions.

Figure 5 presents the comparison between Hawkins' and Stevens' data and those obtained from Experiment I. The dBrnC and VU readings of

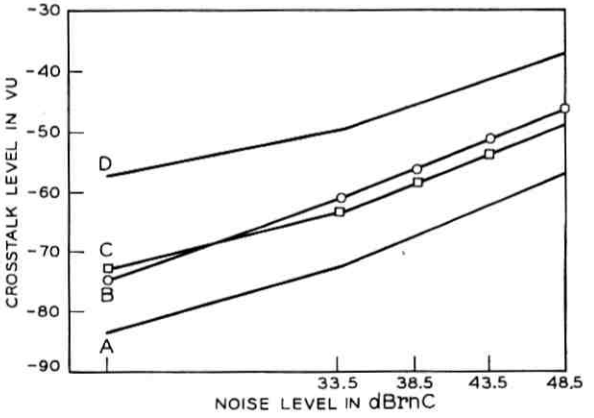

Fig. 4—Crosstalk threshold as a function of circuit noise. A represents detectability threshold and B, the intelligibility threshold in Experiment I; C, the detectability threshold and D, the intelligibility threshold in Experiment II.

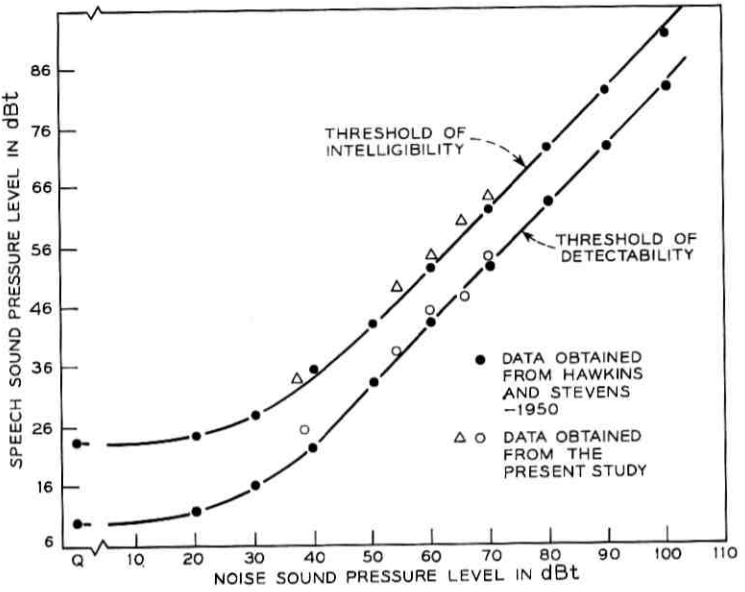

Fig. 5—Speech threshold as a function of background noise: a comparison between the present data and Hawkins–Stevens data.

the present data have been converted to noise and speech sound pressure levels respectively.

A portion of the experimental setup used by Hawkins and Stevens is shown in Fig. 6. In general, three main differences can be pointed out between their experimental conditions and those in Experiment I: (*i*) They used a PDR-10 earphone having a flat response over a much wider frequency band than the U1 telephone receivers used in the present experiments. (*ii*) They used a continuous passage as speech material whereas in Experiment I short sentences were used for the same purpose. (*iii*) They used the *Method of Adjustment*, that is, the subjects themselves adjusted the speech level and judged their own intelligibility threshold.

In Experiment I, on the other hand, the *Method of Limit* was used; that is, the speech level was controlled by the experimenter and the intelligibility threshold was based on the number of correct words reproduced by the subjects. Also, Hawkins and Stevens used a small group of four trained subjects; whereas in Experiment I, a total of 31 subjects were used. In spite of these differences, however, the agreement between the two sets of data is very good. On the average, corresponding

threshold values between the two sets of data differ by less than 2 dB.

Edson's 1952 data had to be corrected for proper comparison with the present data. The final comparison between Edson's data and the present data is shown in Fig. 7. Both measurements are at the line terminals of a 500 type telephone set. The average difference between corresponding threshold values in the two sets of data is of the order of 4 dB here. It should be pointed out, however, that the present data points are for "one word or more intelligibility," whereas Edson's data points are for "four words or more intelligibility." Assuming that these two criteria produce a difference of about 2 to 2.5 dB (this was generally observed in Experiment I), the average difference between Edson's 1952 data and the present data for corresponding thresholds turns out to be of the order of 2 dB. Considering the various differences between the two sets of experimental conditions, a difference of this size is quite probable.

Experiment III was designed to check how much the results of Experiment I might differ by introducing a criterion for the intelligibility threshold which was not so well defined as in Experiment I and also by changing the criterion of intelligibility from "one word or more" to "about a sentence" in a continuous crosstalk situation. The subjects themselves adjusted the level of crosstalk for the threshold and used their own judgment to decide about both detectability and intelligibility thresholds. Both intelligibility and detectability thresholds were

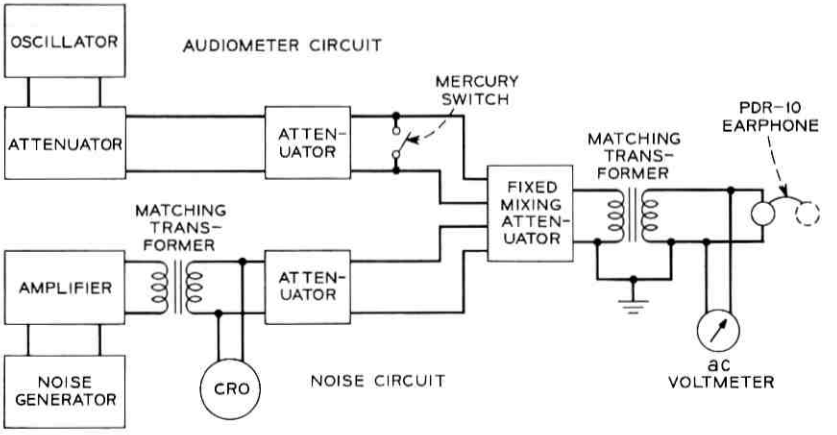

Fig. 6—Block diagram of the apparatus used for the measurement of pure tone threshold in the quiet and in the presence of white masking noise. (From Hawkins-Stevens.)

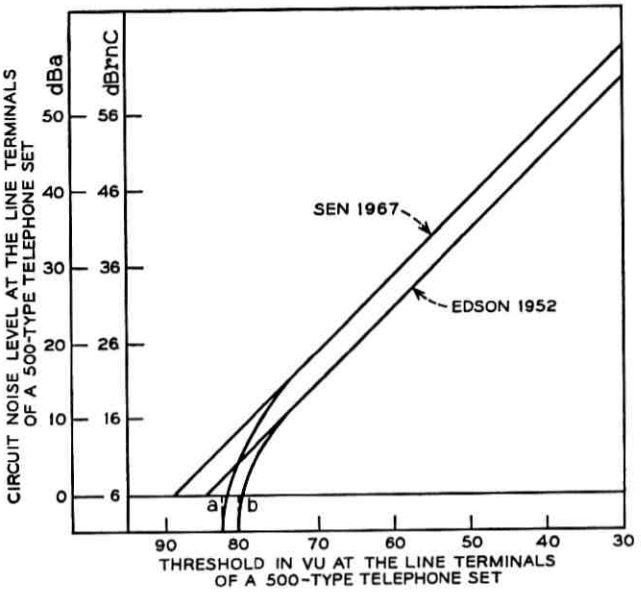

Fig. 7—Crosstalk intelligibility threshold as a function of noise. Note: Data points for noise levels below 18 dBrnC were taken from six trained subjects only in Sen's experiment.

found to be higher in Experiment III than their corresponding values in Experiment I. The average differences were 2.0 dB for intelligibility threshold, and 3.1 dB for detectability threshold. Actual differences were, however, larger for low noise levels than for high noise levels. It may be recalled that the threshold values in Experiment I are 50 percent threshold values. The threshold values of Experiment III compare with 80–90 percent threshold values for corresponding conditions in Experiment I. In other words, while using the *Method of Adjustment*, the subjects preferred to be more than 50 percent confident in making their threshold settings. The average standard deviation was found to be 2.8 dB as compared to 2.5 dB in Experiment I. A comparison between the results of Experiments I and III is shown in Table III.

3.3 *Crosstalk Thresholds for Flat and Capacitive Coupling Systems*

While considering the use of the present data (from Experiment I) for setting transmission objectives, it should be remembered that the experiments reported here were performed using only flat crosstalk coupling between adjacent channels. The data are, therefore, directly

applicable to carrier systems.* A legitimate question, however, arises concerning the applicability of these data for the voice frequency systems in the lower frequency range where the coupling loss between adjacent channels is reduced by 6 dB per octave because of capacitive coupling.

To find out the difference in crosstalk intelligibility thresholds between the two above-mentioned cases, that is, flat and capacitive crosstalk coupling between adjacent channels, an experiment was recently performed by Koenig[9] using both males and females as crosstalk sources. It was found that the capacitive coupling system was, on the average, 2.0 dB more sensitive than the flat coupling system for male crosstalk and 1.06 dB more sensitive for female crosstalk. To be on the conservative side, therefore, it is recommended that in setting crosstalk objectives for the voice frequency systems using the present data from Experiment I, the obtained intelligibility thresholds should be lowered by 2.0 dB.

IV. SUMMARY AND CONCLUSIONS

This paper describes three recently performed laboratory experiments on crosstalk thresholds and presents the results. The experiments were performed using simulated telephone conversations. Detectability and intelligibility thresholds of crosstalk were obtained from the subjects. Thirty-one subjects were used in Experiments I and II, and 39 in Experiment III. Fifteen of these subjects took part in all three experiments. The subjects were chosen from among employees at the Murray Hill location of Bell Telephone Laboratories. Most of them had no previous experience in subjective tests of transmission quality.

Experiment II used both primary speech and circuit noise as masking stimuli while for Experiment I circuit noise was the only masking stimulus. The same five noise conditions were used in both experiments. The primary speech in Experiment II appeared in five levels. In both experiments, the experimenter controlled all levels of speech and noise. The subjects were required to indicate the presence and absence of crosstalk and reproduce the crosstalk words heard whenever they were intelligible. Short sentences spoken by both male and female talkers were used as crosstalk material.

Experiment III was in a way, a repeat of Experiment I with two major exceptions: (*i*) A continuous simulated telephone conversation instead of short sentence was used as crosstalk material. (*ii*) The subjects

* Because the coupling loss between adjacent channels is effectively flat or independent of frequency.

TABLE III—A COMPARISON BETWEEN THE RESULTS OF EXPERIMENTS I & III

Experiment I. Crosstalk Material: Short Beranek Sentences

	Intelligibility Threshold					Detectibility Threshold				
	NOISE LEVEL IN DBRNC									
	18	33.5	38.5	43.5	48.5	18	33.5	38.5	43.5	48.5
M	−75.8	−62.8	−59.5	−50.2	−48.2	−82.2	−72.3	−67.7	−61.3	−55.0
F	−77.2	−60.2	−54.1	−52.7	−44.2	−85.0	−72.8	−66.4	−62.0	−55.2
Avg.	−76.5	−61.5	−56.8	−51.4	−46.1	−83.6	−72.5	−67.0	−61.6	−55.1

Experiment III. Crosstalk Material: Simulated Conversations.

	Intelligibility Threshold					Detectibility Threshold				
	NOISE LEVEL IN DBRNC									
	18	33.5	38.5	43.5	48.5	18	33.5	38.5	43.5	48.5
M	−73.3	−59.6	−55.4	−51.0	−45.3	−79.8	−67.6	−62.1	−58.0	−53.4
F	−72.1	−58.4	−54.1	−50.3	−45.0	−80.1	−68.5	−64.0	−60.5	−55.2
Avg.	−72.7	−59.0	−54.8	−50.6	−45.1	−79.9	−68.0	−63.0	−59.2	−54.3

themselves controlled the crosstalk volume for obtaining thresholds. The criterion for intelligibility threshold was "about one sentence being understood."

In general, the results obtained from Experiments I and III agree fairly well with similar data published earlier. For circuit noise levels above 25 dBrnC measured at the line terminals of a 500-type telephone set, the crosstalk threshold increased almost linearly with noise. In the range of 10 to 25 dBrnC, the "threshold versus noise function" was found to be nonlinear. For low noise (below 10 dBrnC) levels, the threshold was found to be almost independent of noise, that is, the slope of the "threshold versus noise function" is almost zero. The data for low noise levels below 10 dBrnC were obtained from a supplementary experiment using six of the trained subjects.

In Experiment II, where primary speech was also introduced into the circuit, the "threshold versus noise function" was also approximately linear for high-noise level. No data were collected for low-noise level. It was also found in this experiment that a 20 dB shift in the primary speech level between -30 and -50 VU did not produce a significant change in the crosstalk threshold; the main variable affecting the threshold was noise. The five threshold values, corresponding to the five primary speech levels, were therefore averaged for each of the five noise conditions. These values were found to be approximately 10 dB higher than the corresponding values obtained in Experiment I where no primary speech was used. Within each experiment, the intelligibility threshold values were approximately 10 dB higher than the corresponding detectability threshold values. Also for the same amount of noise, the detectability threshold in the presence of speech was about the same as the intelligibility threshold in the absence of speech.

In terms of actual threshold values, the present data from Experiment I agreed extremely well with similar data published by Hawkins and Stevens when proper transformations were carried out. Exact transformation of Edson's data for comparison with the present data could not be done for lack of certain information. So the best possible transformation based on available information was carried out. Comparison of the threshold values for "four words or more" intelligibility showed a difference of the order of 2 dB between Edson's 1952 data and the present data. Considering that there were several differences in the experimental conditions, the latter difference seems quite reasonable. Comparison with any other data on similar studies was not possible because enough information was not available for proper transformation of those data.

The intersubject variability in the present data was found to be rather small, the average standard deviation being of the order 2.5 dB. This figure agrees very well with variability figures published by Falconer and Davis for similar experiments.[10] Most other authors did not supply any figures for intersubject variability but in a paper summarizing the results of masking of speech experiments Miller mentioned that in experiments of this type, the variability between subjects is usually very small.[11]

Finally, there is one suggestion about the criterion of intelligibility threshold that should be considered in setting transmission objectives for crosstalk. Intelligibility of "four words or more" has generally been used. Based on the small variability of the present data as discussed in the preceding paragraph, it is however suggested that a more stringent criterion, that is, intelligibility of "one word or more" should be seriously considered. While analyzing the results of the present experiments it was observed that when one word became easily intelligible, quite a few other words were also intelligible with a high frequency, except in rare cases where one particular word was considerably louder than the average speech level.

V. ACKNOWLEDGMENTS

The author is thankful to the following people who provided valuable help at different stages of this research project: Messrs. M. L. Almquist, Jr., P. T. Brady, P. D. Bricker, C. V. Fanuele, B. C. Griffith, R. W. Hatch, E. T. Klemmer, H. Levitt, D. A. Lewinski, L. M. Padula, H. R. Silbiger, T. C. Spang, J. L. Sullivan, and H. V. Winterberg, and Misses M. Fligiel, A. Kimura and B. Perlmutter.

APPENDIX A

A.1 *Apparatus Used in Experiments I and II*

The laboratory setup for Experiments I and II is shown in Fig. 8 in the form of a block diagram. A 2-channel tape recorder (A) served as the stimulus source, one channel providing the primary speech in Experiment II and the other channel providing crosstalk. A second tape recorder (B) was used for playing the six anchor conditions. The outputs from the 2-channel tape recorder were passed through two 600 ω attenuators, one for each channel, into a 600 ω mixing pad (C). A white noise generator was connected to one port of this mixing pad through a 1 : 1 bridging coil and a 600 ω attenuator designated as NS. The output of this mixing pad was connected to a standard 500-type telephone set through a McIntosh 10 watt program amplifier (No. 2), a 10-dB pad

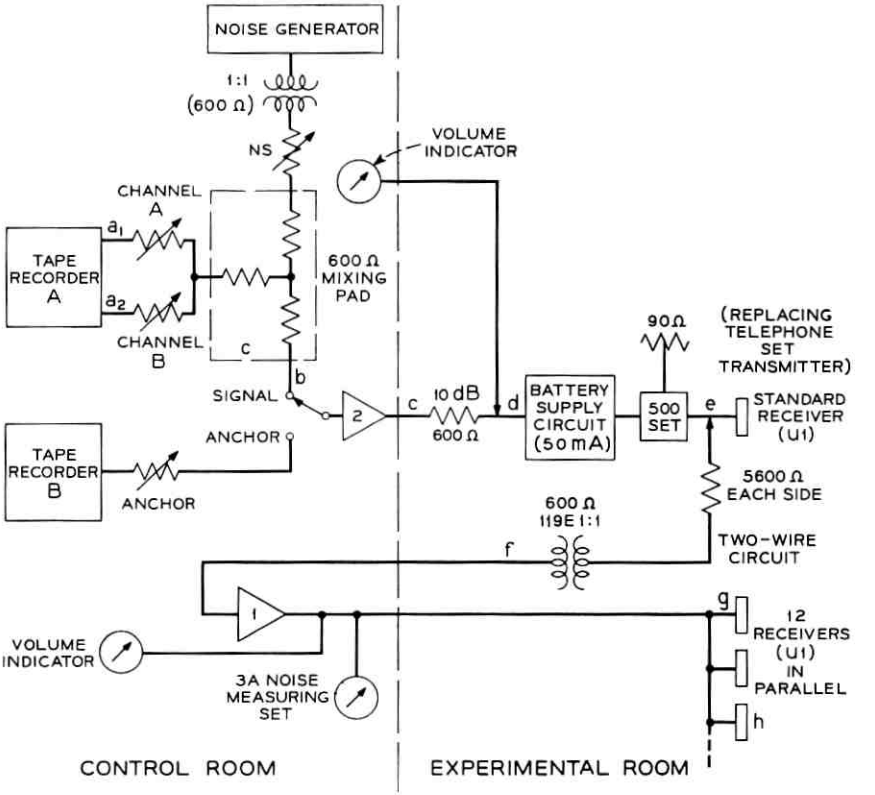

Fig. 8—Laboratory system for crosstalk Experiments I and II.

and a battery supply circuit providing 50 milliamps of current to the telephone set. The transmitter of the telephone set was replaced by a 90 ω resistor and the receiver was connected to 12 other receivers in parallel by means of a bridging arrangement comprising 2 resistors (5,600 ω each), a transformer, and another McIntosh 10 watt program amplifier (No. 1). The purpose of this amplifier was to equate the signal level at each of the 12 receivers with that in the standard receiver. Each one of the 12 parallel receivers (with the associated handset) was located in a separate booth thus permitting testing 12 subjects at a time.

A.2 *Apparatus Used in Experiment III*

The laboratory setup for Experiment III is shown in Fig. 9. This system is a simple version of the one shown in Fig. 8. A tape recorder was used for the crosstalk source. The attenuator termed SUBJECT was a 600 ω continuously variable attenuator which the subject used for

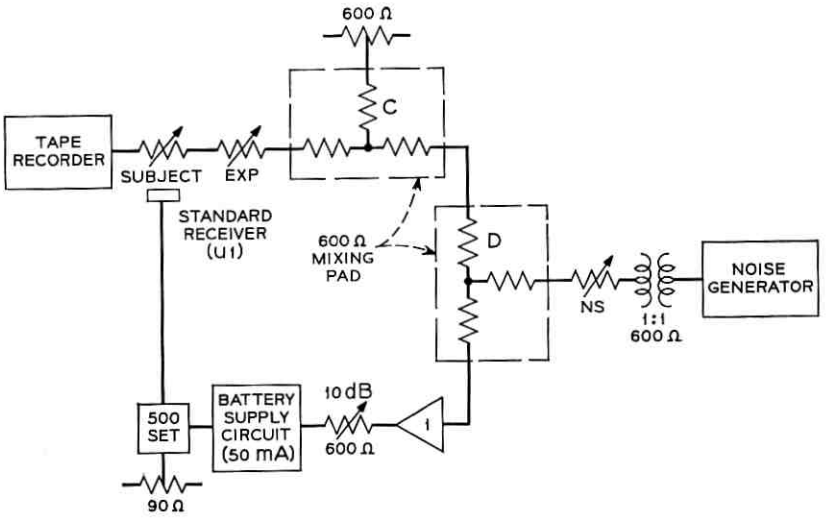

Fig. 9—Laboratory system for crosstalk Experiment III.

adjusting the crosstalk speech level. The attenuators termed EXP and NS were 600 ω attenuators which were under the control of the experimenter. The 600 ω mixing pad (C) was retained in the circuit so that primary speech could also be introduced if wanted. When no such primary speech was used, one port was terminated with a 600 ω resistor. The output of the mixing pad (C) was passed through a similar mixing pad (D) one side of which was connected to a white noise generator through a 600 ω attenuator termed NS and a 1 : 1 bridging coil since the noise generator was unbalanced.

A.3 *Frequency Response of the Experimental System*

Figure 10 presents the frequency response curve of the experimental system used in Experiments I and II. A graphic level recorder was used to plot this electrical to acoustic response of the system. The output of the oscillator was fed to channel A attenuator as shown in Fig. 8. Both A and B attenuators were set at high values and the input to the noise attenuator was terminated in 600 ω. Figure 10 shows the result from receiver No. 6 which had the average sound pressure level of all the 12 receivers used in the experiments. Results from other receivers were similar. The level recorder was plugged into the recorder jack of a B&K amplifier. The calibration was made at 1000 Hz point to correspond to the sound pressure level obtained for No. 6 receiver. The

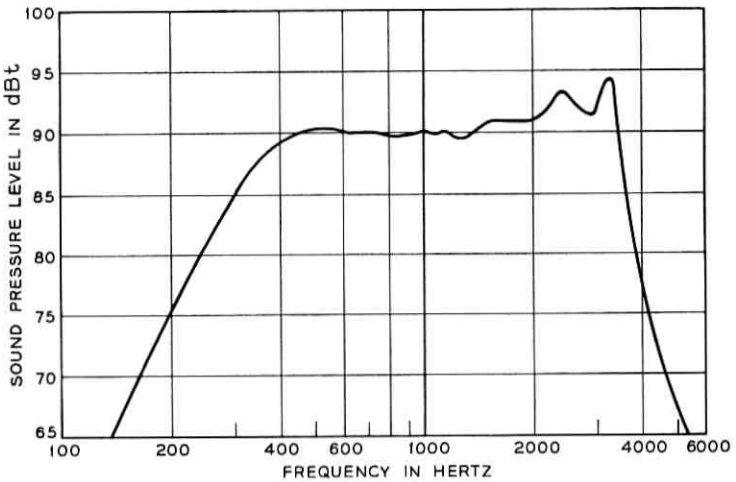

Fig. 10—Frequency response curve of the Laboratory system used in Experiments I and II.

frequency response of the system used in Experiment III was found to be similar.

A.4 *Calibration Data of the Experimental System*

Table IV presents the calibration data for the laboratory system used in Experiments I and II. A calibration tape was used for the bridging and terminated measurements. The input to the noise attenuator was terminated in 600 ω and A&B attenuators were set at 0 dB.

A.5 *Receiver Calibration*

Table V presents the receiver calibration data in terms of dB SPL values. The sound pressure levels (SPL in dB) of the receivers used in

TABLE IV—1000 CYCLE CALIBRATION FIGURES FOR THE LABORATORY SYSTEM SHOWN IN FIGURE 8

Location in the System	600 ω Termination*	Bridging*
a_1	−7 dBO†	−12 dBO
a_2	−7 dBO	−12 dBO
b	−18 dBO	−18 dBO
c	+2.5 dBO	+2.5 dBO
d	−7.5 dBO	−7.5 dBO
e	—	−19.5 dBO
f	−46 dBO	−45.5 dBO
g	—	−19 dBO

* A VU-meter was used to measure the levels of the 1000 Hz tone.
† dBO corresponds to .775 volt.

TABLE V—RECEIVER CALIBRATION DATA

Receiver No.	dB SPL
1	101.9
2	102.9
3	102.9
4	103.2
5	102.4
6	102.7
7	102.5
8	103.1
9	102.6
10	102.5
11	102.7
12	102.8
Standard Receiver	103.2

Note: The overall 250-3000 Hz variation of all the receivers relative to the standard receiver was within ± 1 dB.

Experiments I and II were determined by using an Artificial Ear system. A 1000 Hz calibration tone was used. Its level was −7.5 dBo at the point d in Fig. 8. The attenuators A and B were set to zero and the noise input was terminated in 600 ω. The standard receiver refers to the one shown in Fig. 8.

REFERENCES

1. Edson, R. C., "Tests for Determining the Intelligibility of Crosstalk Volumes," 1938, unpublished work.
2. Aikens, A. J., and Lewinski, D. A., "Evaluation of Message Circuit Noise," B.S.T.J., *39*, No. 4 (July 1960), pp. 879–910.
3. Beranek, Leo L., *Acoustic Measurements*, New York: John Wiley & Sons. 1962, pp. 774–777.
4. Brady, P. T., "A Statistical Basis for Objective Measurements of Speech Levels," B.S.T.J., *44*, No. 7 (September 1965), pp. 1453–1486.
5. Brady, P. T., "Equivalent Peak Level: A Threshold-Independent Speech-Level Measure," Journal Acoustical Society of America, *44*, No. 3 (September 1968), pp. 695–699.
6. Siegel, Sidney, *Nonparametric Statistics for the Behavioral Sciences*, New York: McGraw-Hill, 1956, pp. 47–52.
7. Hawkins, J. E., Jr., and Stevens, S. S., "The Masking of Pure Tones and of Speech by White Noise," Journal Acoustical Society of America, *22*, No. 1 (January 1950), pp. 6–13.
8. Edson, R. C., "Summary of Data from Crosstalk Intelligibility Tests and Results Obtained in Methods for Judging Interference Effects," 1952, unpublished work.
9. Koenig, A. H., "Crosstalk—Comparison of Two Frequency Shaping Systems vs Flat System Relative to Detectability and Intelligibility Thresholds," 1969, unpublished work.
10. Falconer, G. A., and Davis, H., "The Intelligibility of Connected Discourse as a Test for the Threshold for Speech," The Laryngoscope, *57*, No. 9 (September 1947), pp. 581–595.
11. Miller, G. A., "The Masking of Speech," Psychological Bulletin, *44*, No. 2 (March 1947), pp. 105–129.

Contributors to This Issue

D. K. Cohoon, B. S., 1962, Massachusetts Institute of Technology; M. S., 1964, and Ph.D., 1969, Purdue University; Bell Telephone Laboratories, 1968–1969. At Bell Telephone Laboratories Mr. Cohoon undertook the analysis of boundary value problems in the areas of heat transfer and wave propagation. In September 1969, he accepted a Postdoctoral Research Associateship at the University of Wisconsin to study the theory of partial differential equations. Member, American Mathematical Society.

S. C. Liu, B.S. in C.E., 1960, National Taiwan University; M.S., 1964, and Ph.D., 1967, University of California at Berkeley; Bell Telephone Laboratories, 1967—. Mr. Liu has been doing research in applied mechanics, structural dynamics, random vibrations and earthquake engineering. Member, American Society of Civil Engineers, Seismological Society of America.

William K. Pehlert, Jr., B. S., 1959, Drexel Institute of Technology; M. S., 1961, Ph.D., 1966, University of Pennsylvania; U. S. Army, 1961–1963; Bell Telephone Laboratories, 1968—. Mr. Pehlert works in channel characterization and performance analyses of error control systems for data transmission. Member, IEEE, Eta Kappa Nu, Tau Beta Pi, Phi Kappa Phi, Sigma Xi.

Tapas K. Sen, B. Sc. (Physical Sciences), 1951, M. Sc. (Psychology), 1954, Calcutta University; Ph.D. (Psychology), 1963, The Johns Hopkins University; Bell Telephone Laboratories, 1963—. Mr. Sen has been doing human factors research concerning Bell System transmission objectives. He is primarily concerned with the subjective effects of physical interference on both audio and video transmission. Member, American Psychological Association, Optical Society of America, Human Factors Society, Psychonomic Society, AAAS.

S. Y. Tong, B. S., 1955, Taiwan University; M. S., 1961, University of Vermont; Ph.D., 1966, Princeton University; Bell Telephone Laboratories, 1964—. Mr. Tong's current interest is error control in both data transmission and data processing systems. Member, IEEE, American Association for the Advancement of Science, Sigma Xi.

B.S.T.J. BRIEFS

Charge Coupled Semiconductor Devices

By W. S. BOYLE and G. E. SMITH

(Manuscript received January 29, 1970)

In this paper we describe a new semiconductor device concept. Basically, it consists of storing charge in potential wells created at the surface of a semiconductor and moving the charge (representing information) over the surface by moving the potential minima. We discuss schemes for creating, transferring, and detecting the presence or absence of the charge.

In particular, we consider minority carrier charge storage at the Si-SiO_2 interface of a MOS capacitor. This charge may be transferred to a closely adjacent capacitor on the same substrate by appropriate manipulation of electrode potentials. Examples of possible applications are as a shift register, as an imaging device, as a display device, and in performing logic.

A new semiconductor device concept has been devised which shows promise of having wide application. The essence of the scheme is to store minority carriers (or their absence) in a spatially defined depletion region (potential well) at the surface of a homogeneous semiconductor and to move this charge about the surface by moving the potential minimum. A variety of functions can then be performed by having a means of generating or injecting charge into the potential well, transferring this charge over the surface of a semiconductor, and detecting the magnitude of the charge at some location. One method of producing and moving the potential wells is to form an array of conductor-insulator-semiconductor capacitors and to create and move the potential minima by applying appropriate voltages to the conductors. The purpose of this paper is to describe the operation of this basic structure and some possible applications. We present calculations which show feasibility for a simple silicon-silicon dioxide MOS structure.

First consider a single MIS structure on an n-type semiconductor. A diagram of energy vs. distance is shown in Fig. 1 for an applied voltage difference V_1 in which the metal is negative with respect to the semiconductor and large enough to cause depletion. When the

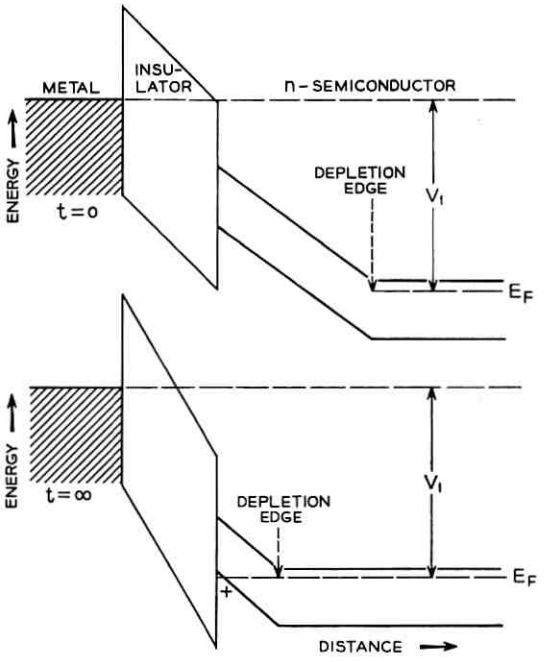

Fig. 1—A plot of electron energy vs distance through an MIS structure both with (at time $t = \infty$) and without (at time $t = 0$) charge stored at the surface.

voltage is first applied at $t = 0$, there are no holes at the semiconductor-insulator interface and the voltage is divided between the semiconductor and insulator as shown. If holes are introduced into the depletion region by some means, they will collect at the semiconductor interface causing the interface potential to become more positive. Eventually the situation shown in Fig. 1 for $t = \infty$ is reached. This is the steady state condition for the structure and it occurs when the valance band at the interface is approximately at the same energy as the Fermi level E_F in the bulk. Any further introduction of holes will cause the interface potential to become yet more positive and holes will be injected into the bulk until the steady state condition is again reached.

Now, consider the linear array of MIS structures on an n-type semiconductor as shown in Fig. 2 where every third electrode is connected to a common conductor. As an initial condition, a voltage $-V_2$ is applied to electrodes 1, 4, 7, and so on, and a voltage $-V_1$ ($V_2 > V_1$) is applied to the other electrodes. The semiconductor is held at zero potential and the V_i's are taken as positive numbers. It is assumed

that $V_1 > V_T$ where V_T is the threshold voltage for the production of inversion under steady state conditions. The edge of the depletion region is indicated by the dashed line. Also, as an example, positive charge is placed under electrodes 1 and 7 and none under electrode 4, as indicated in Fig. 2(a). Now a voltage $-V_3$ ($V_3 > V_2$) is applied to electrodes 2, 5, 8, and so on, as shown in Fig. 2(b) and the charge will transfer from electrode 1 to the potential minimum under electrode 2, and so on. The voltages are now changed to the condition of Fig. 2(c) and, as shown, charge has been shifted one spatial position and the sequence is ready to be continued.

It has been assumed in the foregoing that the voltages were applied and manipulated in a time shorter than the storage time τ where $\tau = Q/I_d$ is the time for the thermally generated current I_d to supply the equilibrium charge density Q. The thermal current I_d results from generation-recombination centers in the depletion region and at the semiconductor-insulator interface. Storage times of the order of seconds have been reported.[1-3]

It is of interest now to consider the capacitance and surface potential

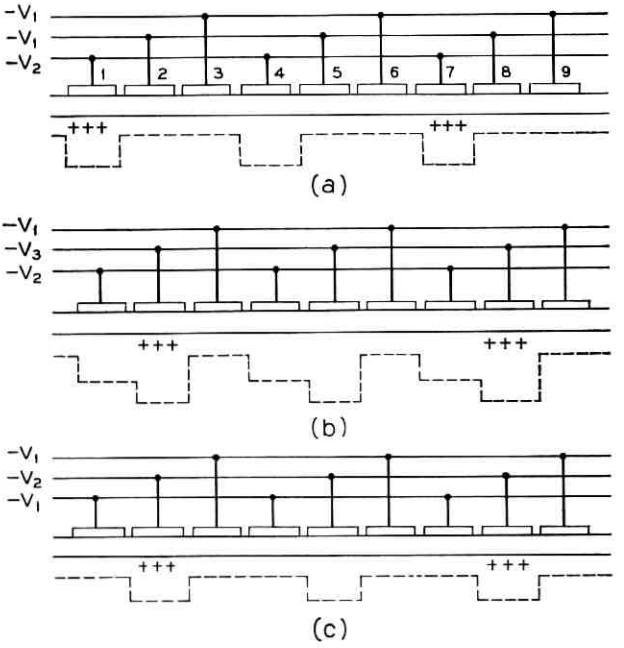

Fig. 2—Schematic of a three phase MIS charge coupled device.

of the structure as a function of stored charge. The capacitance can be used as a measure of the stored charge. Knowledge of the surface potential is necessary to design a structure that insures complete transfer of charge since, referring to Fig. 2, as charge flows from electrode 1 to electrode 2 the potential of 1 will fall and the potential of 2 will rise. Clearly the voltages V_3 and V_2 must be chosen such that the surface potential at electrode 2 is always lower. The steady state minority carrier density Q per unit area for a given gate voltage V_G is given by $Q = C_0(V_G - V_T)$ where $C_0 = K_0\epsilon_0/X_0$ is the oxide capacitance, K_0 is the oxide dielectric constant, and X_0 the thickness. For a charge density $Q' \leqq Q$, the potential φ_s at the semiconductor surface can be shown to be

$$\varphi_s = (V_G - V_{FB}) - \frac{Q'}{Q}(V_G - V_T) - \frac{B}{C_0}\left(\left\{1 + \frac{2C_0(V_G - V_{FB})}{B}\left[1 - \frac{Q'}{Q}\left(\frac{V_G - V_T}{V_G - V_{FB}}\right)\right]\right\}^{\frac{1}{2}} - 1\right) \tag{1}$$

where $B = K_s qN_D X_0/K_0$, K_s is the silicon dielectric constant, V_{FB} is the flatband voltage and N_D the donor density. Similarly, the capacitance between gate and substrate can be shown to be

$$C = C_0\left\{1 + \frac{2C_0V_G}{B}\left[1 - \frac{Q'}{Q}\left(\frac{V_G - V_T}{V_G - V_{FB}}\right)\right]\right\}^{-\frac{1}{2}}. \tag{2}$$

These quantities are plotted as a function of Q'/Q in Fig. 3 for a representative structure with $V_T = 1.2V$. The depletion width $X_d = (2K_s\varphi_s\epsilon_0/qN_D)^{\frac{1}{2}}$ is also plotted. It is seen that these quantities are a reasonably strong function of Q'/Q for the parameters chosen. In a practical situation, the gate voltages chosen ($\sim 10V$) are readily attainable from silicon integrated circuits.

There are two interrelated quantities of interest in describing the transfer of charge from one electrode to the next. One is the time to transfer the charge and the other is the transfer efficiency which we define as the fraction of charge transferred from one electrode to the next. The time constant for transfer of charge from one electrode to another by diffusion will be of the order $\tau_0 = L^2/4D$ where L is the linear dimension of the electrode and D the diffusion constant. It is assumed that the spacings and the applied voltages are such that no potential barrier exists between the electrodes. For $L = 10^{-3}$ cm and $D = 10$ cm^2/sec, it is found that $\tau_0 = 2.5 \times 10^{-8}$ sec. The amount

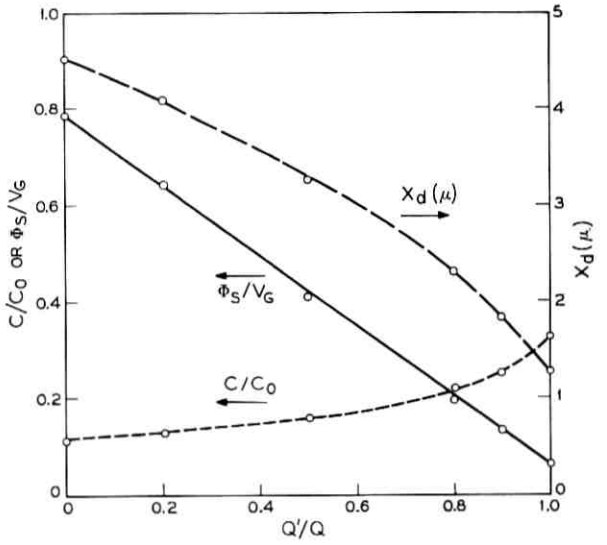

Fig. 3—A theoretical plot of depletion width (X_d), surface potential (φ_s) and capacitance (C) of an MIS structure as a function of charge at the interface (Q'). Edge effects are neglected. The values used in this calculation were:

$$V_G = 10v;$$
$$X_0 = 2 \times 10^{-5}\text{cm};$$
$$N_D = 5 \times 10^{14}/\text{cm}^3;$$
$$C_0 = 1.7 \times 10^{-8}F/\text{cm}^2.$$

of charge remaining will decay in an almost exponential manner with this time constant if trapping in deep surface and bulk states is neglected. If trapping times are comparable to any transfer times of interest, such effects will also detract from the transfer efficiency and for the current Si-SiO_2 technology, it appears that surface states will be the limiting factor.

There will also be a field enhanced component resulting from the change of surface potential with charge density. A qualitative understanding of this is obtained by considering the situation in Fig. 2(b) immediately after $-V_3$ has been applied but before charge has transferred from electrode 1 to electrode 2. As charge from the right hand edge of electrode 1 flows into the potential well under electrode 2, the potential at that edge will become more negative by an amount given by equation (1). This effect results in a field parallel to the interface which adds to the diffusion component. This field will propagate back under the electrode and decrease in magnitude as charge flows but will always add to the diffusion component. The exact nature of

this field has not been calculated but its effect is expected to be significant. For example, an average potential drop of 0.1 volts across the width of a 10^{-3} cm electrode will result in a transit time of 2.5×10^{-8} sec. assuming a mobility of 400 cm^2/v-sec. Further field enhancement may be obtained by making the electrode width plus interelectrode spacing comparable to the oxide thickness and using the fringing field of the neighboring electrode.

The structure in Fig. 2 may be used as a shift register with the addition of a charge generator at one end (input) and a detector at the other. The generation can be accomplished by a forward biased p-n junction, by surface avalanching in an MOS structure,[4] or by radiation induced pair creation. Detection may be accomplished by current detection with a reverse biased p-n junction or Schottky barrier or by utilizing the change of capacitance with charge [see equation (2)].

An estimate of the basic signal-to-noise limitations can be made by considering detection by a reversed biased diode put in place of the last electrode and connected to ground by a resistor. If Q is the average amount of charge stored in an element and f the transfer frequency, then the average signal current is simply $I_s = Qf$. For the example given in Fig. 2, $Q \approx 10^{-13}$ C for an electrode with an area of 10^{-6} cm^2. This results in a signal of 10^{-7} amperes at one megacycle. State of the art video amplifiers have an equivalent noise of about 10^{-9} amperes at one megacycle and would dominate the shot noise which for this example is 2×10^{-10} amperes.

The basic shift register concept may be used to construct a recirculating memory or used as a delay line for times up to the storage time. Clearly, charge transfer in two dimensions is possible as well as the ability to perform logic. An imaging device may be made by having a light image incident on the substrate side of the device creating electron-hole pairs. The holes will diffuse to the electrode side where they can be stored in the potential wells created by the electrodes. After an appropriate integration time, the information may be read out via shift register action. A display device[5] may be constructed by the inverse process of reading in the information (minority carriers) via shift register action and then forward biasing the MIS structure to force the minority carriers into the bulk where radiation recombination takes place.

Aside from problems of yield, the limit to the usefulness device will be determined largely by the speed of transfer, the fractional amount of charge not transferred, and the thermal discharge current. Preliminary experiments[6] show that for existing silicon technology, these parameters lie within the range of usefulness.

The authors wish to thank D. Kahng, C. N. Berglund and E. I. Gordon for stimulating discussions during the course of this work.

REFERENCES

1. Heiman, F. P., "On the Determination of Minority Carrier Lifetime from the Transient Response of an MOS Capacitor," IEEE Trans. on Electron Devices, *ED-14*, No. 11 (November 1967), pp. 781–784.
2. Hofstein, S. R., "Minority Carrier Lifetime Determination from Inversion Layer Transient Response," IEEE Trans. on Electron Devices, *ED-14*, No. 11 (November 1967), pp. 785–786.
3. Buck, T. M., Casey, H. C., Jr., Dalton, J. V., and Yamin, M., "Influence of Bulk and Surface Properties on Image Sensing Silicon Diode Arrays," B.S.T.J., *47*, No. 9 (November 1968), pp. 1827–1854.
4. Goetzberger, A., and Nicollian, E. H., Appl. Phys. Lett. *9*, No. 12 (December 1966), pp. 444–446.
5. Gordon, E. I., private communication.
6. Amelio, G. F., Tompsett, M. F., and Smith, G. E., "Experimental Verification of the Charge Coupled Device Concept," B.S.T.J., this issue, pp. 593–600.

Experimental Verification of the Charge Coupled Device Concept

By G. F. AMELIO, M. F. TOMPSETT and G. E. SMITH

(Manuscript received February 5, 1970)

Structures have been fabricated consisting of closely spaced MOS capacitors on an n-type silicon substrate. By forming a depletion region under one of the electrodes, minority carriers (holes) may be stored in the resulting potential well. This charge may then be transferred to an adjacent electrode by proper manipulation of electrode potentials. The assumption that this transfer will take place in reasonable times with a small fractional loss of charge is the basis of the charge coupled devices described in the preceding paper.[1] *To test this assumption, devices were fabricated and measurements made. Charge transfer efficiencies greater than 98 percent for transfer times less than 100 nsec were observed.*

The basic principles of the charge coupled device, as already described,[1] are very simple indeed, but it is not clear whether the properties of an MIS system are adequate to give viable devices. The purpose

The authors wish to thank D. Kahng, C. N. Berglund and E. I. Gordon for stimulating discussions during the course of this work.

REFERENCES

1. Heiman, F. P., "On the Determination of Minority Carrier Lifetime from the Transient Response of an MOS Capacitor," IEEE Trans. on Electron Devices, *ED-14*, No. 11 (November 1967), pp. 781–784.
2. Hofstein, S. R., "Minority Carrier Lifetime Determination from Inversion Layer Transient Response," IEEE Trans. on Electron Devices, *ED-14*, No. 11 (November 1967), pp. 785–786.
3. Buck, T. M., Casey, H. C., Jr., Dalton, J. V., and Yamin, M., "Influence of Bulk and Surface Properties on Image Sensing Silicon Diode Arrays," B.S.T.J., *47*, No. 9 (November 1968), pp. 1827–1854.
4. Goetzberger, A., and Nicollian, E. H., Appl. Phys. Lett. *9*, No. 12 (December 1966), pp. 444–446.
5. Gordon, E. I., private communication.
6. Amelio, G. F., Tompsett, M. F., and Smith, G. E., "Experimental Verification of the Charge Coupled Device Concept," B.S.T.J., this issue, pp. 593–600.

Experimental Verification of the Charge Coupled Device Concept

By G. F. AMELIO, M. F. TOMPSETT and G. E. SMITH

(Manuscript received February 5, 1970)

Structures have been fabricated consisting of closely spaced MOS capacitors on an n-type silicon substrate. By forming a depletion region under one of the electrodes, minority carriers (holes) may be stored in the resulting potential well. This charge may then be transferred to an adjacent electrode by proper manipulation of electrode potentials. The assumption that this transfer will take place in reasonable times with a small fractional loss of charge is the basis of the charge coupled devices described in the preceding paper.[1] *To test this assumption, devices were fabricated and measurements made. Charge transfer efficiencies greater than 98 percent for transfer times less than 100 nsec were observed.*

The basic principles of the charge coupled device, as already described,[1] are very simple indeed, but it is not clear whether the properties of an MIS system are adequate to give viable devices. The purpose

of this paper is to describe experiments which have been carried out using the silicon-silicon dioxide system to investigate these properties and their effect on device performance in terms of charge transfer speed and efficiency.

The requirements on the silicon-silicon dioxide interface and on the oxide itself are very demanding. One essential feature is a long storage time which is the time required for a pulsed MOS element to reach the steady state condition. The storage time is a function of the flat-band voltage, the pulse voltage and the number of generation-recombination centers at the interface and in the neighboring bulk. Ignoring bulk states and using the capacitance of a 1200 Å thick oxide, it is readily calculated that for zero threshold voltage, a pulse voltage of 20 V and the surface recombination current[2-4] of 3.7×10^{-8} A cm^{-2} appropriate to a fast state density of $2 \times 10^{+10}$ states/cm^2, the storage time is about 16 seconds.

The operational requirement of a charge coupled device is that it must be able to transfer charge with only minimal loss at high speeds. The object of our experiments has been to evaluate this. Estimates of the rate of charge transfer have been made[1] but estimates of transfer efficiency are much more speculative on account of ambiguity in the density of surface states in the energy region near the band edge for a particular oxide.

Several types of oxide on nominal 10 Ω-cm n-type (100) and (111) orientated silicon have been tried. Steam grown oxides with a fast surface state density as low as $N_{ST} = 2 \times 10^{10}$ states/cm^2 gave oxide storage times less than 100 msecs for a 20 V pulse. This unexpected result was attributed to generation-recombination centers caused by impurities which had diffused into the bulk. A silane deposited oxide had storage times greater than one second but was not stable with respect to migration of positive charge. The oxide which has given the best results so far is a dry oxide 1200 Å thick grown in oxygen at 1100°C for one hour and annealed in a nitrogen atmosphere for one hour at 400°C. The flatband potential for this oxide is typically −5 V.

The initial device configuration used in the experiments described below is a linear array of Cr-Au squares 0.1 × 0.1 mm and separated by 3 μm gaps. These squares were produced by conventional photolithography on the oxidized silicon slice. The slice was diced, each die mounted on a 10 pin header and each square gold-wire bonded to a pin.

The device as described above was designed principally for ease of fabrication and is in no way optimized in either material processing

or geometry. Indeed, there are reasons for supposing that p-type material might be preferable since the minority carrier mobility will be greater than in n-type silicon.

Evaluation of charge coupled device performance is based on the measurement of several parameters including percentage of charge transferred (efficiency), the limiting speed of transfer and the storage time. For times greater than about one-half second, the latter property is easily measured by applying a negative step voltage and observing the change of capacitance with time using a capacitance bridge and an xy recorder. Storage times less than one-half second are normally associated with high interface state density oxides or a large number of bulk generation-recombination centers and are of no interest in the present application.

Observation of charge transfer including the determination of efficiency and speed requires a different approach. The experimental configuration chosen in the measurements is shown in Fig. (1). Capacitor P_0 in this figure is used to supply a source of holes to the other units (P_1, P_2, $\cdots$) by surface avalanching. The avalanching pulse, is adjustable 0-200 volts with a full width half maximum of 60 nanoseconds. For the 10 Ω-cm substrate material and 1200 Å oxide thickness used, avalanching occurs in the vicinity of -165 volts. Unit pulse generators are attached to pads P_1, P_2, and P_3. In a many

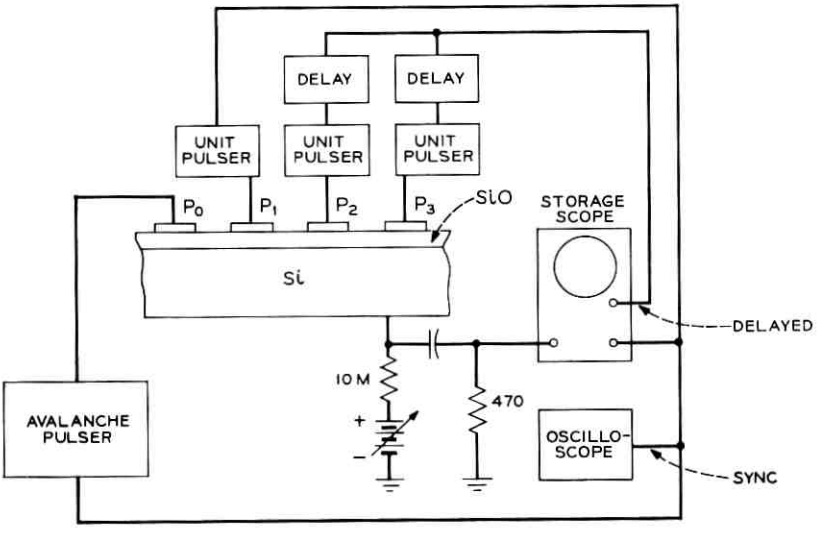

Fig. 1—Schematic of experimental configuration used to evaluate charge transfer.

transfer application, P_1 is attached to each P_{1+3n}, P_2 attached to each P_{2+3n} and P_3 attached to each P_{3+3n}.[1] The substrate is connected to a load resistor and a positive potential for the purpose of biasing the MOS elements beyond threshold voltage. The output signal is capacitively coupled to a relatively low impedance so that response times on the order of 100 nanoseconds are achieved. As each MOS capacitor is pulsed by the supply generators, a charging and discharging spike is observed at the oscilloscope which, for the circuit shown, is proportional to the current flow. The pulsing sequence for capacitors P_0, P_1 and P_2 is illustrated in Fig. (2) for the conditions when the P_1 and P_2 pulse voltages (V_{P_1} and V_{P_2}) do and do not overlap in time. Note the avalanche pulse occurs shortly after P_1 is turned on. Of interest is the charge transfer from P_1 to P_2, all others being ignored for the sake of simplicity. Below each pulse sequence is shown the expected (idealized) oscilloscope display with a positive going signal taken in the downward direction.

For the nonoverlap condition, there are two essentially separate events. Notice that the turn-off pulse of P_1 is larger than the turn-on pulse when avalanching of P_0 occurs during the on-time of P_1. This is easily understood. Each current pulse is given by the relation

$$i(t) = \frac{dQ}{dt} = \frac{dQ}{dV}\frac{dV}{dt} = c(V)\frac{dV}{dt} \tag{1}$$

where $c(V)$ is the differential capacitance of the device, V is the voltage across the capacitor and Q is the charge flowing from ground. Assuming the turn-on and turn-off characteristics of each voltage pulser are made the same, the magnitude of the current is determined by the differential capacitance $c(V)$. At turn-on, the capacitance which must be charged to an additional V_p volts from the bias voltage V_b is represented by the oxide and depletion capacitance in series. When P_0 is avalanched, the holes generated diffuse to P_1 and invert the surface there. The depletion region under P_1 diminishes and the associated capacitance increases. Now at turn-off when the voltage across the device is returned to V_b, the relaxation pulse is of greater magnitude than the turn-on pulse by an amount related to the change in differential capacitance. When no holes are stored, as in the case of P_2, the turn-on and turn-off pulses are of equal amplitude.

Consider now the overlap case. There, instead of the turn-off pulse of P_1 resulting in a large hole injection into the bulk, the holes are transmitted to the adjacent MOS capacitor. The turn-off pulse amplitude of P_1 should therefore decrease. On the other hand, the turn-off

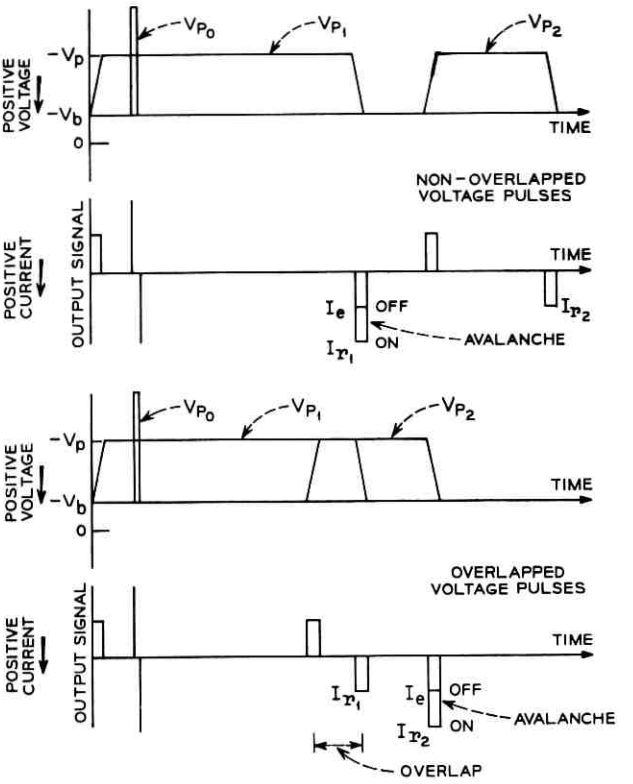

Fig. 2—The pulsing sequence for capacitors P_0, P_1 and P_2. Below each pulse sequence is shown the expected (idealized) oscilloscope display with positive going signal taken in the downward direction.

pulse of P_2 is expected to increase as a result of the charge transmitted to it from P_1.

The efficiency of a single charge transfer can be defined as

$$\eta = \frac{\text{charge arriving at } P_2}{\text{charge originally stored in } P_1} \tag{2}$$

where the charge is given by the integral from V_b to $V_b + V_p$ of the difference in differential capacitance during turn-off and turn-on. This charge can be approximately related to the current pulses discussed above if equal voltage pulses and similar MOS capacitance properties for the two pads are assumed. Thus, for bias voltages significantly beyond threshold where the $c(V)$ curve is relatively flat, the efficiency

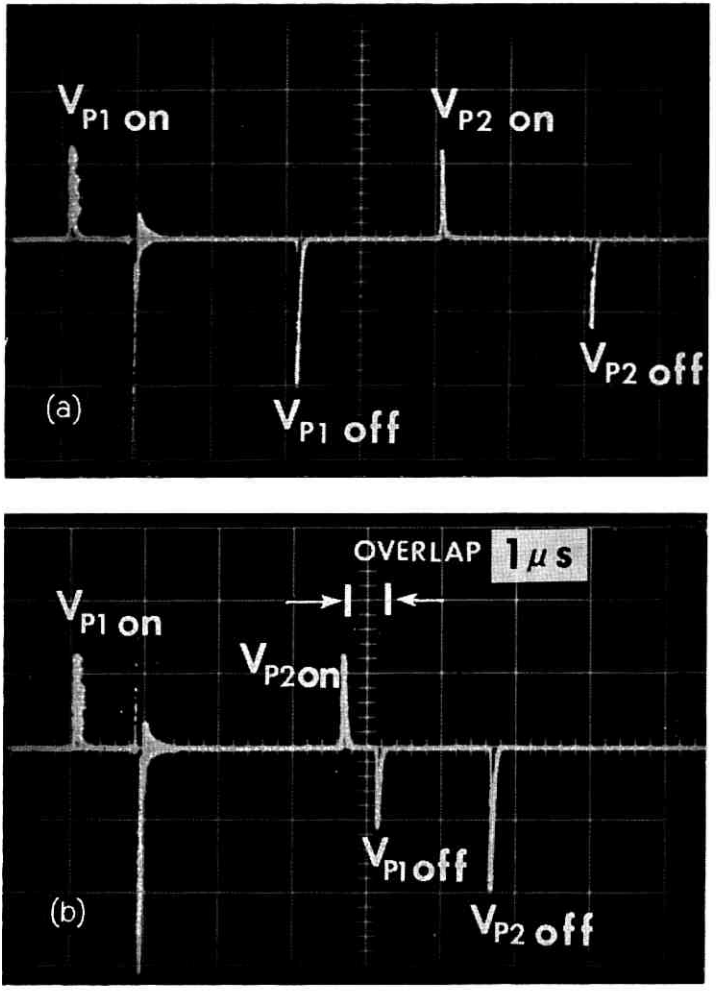

Fig. 3—Oscilloscope traces showing the (a) nonoverlap and (b) overlap charging pulses for an actual device with $V_b = -5$V and $V_p = -20$V. The time base is 2 μs/cm.

can be reasonably approximated in terms of the peak amplitudes of the relaxation current pulses as

$$\eta \approx \frac{I_{r2} - I_e}{I_{r1} - I_e} \tag{3}$$

where I_{r2} is the turn-off pulse when P_2 contains charge, I_{r1} is the turn-

off pulse when P_1 contains charge and I_e is the turn-off pulse when either is empty.

In Figs. 3(a) and (b), the nonoverlap and overlap charging pulses for an actual device with $V_b = -5$ V and $V_p = -20$ V are given. The threshold voltage for this unit is -1.5 volts. The evidence of charge transport is unmistakable. In Fig. 4 a similar, although somewhat more complicated, photograph shows the superposition of many events (using a storage oscilloscope) in which the pulse duration of V_{P_1} is increased until it overlaps V_{P_2} by one microsecond. Following this, V_{P2} is additionally delayed until there is once again no overlap. The rounding seen in the turn-off pulse of P_2 after it goes out of overlap is attributable to holes remaining in the vicinity of P_1 and P_2 after P_1 is turned off. The high transfer speed of the device is seen by the rapidity with which the relaxation pulse P_1 falls off as the pulses overlap. Although not evident in Fig. 2, the charge transfer efficiency is not a function of time for overlap times greater than 100 nanoseconds (the rise time of the pulses used in the experiment). Using enlarged photographs similar to that shown in Fig. 3 and equation (3), the measured efficiency in $\eta = 94 \pm 6$ percent. Measurements made in this manner have been performed on devices with wet, dry and deposited oxides on ⟨111⟩ and ⟨100⟩ oriented surfaces. To date, the best results have

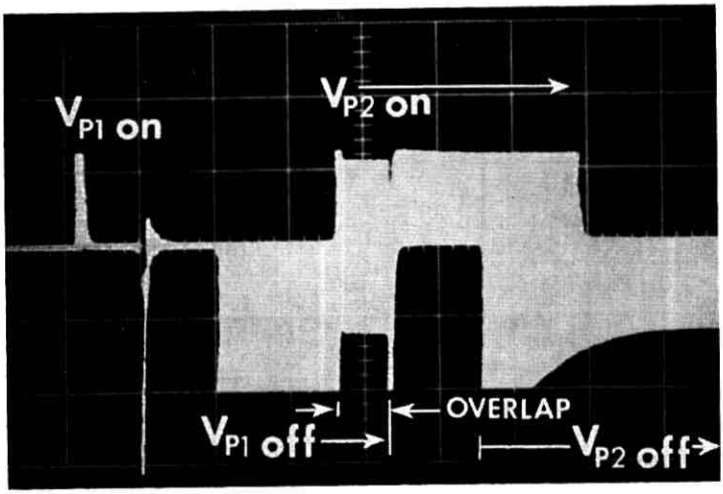

Fig. 4—Oscilloscope traces showing the superposition of many events (using a storage oscilloscope) in which the pulse duration of V_{P_1} is increased from 4 μs until it overlaps V_{P_2} by one microsecond. The turn-on of V_{P_2} is then additionally delayed until there is once again no overlap. The same device is used as for Fig. 3.

been obtained for a 1200 Å dry oxide on the ⟨100⟩ surface of silicon.

More recently, multiple transfer measurements have been conducted for which efficiencies greater than 90 percent have been demonstrated after five transfers, again with pulse widths of 3 μs and overlap times of 1 μs. This implies an η of over 98 percent. For these measurements, current integration has been employed for more accurate determination of the charge transferred.

The authors wish to acknowledge the help of R. A. Furnanage in fabricating the devices and the assistance of P. M. Ryan and E. J. Zimany, Jr. in making the measurements.

REFERENCES

1. Boyle, W. S., and Smith, G. E., "Charge Coupled Semiconductor Devices," B.S.T.J., this issue, pp. 587–593.
2. Heiman, F. P., "On the Determination of Minority Carrier Lifetime from the Transient Response of an MOS Capacitor," IEEE Trans. on Electron Devices, *ED-14*, No. 11 (November 1967), pp. 781–784.
3. Hofstein, S. R., "Minority Carrier Lifetime Determination from Inversion Layer Transient Response," IEEE Trans. on Electron Devices, *ED-14*, No. 11 (November 1967), pp. 785–786.
4. Buck, T. M., Casey, H. C., Jr., Dalton, J. V., and Yamin, M., "Influence of Bulk and Surface Properties on Image Sensing Silicon Diode Arrays," B.S.T.J., *47*, No. 9 (November 1968), pp. 1827–1854.